Wideband Planar Array Antennas: Theory and Measurements

by

David Grant Shively

Thesis submitted to the Faculty of the

Virginia Polytechnic Institute and State University

in partial fulfillment of the requirements for the degree of

Master of Science

in

Electrical Engineering

APPROVED:

Warren L. Stutzman, Chairman

Gary S. Brown

William A. Davis

May, 1988

Blacksburg, Virginia

Wideband Planar Array Antennas: Theory and Measurements

by

David Grant Shively

Warren L. Stutzman, Chairman

Electrical Engineering

(ABSTRACT)

The need for a wide bandwidth array is introduced and explained. Basic planar array principles are reviewed as well as previous work performed on wide bandwidth planar array design. An Archimedean spiral is suggested for the array element and a model for the element radiation pattern is presented. A wide bandwidth linear array is then analyzed using the element model. The array is made to operate over a two octave bandwidth by using an alternate number of elements. This idea is then extended to two dimensions to form a wide bandwidth planar array design. An improved array design is then suggested using fewer elements. This array was fabricated and tested and showed close agreement to theoretically predicted radiation patterns.

Acknowledgements

I would like to thank Dr. Warren Stutzman for the constant advice and encouragement. Claudia deserves a special thanks for always listening and bringing those great brownies to work. Everyone in the lab has been a tremendous help. Thanks to Dennis for all of the microwave advice. Thanks to Ko and Bob for all of the computer help. Thanks to my parents who made all of this possible. A special thanks to Brian, Kathleen, Mark, Mike, Steve, Ken, Kim and John who have all had to put up with me for the past two years. Thanks to Ton-80 for just being there.

Table of Contents

I. Introduction

Wideband antennas have many practical uses which include antennas for wideband measurement systems, spread spectrum communications systems such as "frequency hopping", feeds for reflectors and multifunctional antenna systems. The time required for data acquisition with wideband antenna or scattering measurements can be reduced by using a single antenna system which operates over a large bandwidth instead of switching between narrow band antennas. Likewise for "frequency hopping" communications, if a single antenna could operate over all frequencies of interest only one antenna would be needed. Reflectors are inherently wideband devices but the bandwidth is limited by the feed antenna. Feed antennas for reflectors could also be made wideband if the feed has suitable radiative characteristics over the frequencies of interest.

Wideband operation can be achieved with a single wideband antenna. Examples of wideband antennas are spiral, log-periodic, and helix antennas [1]. The basic tradeoffs when using a single wideband antenna are reduced gain and lack of control over the radiation pattern.

Wide bandwidths can also be realized by switching between narrow or moderate bandwidth antennas. In this way the gain and radiation pattern can be controlled by

using a different antenna when utilizing a different frequency. This approach, however, does not address the problem of wide bandwidth antenna design.

A possible technique for maintaining gain and pattern control is to use an array of antenna elements. This idea has received some attention in the last two decades with some success. There are several advantages to using arrays in wideband applications. In an array several small antennas replace one large (possibly expensive) antenna. Also, the performance of an array can be controlled by weighting the excitation of each array element. Arrays offer high gain and flexibility of construction including conformal structures. The problem is to design an antenna array that will perform satisfactorily at all of the frequencies of interest. This, however, is not easy to do because of problems encountered with array geometries when frequency is changed. Obviously, as frequency is increased the effective electrical spacing between each element will increase, and this causes higher sidelobes and grating lobes to appear in the visible region of the radiation pattern. Also, if the elements themselves are of large electrical size they will not fit closely together in an array. The element size will determine the minimum spacing allowed in the array.

An architecture is proposed here which resolves the basic wideband array conflict between avoiding large electrical interelement spacings while needing electrically large elements. The new concept is to abandon the requirement of identical elements in a uniform spatial grid. Here, nonidentical elements are used in a grid arrangement that is changed electrically as frequency is increased. In this study several geometries are examined and the performance of each is reported. One particularly well-performing architecture was found by using eight array elements of two different sizes.

Attention here is restricted to planar arrays, but the ideas can be applied to other surfaces. This study was not driven by any specific application but the following performance objectives are assumed: moderate to high gain and not exceedingly high

sidelobes over the complete operating band. The bandwidth goal is two octaves, but the ideas presented may be extended to even wider bandwidths.

II. Basics of Planar Arrays

Although the overall geometry of an array may take on any shape, arrays are generally catagorized by the shape formed by connecting the centers of adjacent elements. This defines the array lattice, similar to the lattice structure of crystals. Antenna arrays are customarily constructed with the element centers maintaining a rectangular or triangular lattice structure. It is also customary to locate planar arrays in the xy-plane with the broadside direction along the +z-axis [2,3]. This convention will be followed in this paper.

2.1 Rectangular Lattice Structure

Arrays are said to have a rectangular lattice structure if the element centers are arranged in a rectangular grid. The overall shape of the array, however, need not be rectangular. An example of a rectangular lattice array is shown in Fig. 2.1-1. The element spacings are designated by S_x in the x-direction, S_y in the y-direction and S_d in the

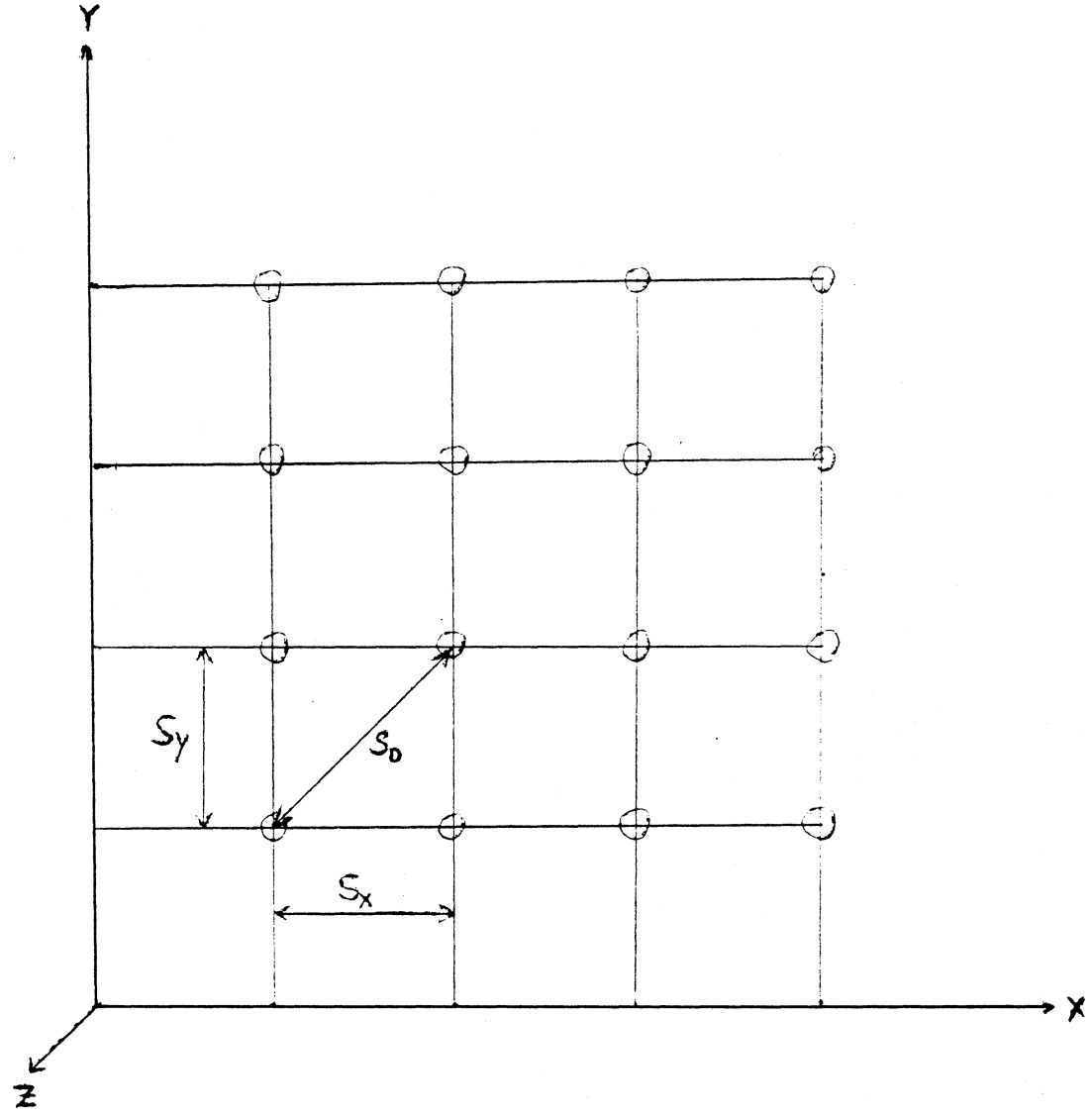

Figure 2.1-1. Rectangular lattice array structure. Element locations are indicated by circles.

diagonal direction. A regular rectangular array has the constraint $S_x = S_y$. The radiation pattern will only be the same in both principal planes if the number of elements is the same in the x- and y-directions and $S_x = S_y$ and the element pattern is the same in both planes.

2.2 Triangular Lattice Structure

When the center points of the array elements form triangles the array is said to have a triangular lattice structure. The most common form of this arrangement is that of an equilateral triangle. In this case each element is equidistant from each neighboring element as shown in Fig. 2.2-1. However, because of the different element spacings in the principal planes the radiation patterns will not be the same in these two planes.

2.3 Array Radiation Pattern Evaluation

The radiation pattern for an array is obtained by the principle of pattern multiplication [1]. Thus, the complete normalized radiation pattern is

$$F(\theta, \phi) = g(\theta, \phi) f(\theta, \phi) \tag{2.3-1}$$

where $g(\theta, \phi)$ is the normalized radiation pattern of one element and $f(\theta, \phi)$ is the normalized array factor expression. This assumes that mutual coupling between elements is either negligible, or is uniform across the array and included in the element pattern [1].

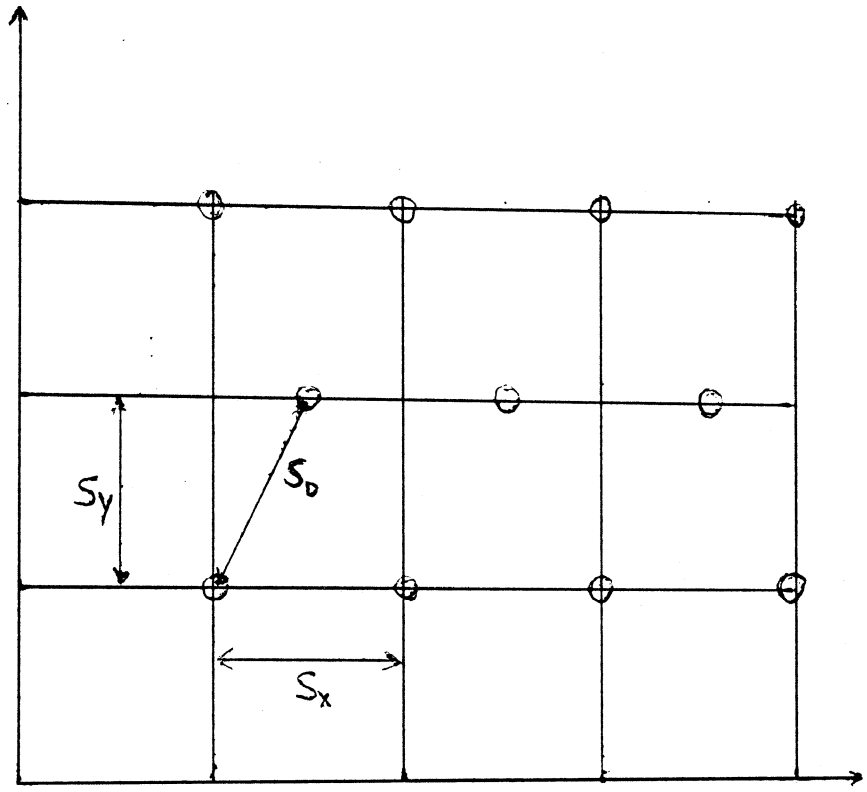

Figure 2.2-1. Triangular lattice array structure. Element locations are indicated by circles.

The unnormalized array factor expression for an arbitrary array is given by

$$AF = \sum_{n=0}^{N-1} A_n e^{j\alpha_n} e^{j\beta \vec{r}_n \cdot \hat{r}} \tag{2.3-2}$$

where A_n is the relative magnitude of element n, α_n is the relative phase of element n and B is the free space propagation constant [1]. For planar arrays in the xy-plane, $\vec{r}_n = x_n\hat{x} + y_n\hat{y}$ and (2.3-2) reduces to

$$AF = \sum_{n=0}^{N-1} A_n e^{j\alpha_n} e^{j\beta(x_n \sin\theta \cos\phi + y_n \sin\theta \sin\phi)} \tag{2.3-3}$$

where x_n and y_n are the coordinates of element n.

III. Previous Research Involving Wideband Arrays

Several successful implementations of wide bandwidth arrays have been reported. Because planar arrays involve two dimensions and are therefore more complex to analyze, most research has been done on linear arrays. It is possible, however, to apply some principles of wideband linear array design to wideband planar array design. In this chapter we review the literature on the subject.

3.1 Wideband Linear Arrays

King, et al. [2] define a "broad band array" as an array that is a specific length in meters and at all frequencies of interest has sidelobes less than a specific value. They used unequal spacings as a means to reduce the number of elements in the array while retaining constant beamwidth and low sidelobe levels. Also, they confined their study to equally excited elements. King, et. al. assumed that the smallest spacing should be 1/2 wavelength at the lowest frequency. Resulting linear array designs were reported to

have sidelobes less than -5 dB relative to the peak of the main beam over a 2:1 bandwidth.

Ishimaru and Chen [3] claimed that bandwidths of 5:1 or even 20:1 were possible with unequal spacings and equal amplitude weightings. The array should be designed for the highest frequency of interest so that as frequency is reduced the sidelobe level is also reduced. This is because as frequency is reduced the element spacing decreases electrically. The authors noted that if unequal amplitudes are allowed, the sidelobe level can be further reduced. The arrays considered by Ishimaru and Chen, however, were linear and contained a large number of elements.

Bratkovic [4] also suggested designing for the highest frequency and claimed that any bandwidth is possible, specifically mentioning as much as 27:1. The array analyzed by Bratkovic was linear and contained a large number of elements. The author used unequal spacings and each element was equally excited.

3.2 Wideband Planar Arrays

Some wideband planar arrays have been built, but most contain complicated feeding mechanisms such as ferrite phase shifters and time delay devices. DuFort [5] suggested that time delay devices should be used instead of phase shifters when wide bandwidth is desired to maintain constant gain and low sidelobes. This is because the phase shifters considered by DuFort operated at only one frequency. Laughlin and others [6] built a planar array that operated over a 2:1 bandwidth. This array consisted of 96 waveguide radiators in a triangular lattice fed by broadband ferrite phase shifters and dielectric impedance matching transformers on a radiating aperture. A similar de-

sign considered by Boyns and Provencher [7] consisted of three different sizes of waveguide radiators interlaced in an array. The array was operated at three discrete frequencies and maintained sidelobes lower than -7 dB at these three frequencies. However, this array was not operated over the entire frequency band and contained a large number of elements. This shared aperture concept was also investigated by Stutzman [8,9] who stacked different size Archimedean spirals in layers, thus creating a three dimensional array of spirals. The array was successfully operated over two octaves and the blockage due to the different layers of the array was found to be minimal. Newman and Schrote [10] achieved a 3:1 bandwidth array with only four elements by utilizing superdirective techniques. The superdirective techniques allowed a reduced size array while maintaining moderate directivity. Superdirectivity, however, made the feed system more complex and more lossy than desired.

3.3 Spiral Elements for Wideband Arrays

Although any wideband element could be considered for a wideband array, spiral antennas have the advantages of small size and a nearly constant radiation pattern over a wide frequency range. Planar cavity backed spirals also offer a low profile. Equiangular, Archimedean, hyperbolic and square spirals exhibit wideband properties although only the equiangular spiral is a truly frequency independent antenna [11]. Both circular and square spirals are possible choices as elements. Both such spirals possess the property that, in order to operate, the perimeter of the spiral must be at least one wavelength at the frequency of interest. The spiral will continue to radiate as the frequency is increased above the cutoff frequency over a three to four octave range. The

radiation from circular and square spirals is inherently circularly polarized. The arms of a spiral may also be zig-zagged in order to form a "slow wave" spiral. This allows reduced aperture size while maintaining similar radiative characteristics as those of a regular spiral [8,9]. For more detailed information concerning spiral operation see [12].

Spiral antennas were investigated in great detail in the early 1960's and some planar arrays were built with spiral elements but were not operated over a wide bandwidth. Donnellan and Close [13,14] built planar arrays of spirals with low sidelobe levels and linear polarization. These spiral arrays were only operated at one frequency and had Chebyshev amplitude weighting to attain sidelobe levels better than -25 dB. The sidelobes were found to increase as the main beam was scanned off axis.

IV. Directivity of Planar Arrays

4.1 Directivity of Planar Arrays of Isotropic Elements

Directivity, in general, is given by

$$D = \frac{4\pi}{\Omega_A} \tag{4.1-1}$$

where Ω_A is the beam solid angle. For an array of isotropic elements the beam solid angle is given by the integral of the power pattern as

$$\Omega_{A_i} = \int_0^{2\pi} \int_0^{\frac{\pi}{2}} |f(\theta, \phi)|^2 d\Omega \tag{4.1-2}$$

and $d\Omega = \sin\theta d\theta d\phi$. In this case the integration over θ is from 0 to $\frac{\pi}{2}$ because the pattern is assumed to vanish beyond $\theta = \frac{\pi}{2}$. The integrand is the magnitude square of the array factor expression for a planar array given by (2.3-3). The integral was evaluated numerically with the IMSL routine DBLIN which was called by the Fortran pro-

gram listed in Appendix A. A plot of directivity for an array of four isotropic elements as a function of element spacing is shown in Fig. 4.1-1.

4.2 Element Pattern Modeling

Before directivity can be evaluated with element pattern effects included, the element pattern expression must be modeled. Spiral antennas were chosen as the element for a wideband array because of their small size and wide bandwidth properties. See Sec. 3.3 for a discussion of spiral elements.

Pattern data supplied with commercially available spirals manufactured by American Equipment Laboratories [15] for several circular, cavity backed, Archimedean spiral antennas were examined. The following were found to be typical radiation pattern points:

$$\begin{matrix} -4.5\,dB \;\; at\; \theta = 45° \\ \\ -20.0\,dB \;\; at\; \theta = 90° \end{matrix} \qquad (4.2\text{-}1)$$

A smooth pattern through these points results if the following element pattern model is used:

$$g(\theta, \phi) = \cos^q(n\theta) \qquad (4.2\text{-}2)$$

with a value for q of 5.8 and a value for n of 0.53. Note that such an element pattern depends only on the angle θ. A plot of this radiation pattern appears in Fig. 4.2-1.

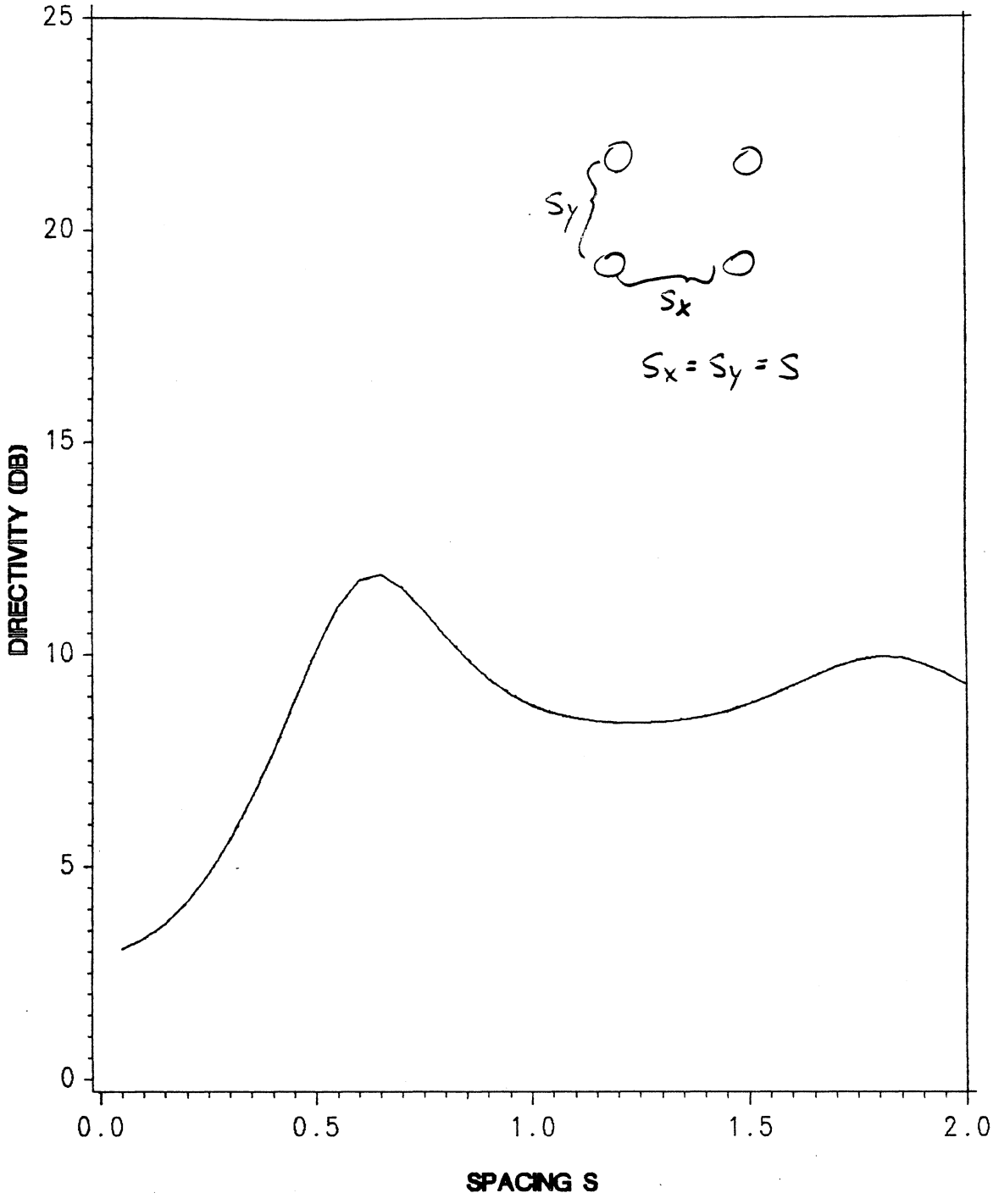

Figure 4.1-1. Directivity for a planar array of four isotropic elements evaluated using (4.1-2). Element spacing is given in wavelengths.

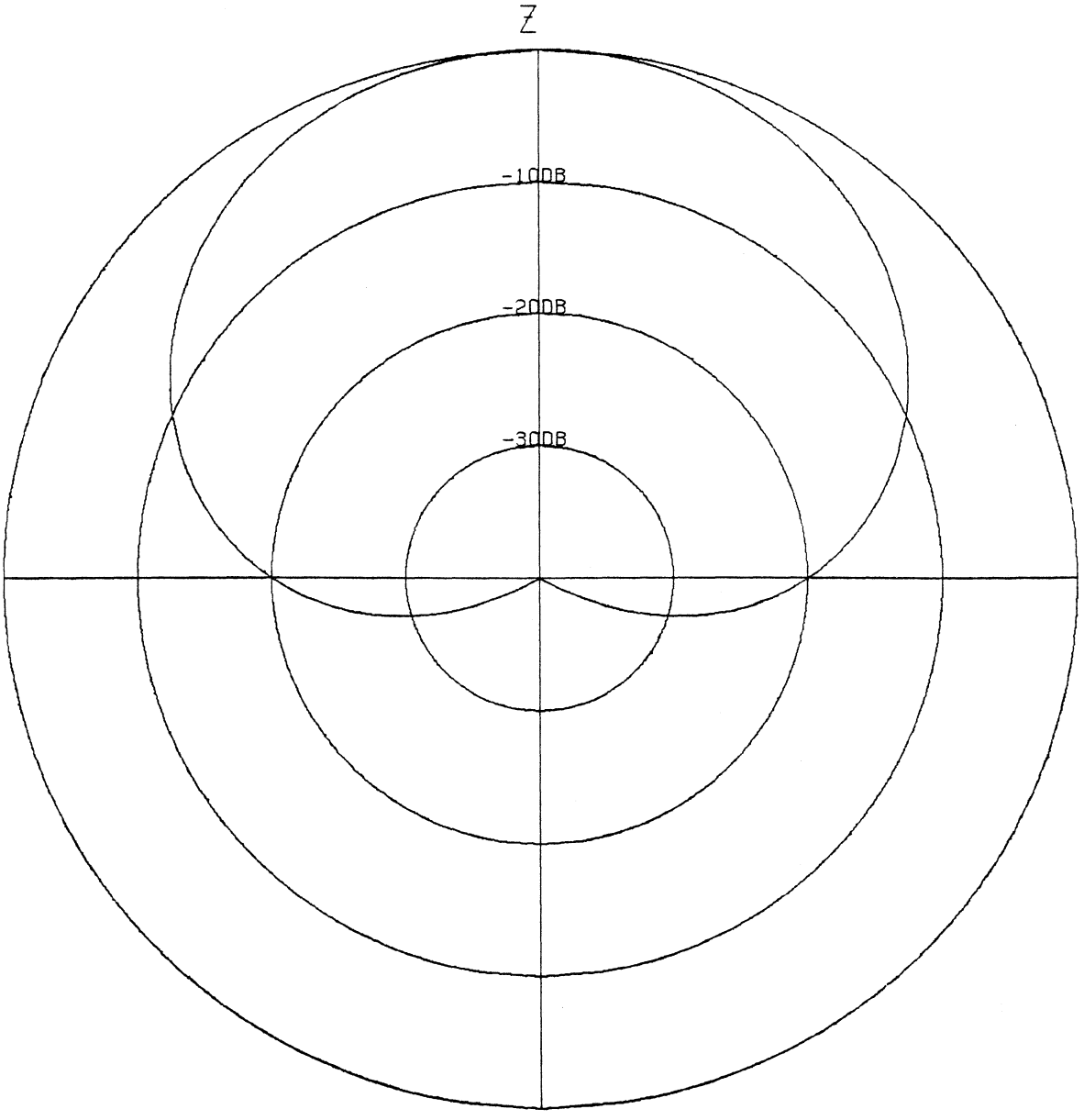

Figure 4.2-1. Proposed pattern model of (4.2-2) for an Archimedean spiral antenna.

4.3 Directivity Including Element Pattern Effects

The directivity of an array including element pattern effects is given by (4.1-1) with Ω_A now defined as

$$\Omega_A = \int_0^{2\pi} \int_0^{\frac{\pi}{2}} |g(\theta)|^2 |f(\theta, \phi)|^2 d\Omega \tag{4.3-1}$$

where $g(\theta)$ is given by (4.2-2) for spiral antenna elements. The directivity was evaluated by numerically integrating (4.3-1) using the program in Appendix A and is shown in Fig. 4.3-1 for a four element rectangular array.

Rahmat-Samii [16] and others [17] have derived matrix equations for directivity which do not depend on numerical integration and have obtained similar results. In Fig. 4.3-2 a comparison is made between numerical integration and Rahmat-Samii's matrix technique for a four element planar array with the element pattern $g(\theta) = \cos^{3.54}(\theta)$. The original figure was borrowed from [16]. Both methods have similar results for the element spacings shown. Because of the close agreement between these two results and the availability of the IMSL integration routines numerical integration was used for directivity calculations throughout this paper.

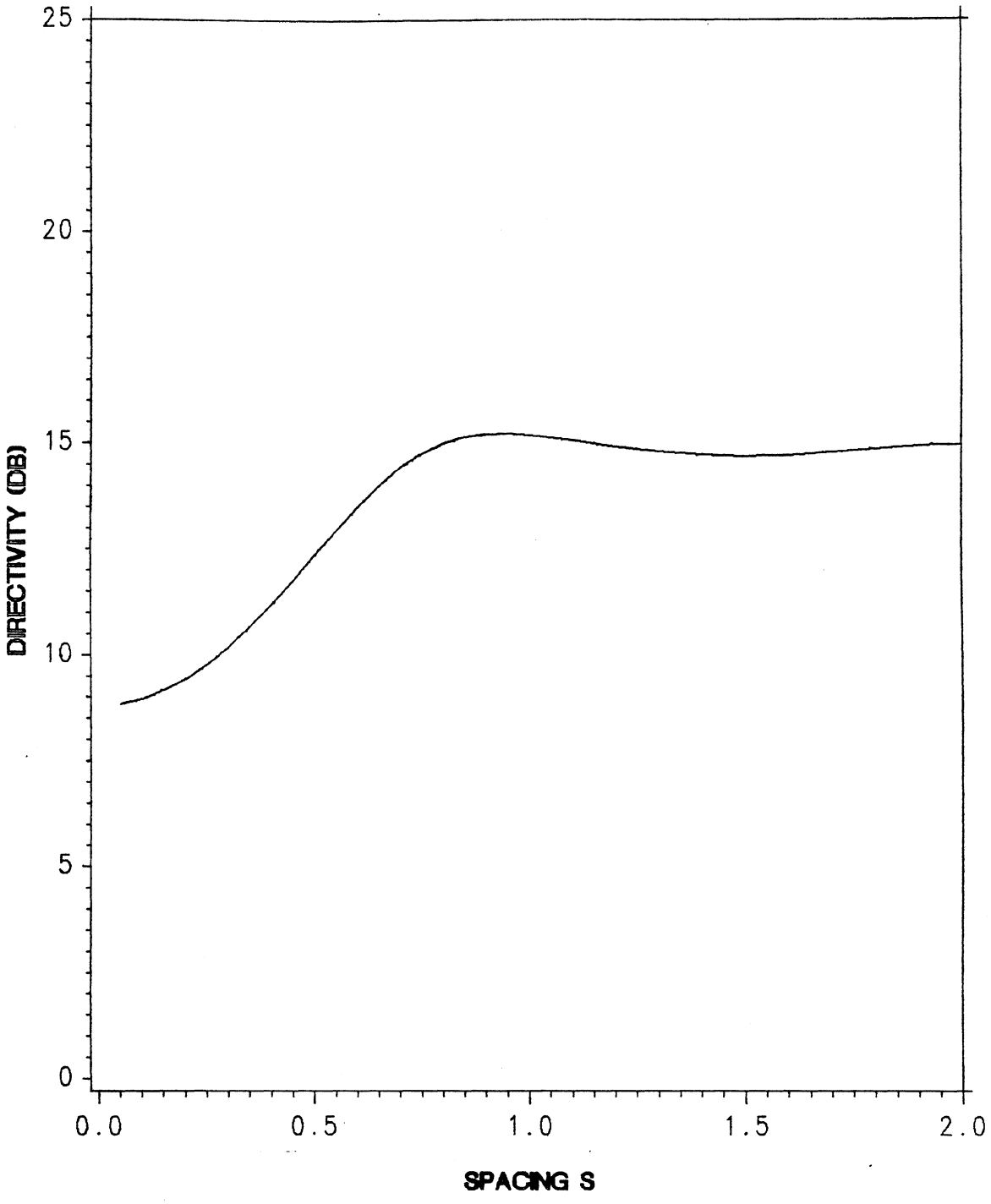

Figure 4.3-1. Directivity of a four element array of spiral elements with the element pattern (4.2-2) evaluated by numerical integration using the program in App. A. Element spacing is given in wavelengths.

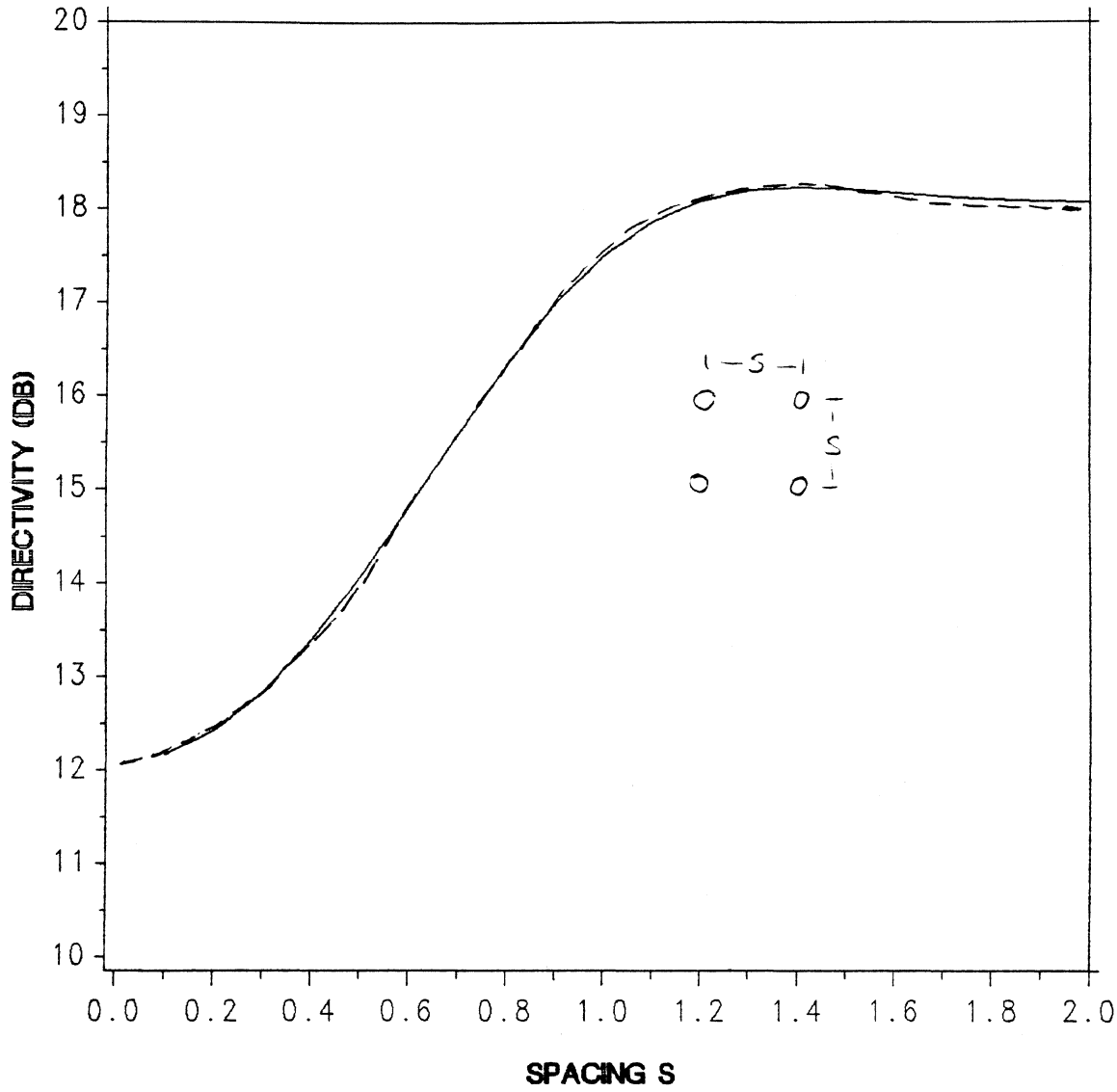

Figure 4.3-2. Directivity comparison for four element planar array with element pattern $\cos^{3.54}\theta$. Rahmat-Samii solid and numerical integration dashed. Element spacing is given in wavelengths.

V. Investigation of Wideband Array Architectures

5.1 An Idea for a Wideband Array

Most arrays are designed so that the element centers are between one half and one wavelength apart. As element spacing approaches one wavelength, sidelobe levels increase and directivity decreases due to the appearance of grating lobes in the visible region of the radiation pattern [1]. In order to achieve wide bandwidth it is necessary to retain the desirable characteristics of 1/2 to 1 wavelength element spacing with increasing frequency. The exact range of spacings allowed depends on the element pattern and element excitations. A layered array geometry was developed that successfully solved this problem [8,9]. The array was composed of three different size elements located in three different layers and is shown in Fig. 5.1-1. The blockage due to the outer layers was found to have only a small effect on the performance of the innermost elements. In this research a planar array arrangement is suggested because of the simpler construction. The planar configuration is more space efficient, of lower profile, and eliminates all blockage. The 1/2 to 1 wavelength element spacing can be preserved over a two

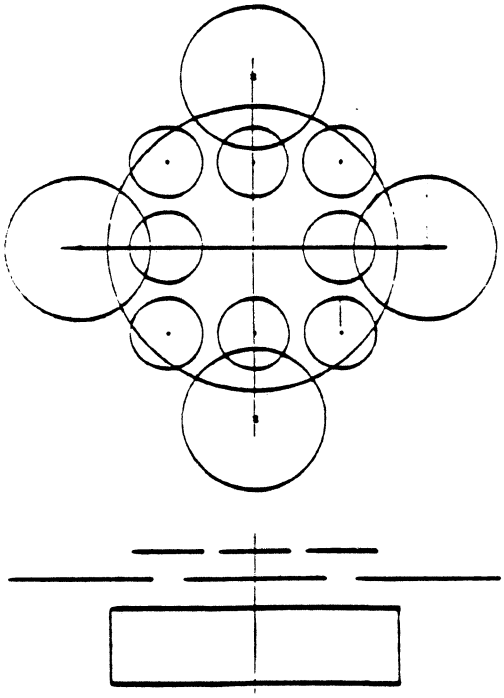

Figure 5.1-1. Shared aperture array configuration (top, side views).

octave range if the number of active elements in the array can be changed when the element spacing becomes 1 wavelength. By locating small elements in between large elements as indicated in Fig. 5.2-1 and the activating the small elements when the spacing between the two large elements becomes one wavelength the spacing between the elements again becomes 1/2 wavelength. Although this changes the number of elements in the array, it does insure that the element spacing never goes beyond one wavelength as frequency is increased over a two octave range, assuming that at the lowest frequency of operation the two outer elements are a half wavelength apart or less. The small elements can be switched in and out of operation when needed. In the case of spirals, if the operating frequency of the array is below the cutoff frequency of the small elements, then the presence of the small element should have no effect on the array operation because of large input impedance and poor radiation efficiency. Of course, in this approach element size will be critical because of the close packing required.

For the case of a linear array this uniform spacing is in contrast to the unequal element spacings suggested in Sec. 3.2 for wideband arrays. Also, this array is not designed for the highest frequency of operation as was suggested in Sec. 3.2. Naturally the array performance will change as the frequency is increased. Before a planar array design will be attempted a linear array similar to that described above will be analyzed in order to try to understand the performance of such an array.

5.2 A Wideband Linear Array of Spirals

Consider the array shown in Fig. 5.2-1 composed of three large spirals and three small spirals. The diameter of the larger spirals is twice that of the smaller spirals. At

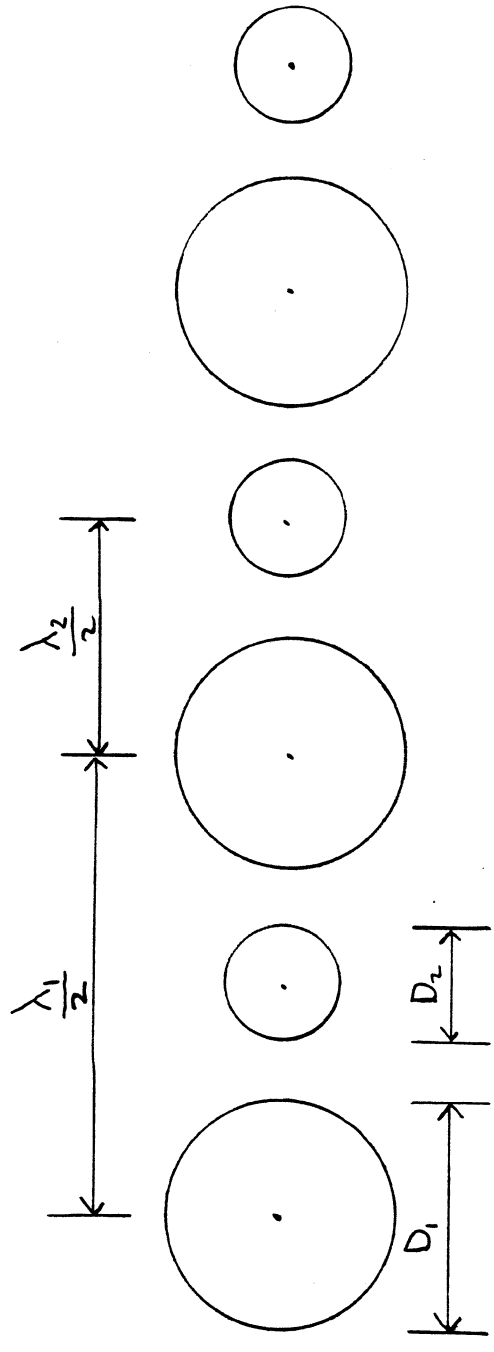

Figure 5.2-1. Linear array of spirals designed for two octave performance.

the lowest frequency of operation, f_1, only the three larger spirals will operate. At frequency f_1 the element spacing is $\frac{\lambda_1}{2}$, where λ_1 is the wavelength at frequency f_1. As the frequency is increased the element spacing in wavelenths increases linearly. At $f_2 = 2f_1$ the element spacing is $1\lambda_2$, and the three smaller spirals begin to operate so the element spacing becomes $\frac{\lambda_2}{2}$. The frequency can then be increased another octave to $f_4 = 4f_1$ when the element spacing once again becomes $1\lambda_4$. To summarize, the large elements operate over a two octave range and the small elements operate only over the upper octave.

The inclusion of the three smaller elements serves two purposes. First, as the element spacing approaches one wavelength sidelobes become greater than -10 dB. With the inclusion of the three smaller elements in the upper octave the sidelobes remain below -10 dB over a two octave range of frequency. Assume that $A_n = 1$ and $\alpha_n = 0°$ in the array factor expression of (2.3-3). The element pattern is given by (4.2-2). Sidelobe levels were predicted with the TURBO Pascal program listed in Appendix B and are plotted versus frequency in Fig. 5.2-2. Second, the inclusion of the three smaller elements at f_2 means that the directivity of the array increases over the two octave band. Directivity calculated with the program in Appendix A is plotted versus frequency in Fig. 5.2-3. Radiation patterns for the array were calculated by evaluating (2.3-1) with the TURBO Pascal program listed in Appendix C and are shown in Figs. 5.2-4 through 5.2-6 for frequencies f_1, f_2, and f_4, respectively. In Fig. 5.2-5 a comparison is shown between the three element array and the six element array at frequency f_2. Note the pattern improvement provided by the inclusion of the three smaller elements.

Our original idea used the same number of small elements as large elements. However, if the small element at the end of the array is removed, the performance does not degrade drastically. The sidelobe level is actually lower over part of the two octave bandwidth than that of the previous array and is below -10 dB at the highest frequency

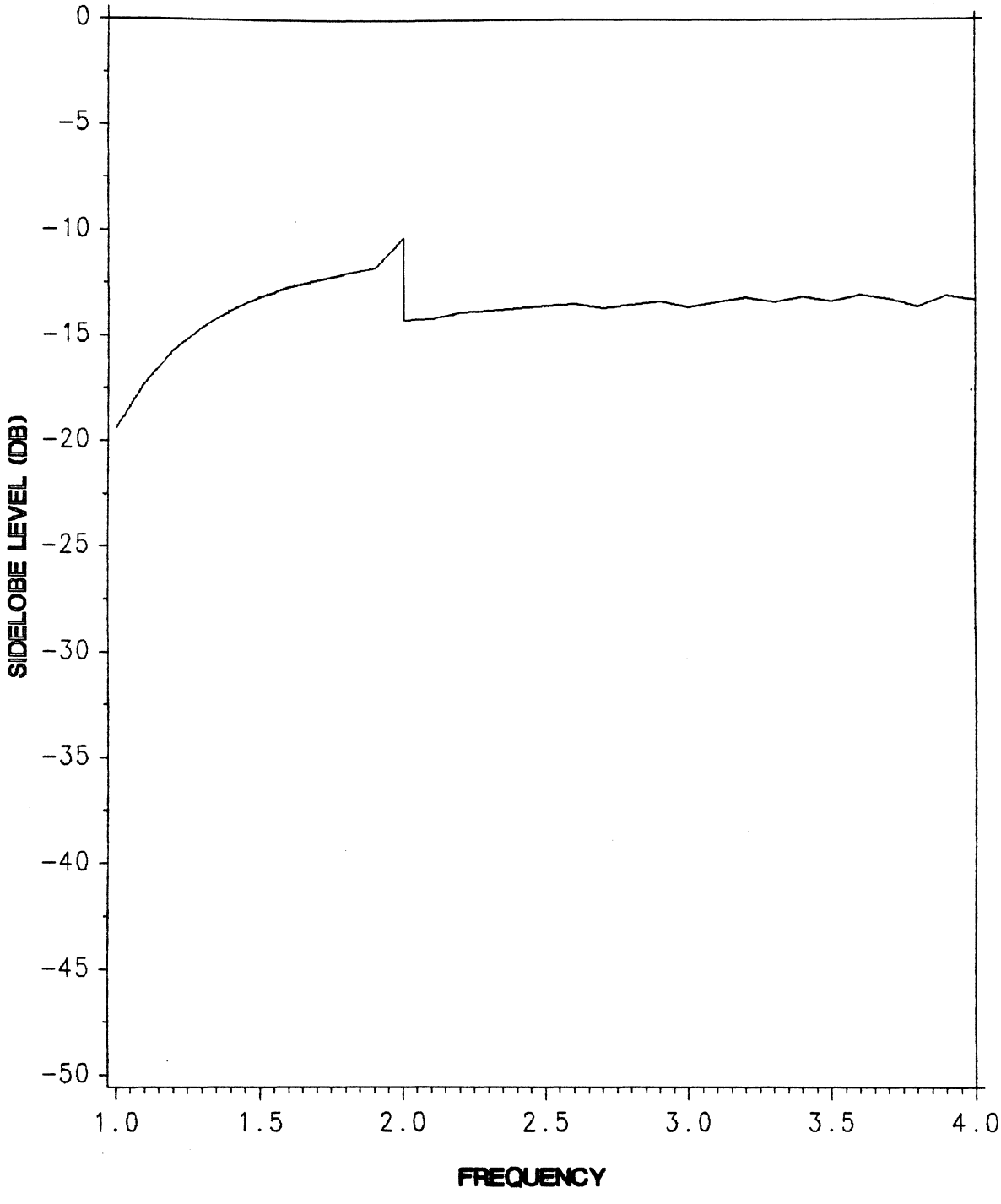

Figure 5.2-2. Calculated sidelobe level for the linear array in Fig. 5.2-1 with uniform amplitude and phase excitation. Abscissa is normalized to f_1 Four large elements are active up to $2f_1$. Above $2f_1$ all eight elements are active.

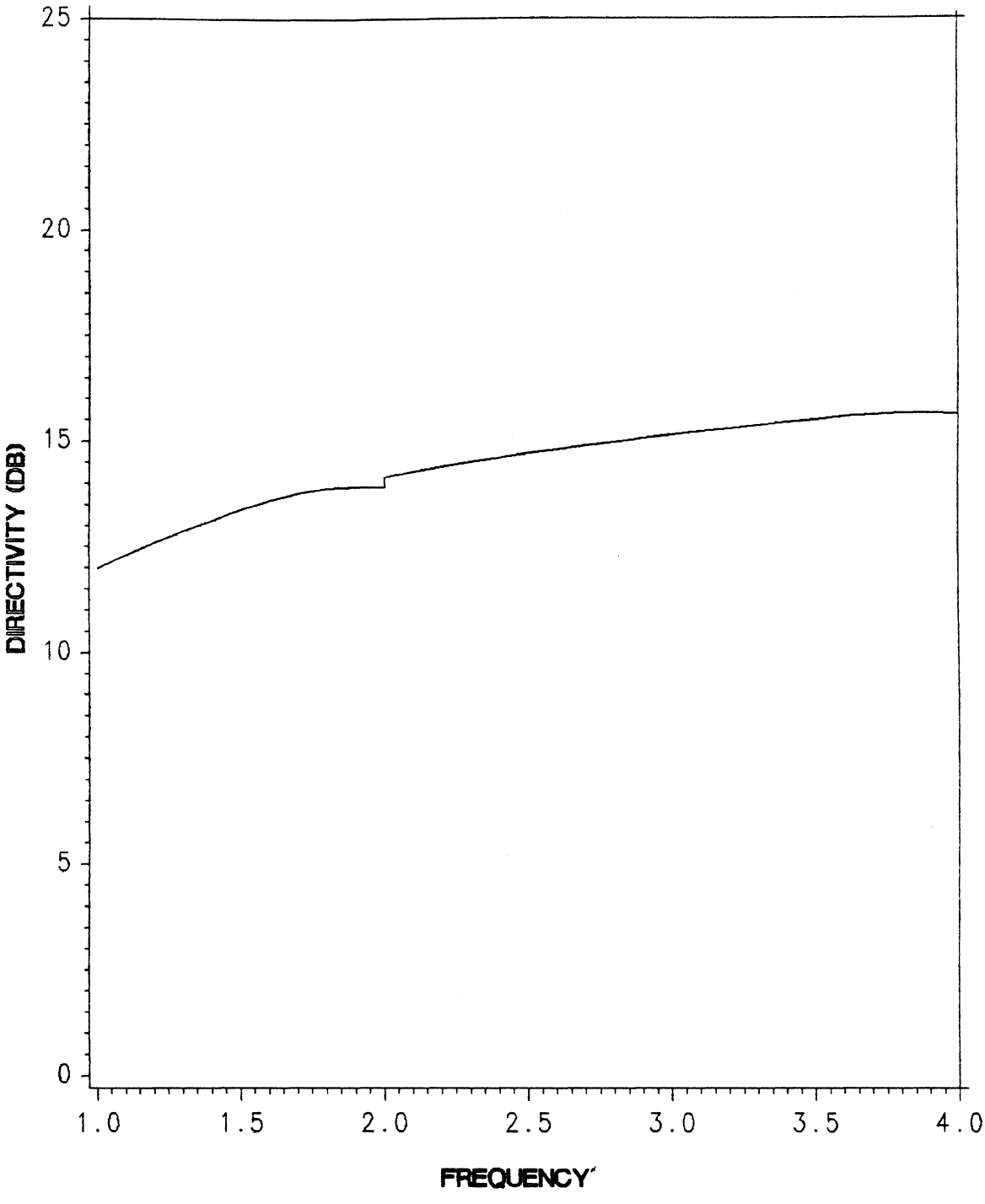

Figure 5.2-3. Calculated directivity for the linear array in Fig. 5.2-1 with uniform amplitude and phase excitation. Abscissa is normalized to f_1 Four large elements are active up to $2f_1$. Above $2f_1$ all eight elements are active.

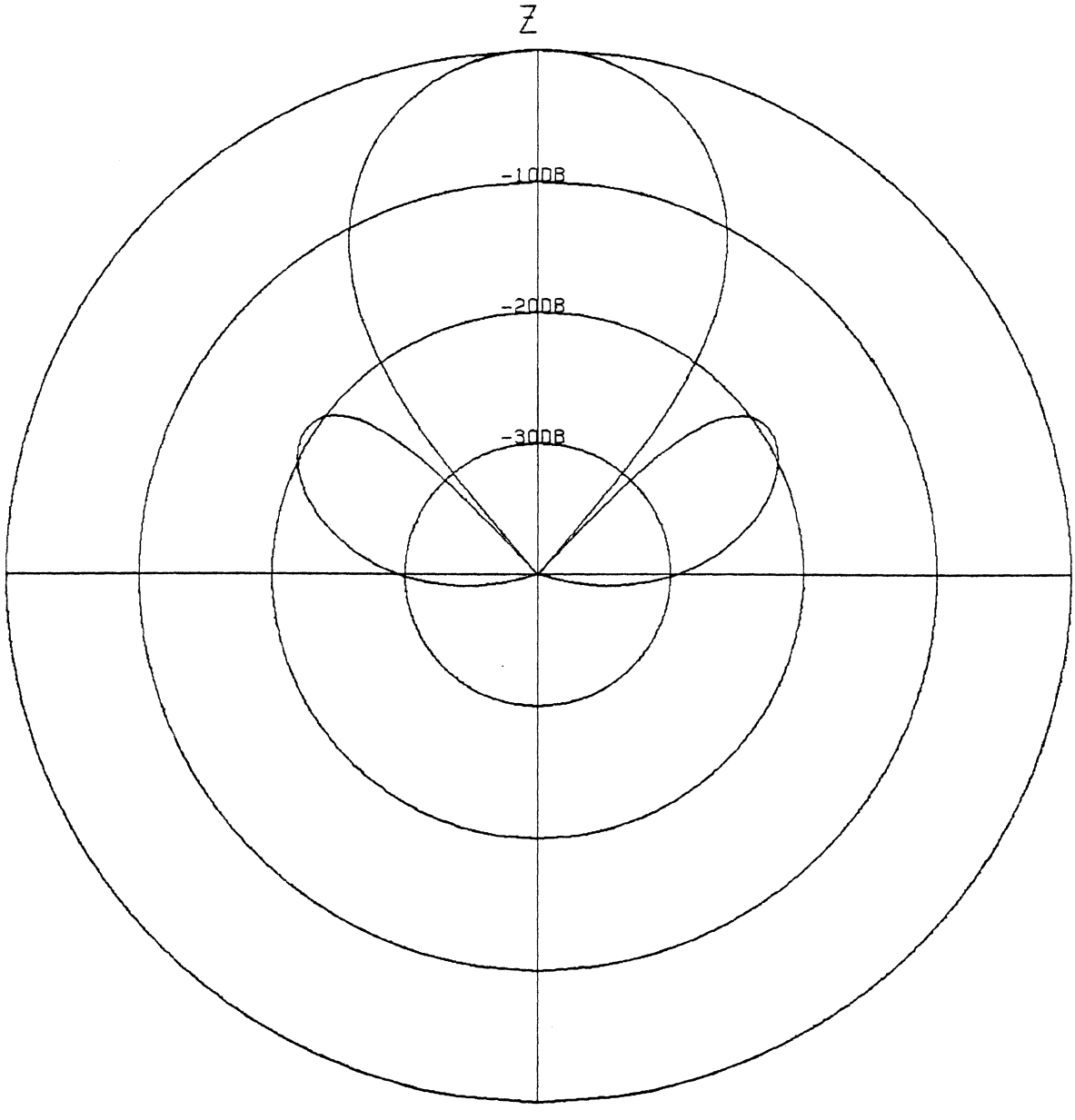

Figure 5.2-4. Calculated radiation pattern for the three large elements in the linear array of Fig. 5.2-1 at frequency f_1 with uniform amplitude and phase excitation.

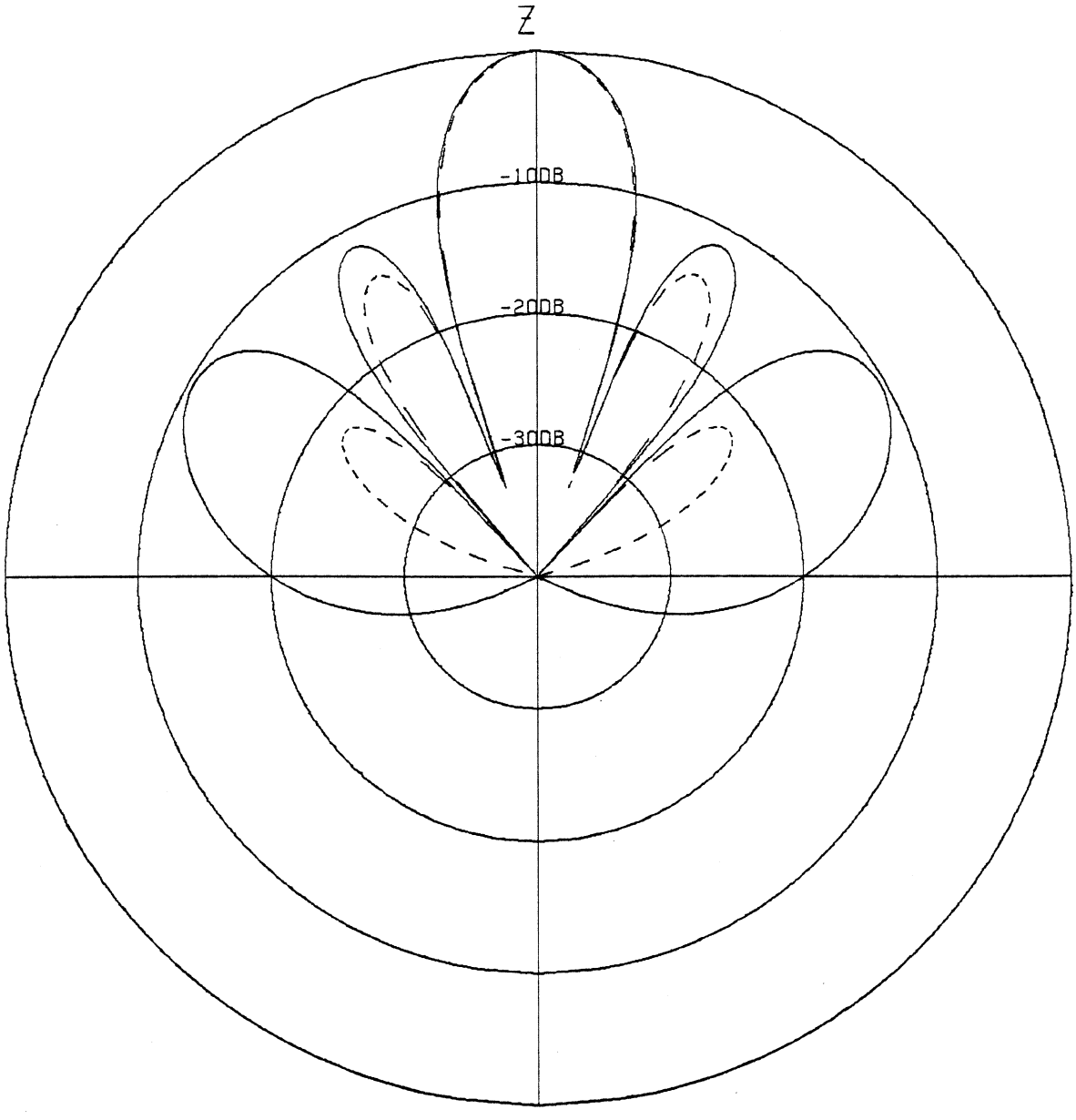

Figure 5.2-5. Calculated radiation patterns for the linear array of Fig. 5.2-1 at frequency f_2 with uniform amplitude and phase excitation (3 large elements active-solid, all 6 elements active-dashed).

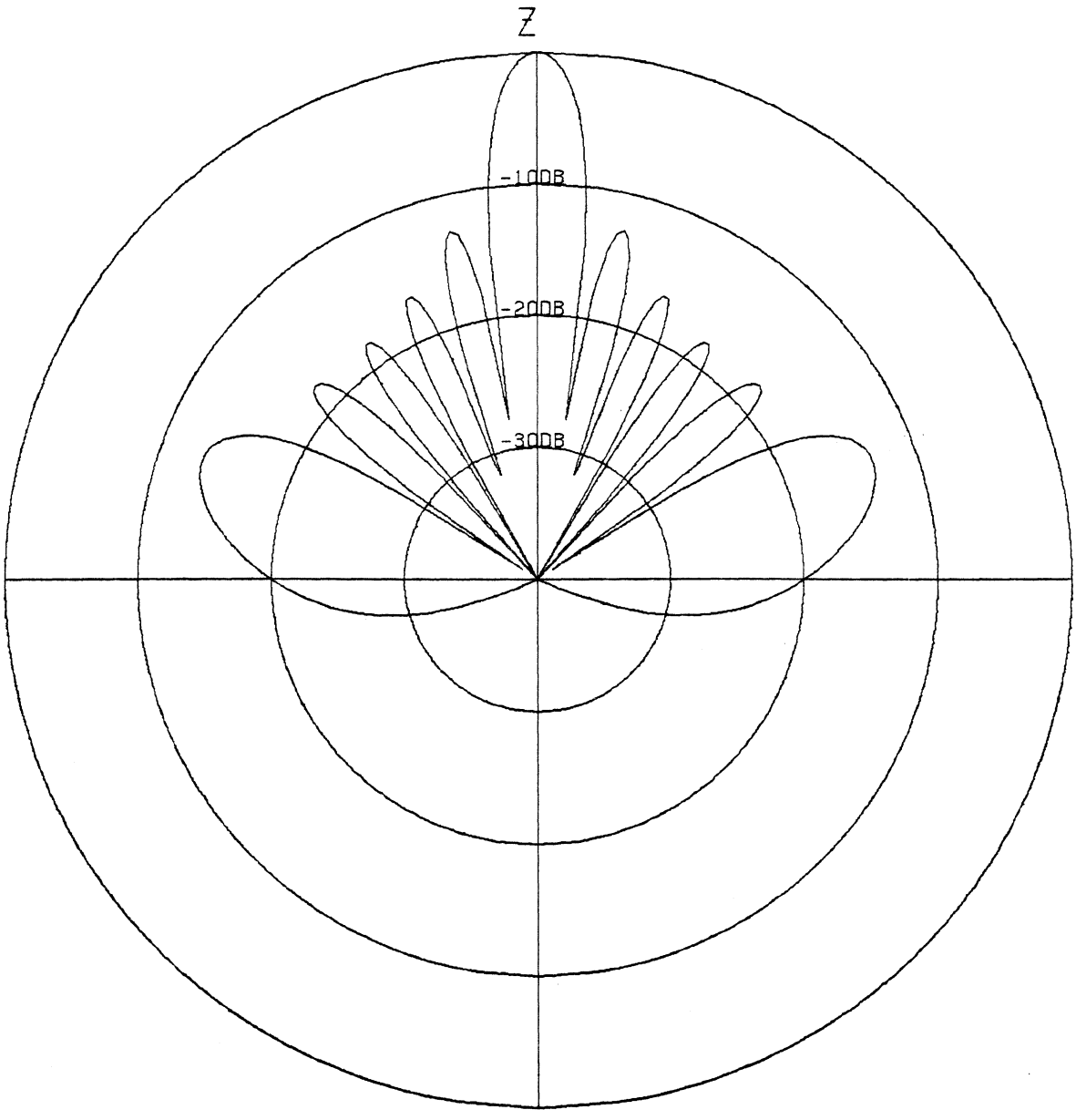

Figure 5.2-6. Calculated radiation pattern for 6 element linear array of Fig. 5.2-1 at frequency f_4 with uniform amplitude and phase excitation.

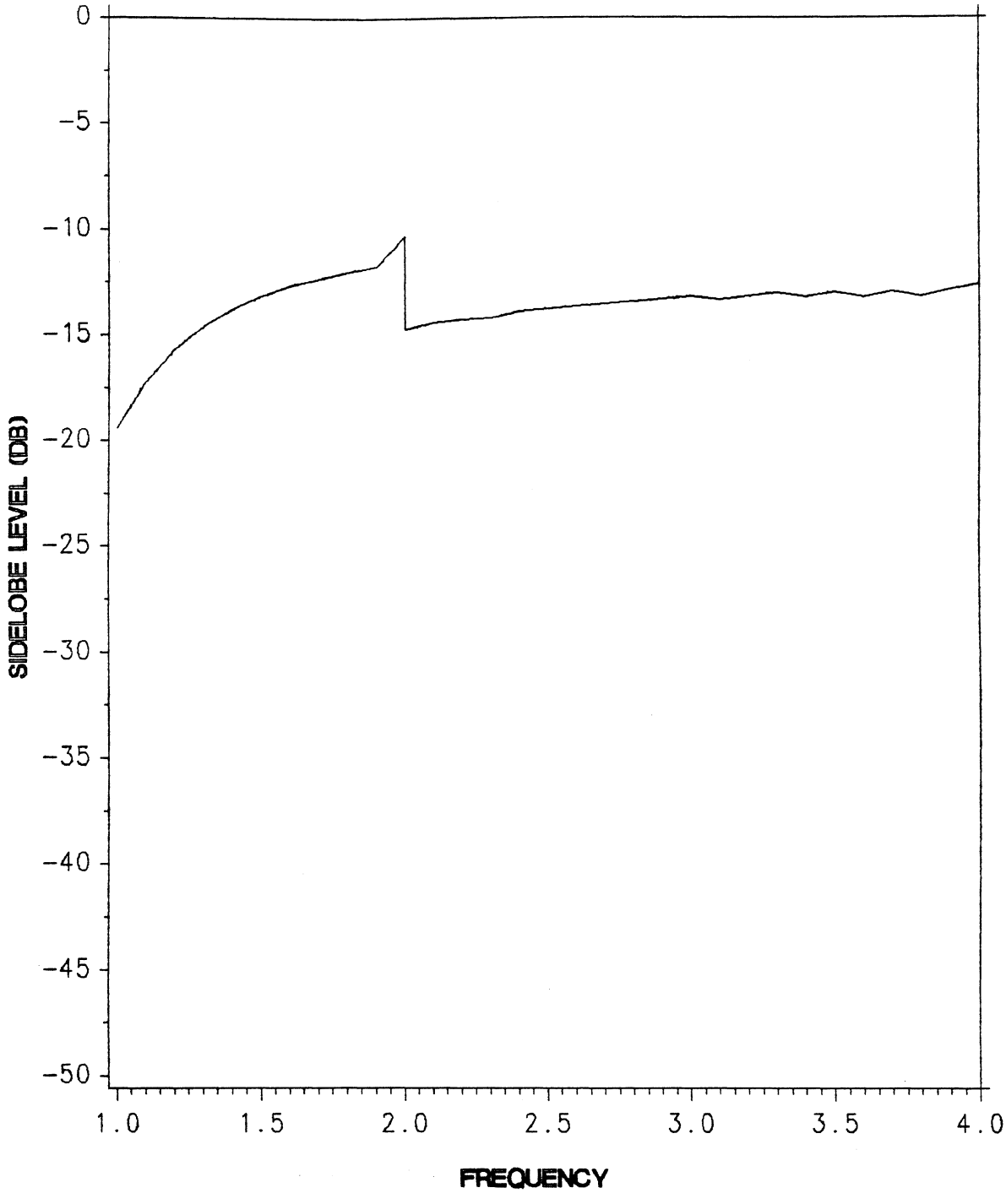

Figure 5.2-7. Calculated sidelobe level for the 3 and 5 element array of Fig. 5.2-1 with the small element removed and uniform amplitude and phase excitation. Ascissa is normalized to f_1.

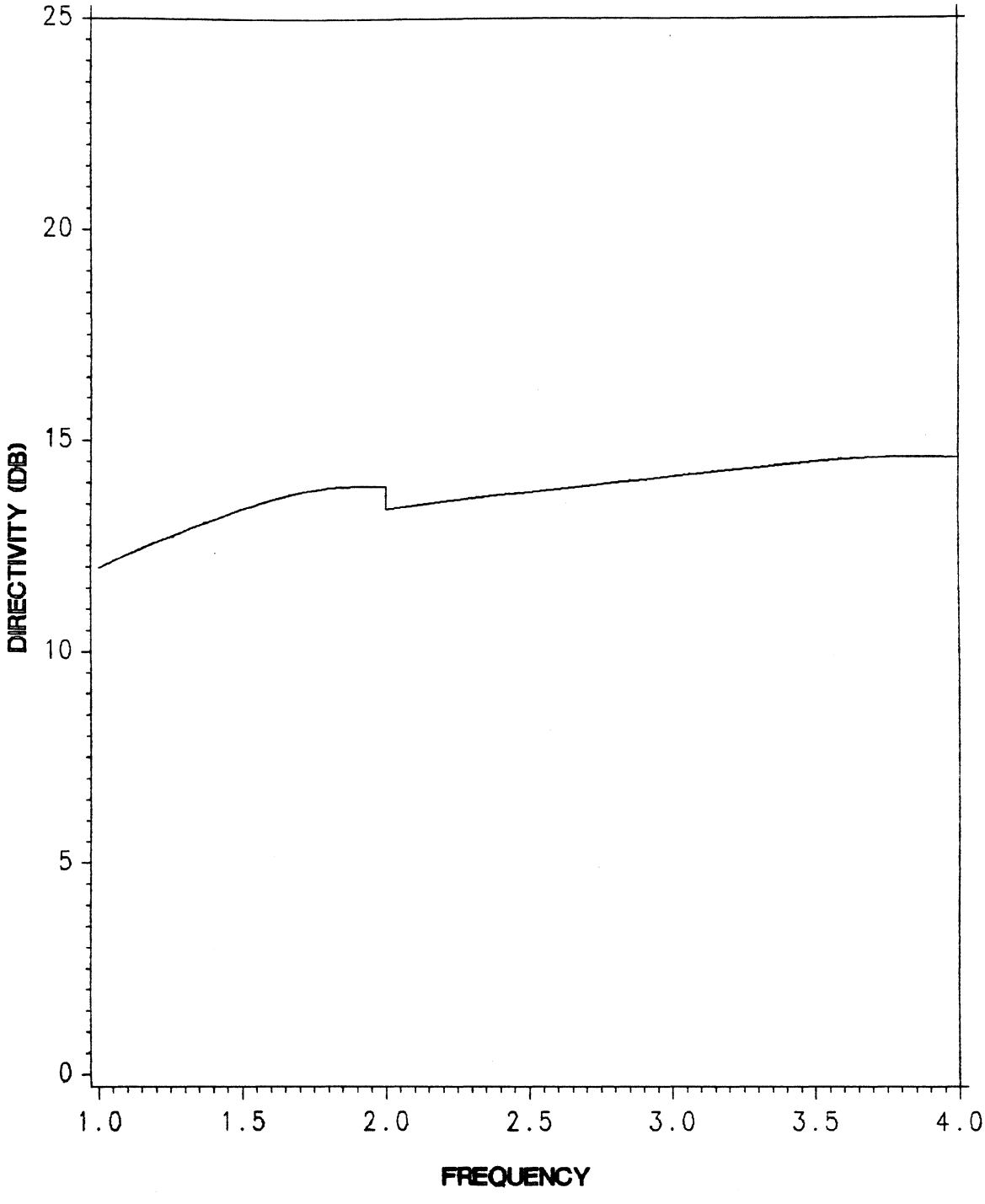

Figure 5.2-8. Calculated directivity for the 3 and 5 element array of Fig. 5.2-1 with the small element removed and uniform amplitude and phase excitation. Abscissa is normalized to f_1.

f_4, as shown in Fig. 5.2-7. The directivity of this array is plotted in Fig. 5.2-8 and is slightly lower than that of the previous array in the range f_2 to f_4. This is due to the changes in the array factor expression. Radiation patterns are similar to those shown in Figs. 5.2-4 through 5.2-6.

5.3 A Wideband Planar Array of Spirals

A natural extension of the linear array of the previous section would be a wideband planar array of spiral elements. In order to maintain similar patterns in the principal planes, the array should have similar element spacings in the $\phi = 0°$ and $\phi = 90°$ directions. Consider the planar array arrangement shown in Fig. 5.3-1 consisting of nine large elements and nine small elements. As in the linear array case, only the large elements radiate in the frequency range f_1 to f_2 and all elements radiate in the frequency range f_2 to f_4. Also as before, the element excitations are uniform, i.e. $A_n = 1$ and $\alpha_n = 0°$. The large elements are spaced a half wavelength apart at f_1 ; with the small elements centered between the large elements in both the x and y directions. Because rays are assumed to travel parallel to each other to the far field, the offset of the small elements in the y direction does not affect the the radiation pattern when $\phi = 0°$. Likewise the offset of the small elements in the x direction does not affect the radiation pattern when $\phi = 90°$. This is verified in the array factor expression (2.3-3) when, in the principal planes, the x_n or the y_n term equals zero because of the trigonometric factors. The planar array arrangement can then be considered to be a linear array projected onto the x axis when $\phi = 0°$ or the y axis when $\phi = 90°$ with an amplitude distribution determined by the number of elements that fall on top of one another. This effect was noted by

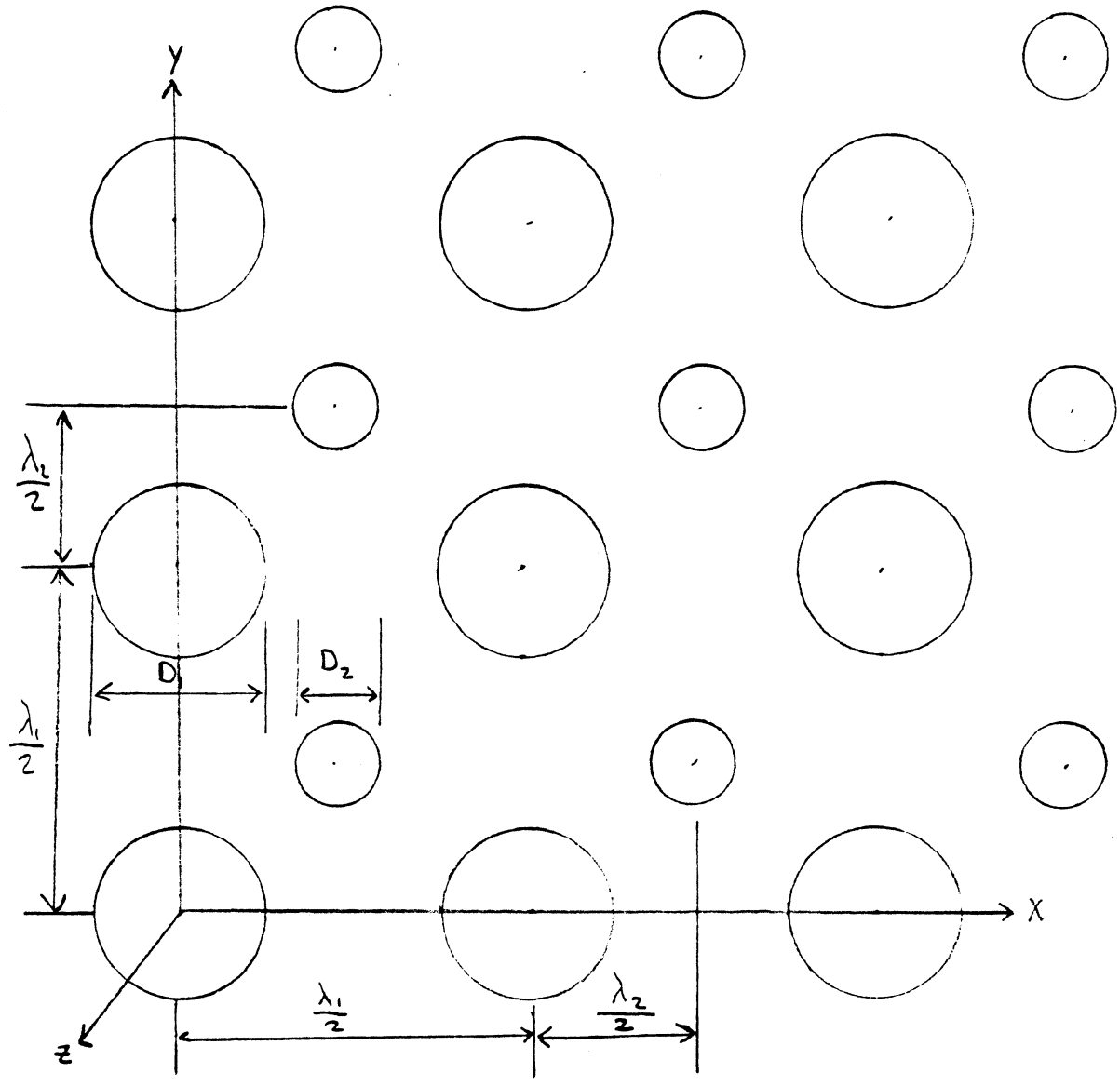

Figure 5.3-1. Wideband planar array designed for two octave bandwidth. The elements are circular spirals antennas with the element pattern (4.2-2).

Elliot in [18]. The planar array of Fig. 5.3-1 would thus have an amplitude distribution of 3:3:3:3:3:3 on the x or y axis when all of the elements are radiating. The $\phi = 45°$ axis would have an amplitude distribution of 1:3:5:5:3:1 when all elements are radiating. This array arrangement has principal plane radiation patterns that are exactly the same as those shown in Figs. 5.2-4 through 5.2-6 for the linear array described in Sec. 5.2. Thus, the sidelobe levels are the same as before and are given by Fig. 5.2-2. Sidelobe levels for the $\phi = 45°$ plane are slightly higher and the values are given in Fig. 5.3-2. The directivity for this array is plotted in Fig. 5.3-3 as a function of frequency.

As was the case for the linear array described in Sec. 5.2, the small elements that are not centered between any large elements can be omitted from the array altogether without drastically changing the radiation properties of the array. This was found to be the case for the above planar array leading to the array arrangement shown in Fig. 5.3-4. As above there are nine large elements but now there are only four small elements centered between the large elements. Element spacings, amplitudes, and phases remain the same as in the above cases. When projected onto the x or y axis, the amplitude distribution becomes 3:2:3:2:3 when all of the elements are radiating. The amplitude distribution for the $\phi = 45°$ axis becomes 1:3:5:3:1 when all elements are radiating. As expected, this simpler array arrangement did not have a severe effect on the radiation properties described above for the 9-18 element array. The sidelobe levels for the principal planes are shown in Figure 5.3-5 and as before remain below -10 dB across the two octave frequency band. The sidelobe levels in the $\phi = 45°$ plane do not differ greatly from the previous case and are shown in Figure 5.3-6. The directivity, shown in Fig. 5.3-7 as a function of frequency, is slightly lower than that of the previous array between f_2 and f_4 as expected because of the smaller number of elements. However, the discontinuity at f_2 is smaller and the variation in directivity above f_2 is less than in the previous case.

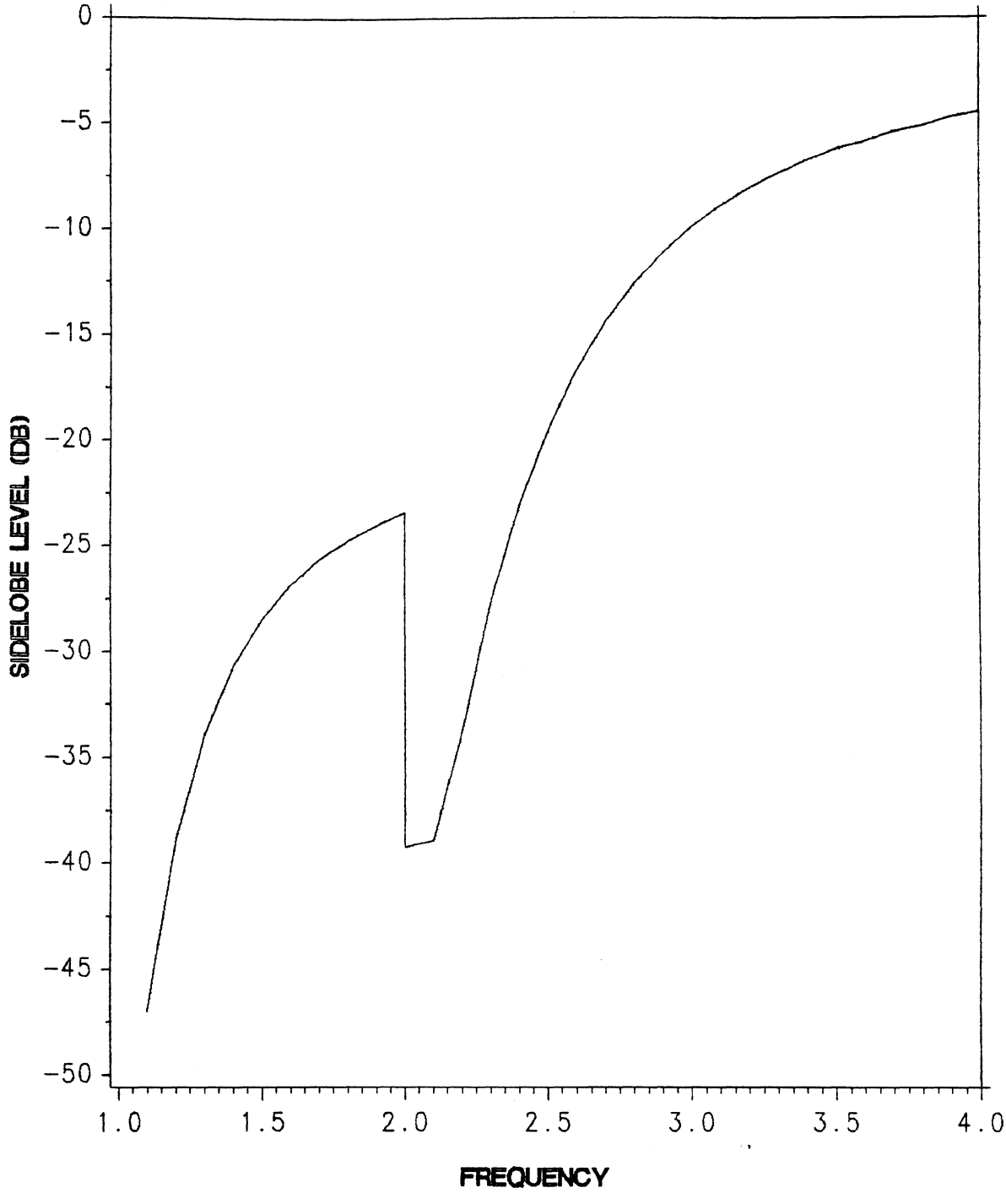

Figure 5.3-2. Calculated $\phi = 45°$ plane sidelobe levels for the array in Fig. 5.3-1 with uniform amplitude and phase excitation. Abscissa is normalized to f_1. The nine large elements are active up to $2f_1$. Above $2f_1$ all elements are active.

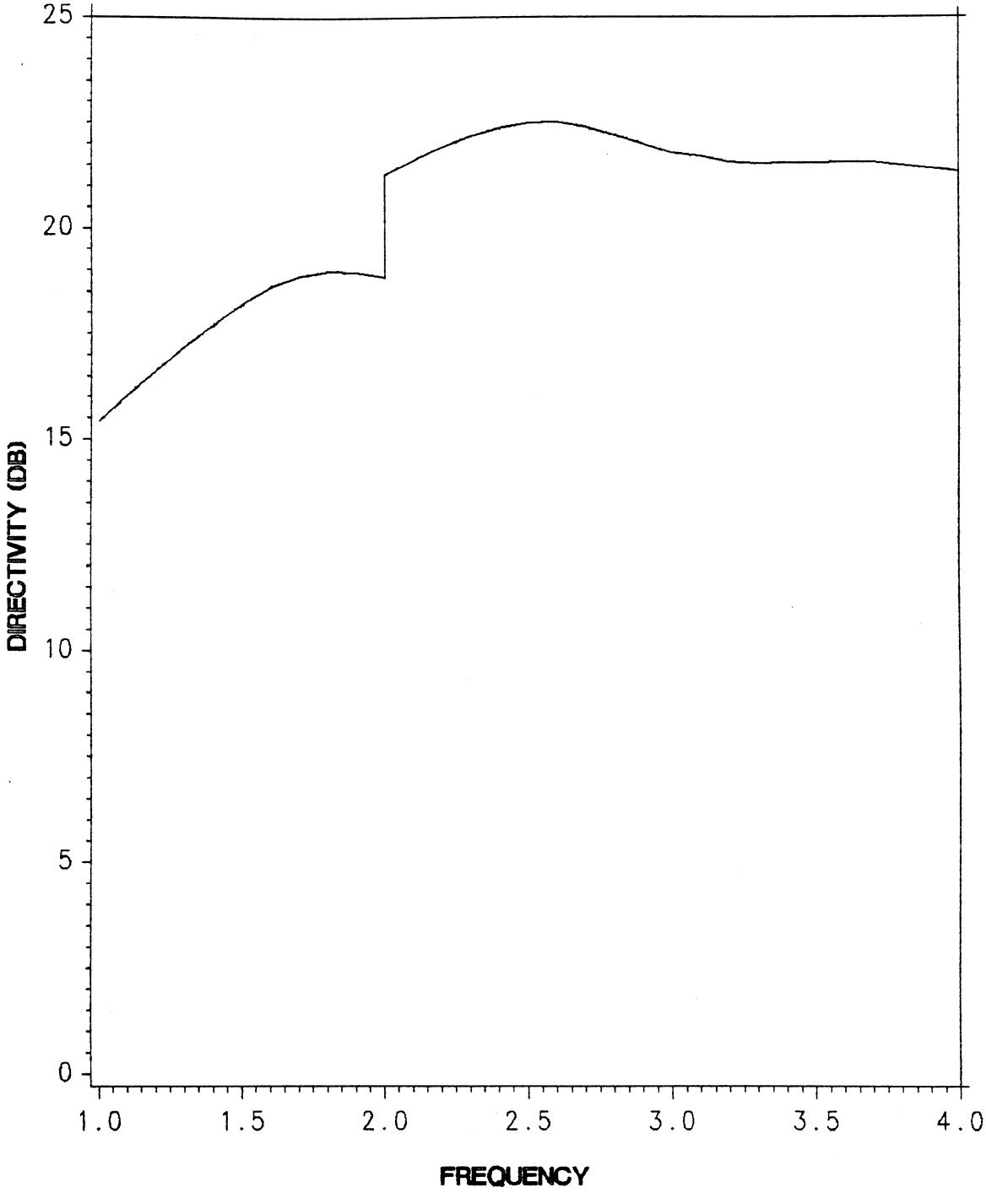

Figure 5.3-3. Calculated directivity for the array of Fig. 5.3-1 with uniform amplitude and phase excitation. Abscissa is normalized to f_1 . The nine large elements are active up to $2f_1$. Above $2f_2$ all elements are active.

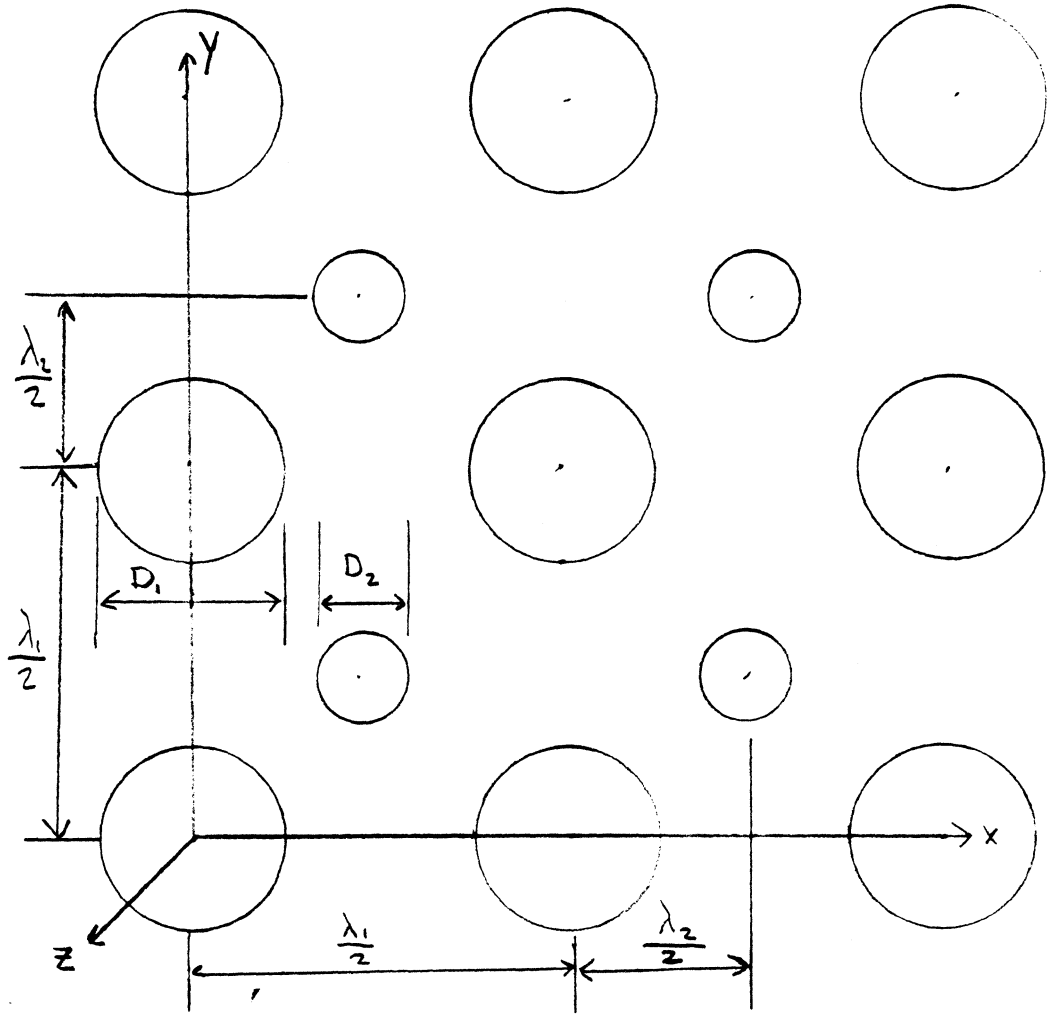

Figure 5.3-4. Wideband array designed for two octave bandwidth with 13 elements and element pattern (4.2-2).

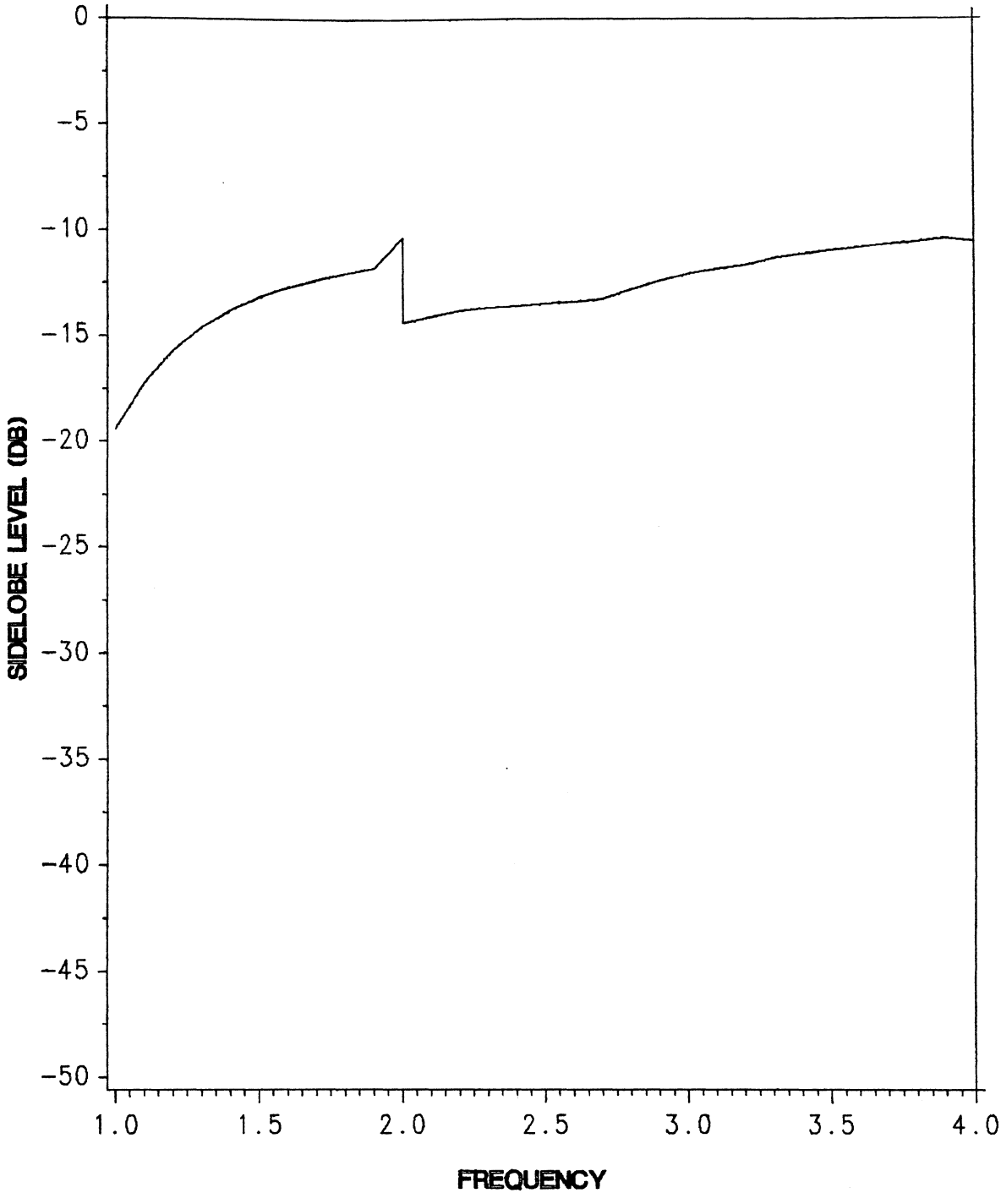

Figure 5.3-5. Calculated principal plane sidelobe level for the array of Fig. 5.3-4 with uniform amplitude and phase excitation. Abscissa is normalized to f_1. The nine large elements are active up to $2f_1$. Above $2f_1$ all elements are active.

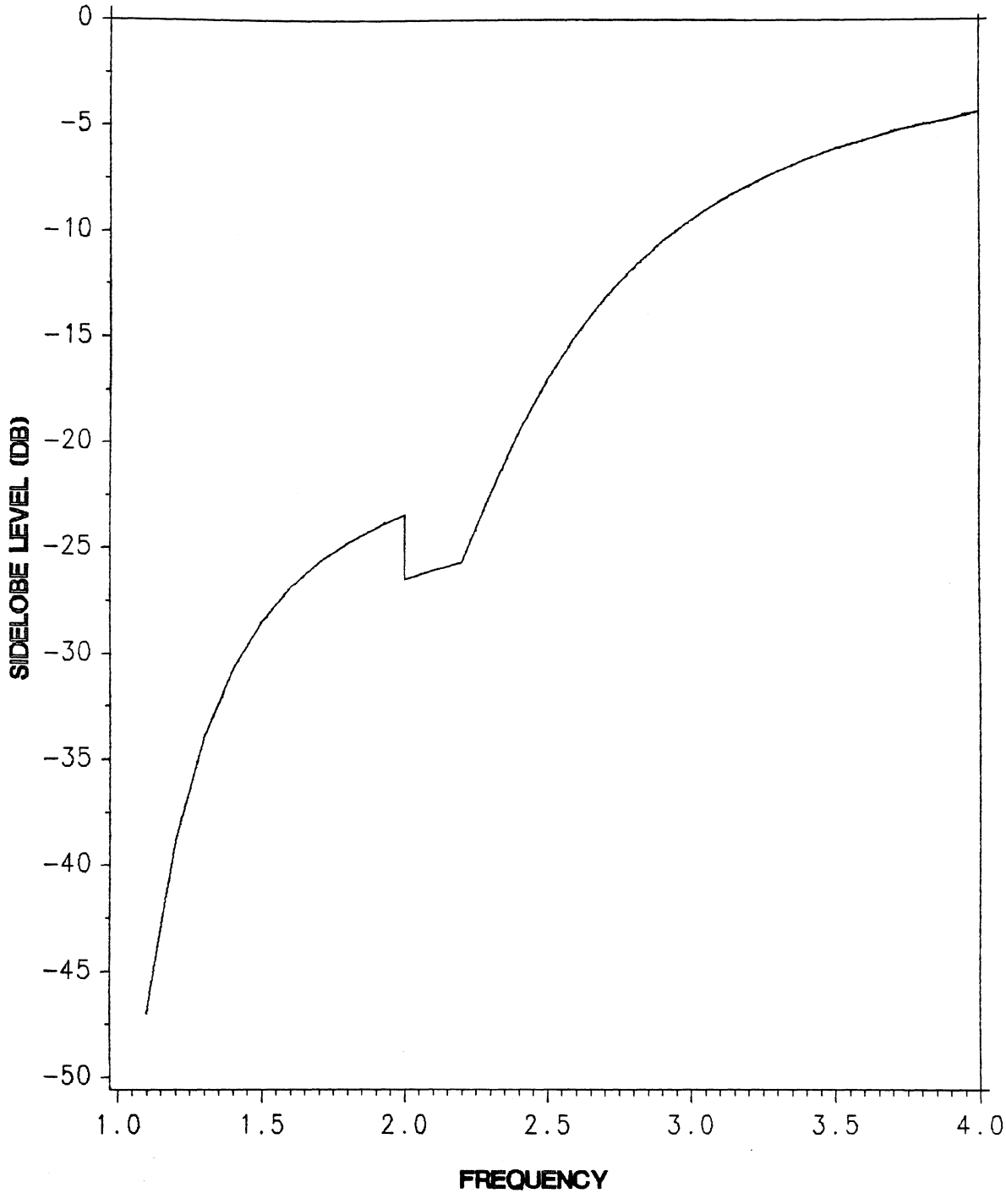

Figure 5.3-6. Calculated $\phi = 45°$ plane sidelobe levels for the array of Fig. 5.3-4 with uniform amplitude and phase excitation. Abscissa is normalized to f_1. The nine large elements are active up to $2f_1$. Above $2f_1$ all elements are active.

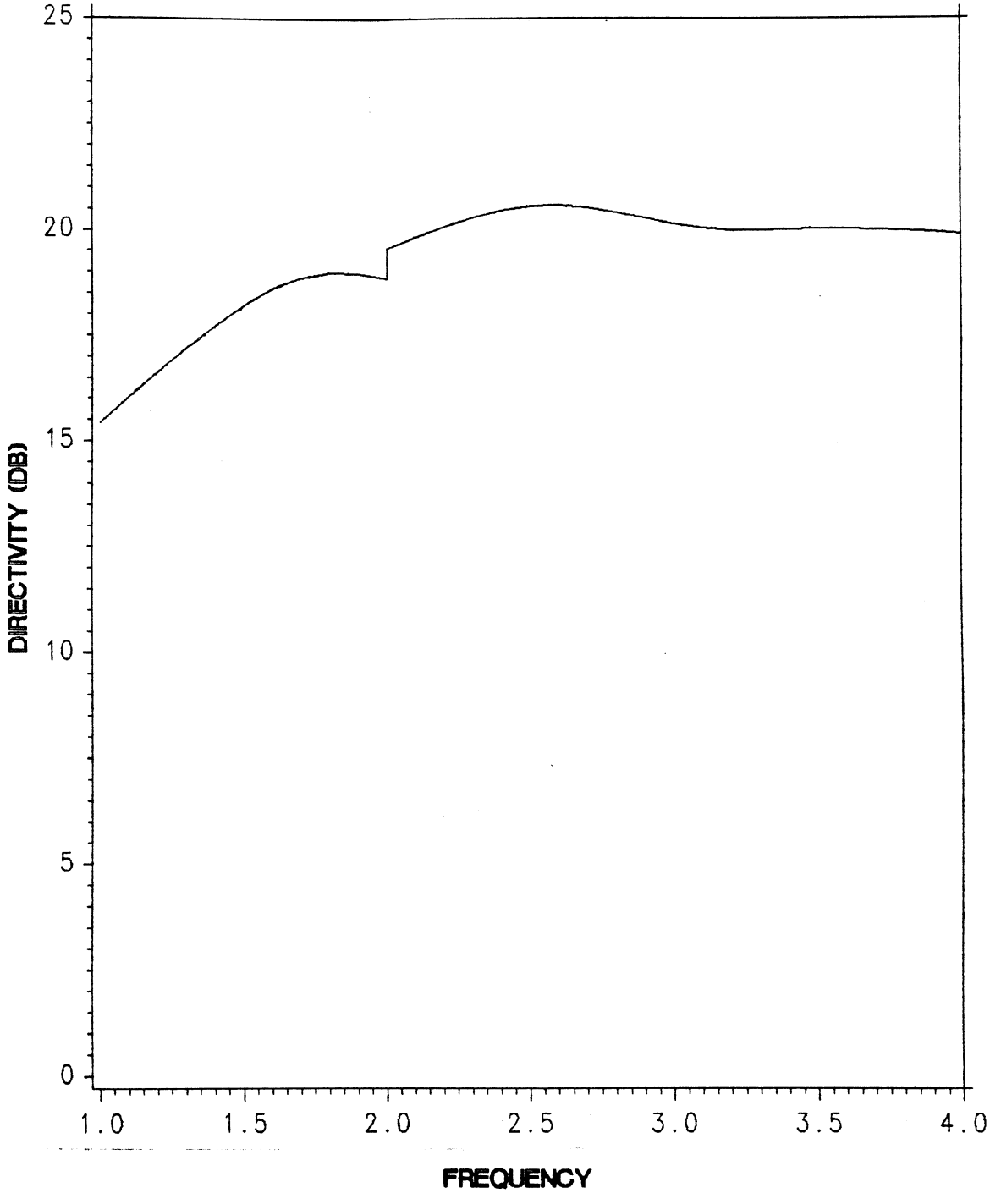

Figure 5.3-7. Calculated directivity for the array of Fig. 5.3-4 with uniform amplitude and phase excitation. Abscissa is normalized to f_1 . The nine large elements are active up to $2f_1$. Above f_1 all elements are active.

5.4 Geometrical Constraints for Wideband Arrays of Circular Spirals

The size of the elements in the array will be determined by the geometrical constraints encountered when packing the elements as close as possible. Consider the array geometry shown in Fig. 5.4-1, which is a portion of the array in Fig. 5.3-5. The diameter of the large elements, D_1, is twice that of the small elements, D_2. The large elements are spaced a distance $S_x = S_y = S$ apart with the small element spaced a distance S_D from any large element. It is assumed that the elements are not allowed to overlay one another. As the array size is reduced, overlap will occur first either along a diagonal or along a principal axis. This leads to the two following constraints:

$$\frac{D_1 + D_2}{2} < S_D = \frac{S}{\sqrt{2}} \tag{5.4-1}$$

$$D_1 < S \tag{5.4-2}$$

By replacing D_2 in (5.4-1) with $\frac{1}{2} D_1$, the following inequality results:

$$\frac{3}{2\sqrt{2}} D_1 = 1.06 D_1 < S \tag{5.4-3}$$

which is more restrictive than (5.4-2).

If $S = \frac{\lambda_1}{2}$, then the maximum diameter of the large spirals is given by

$$\frac{\lambda_1}{2} = 1.06 D_{1max}$$

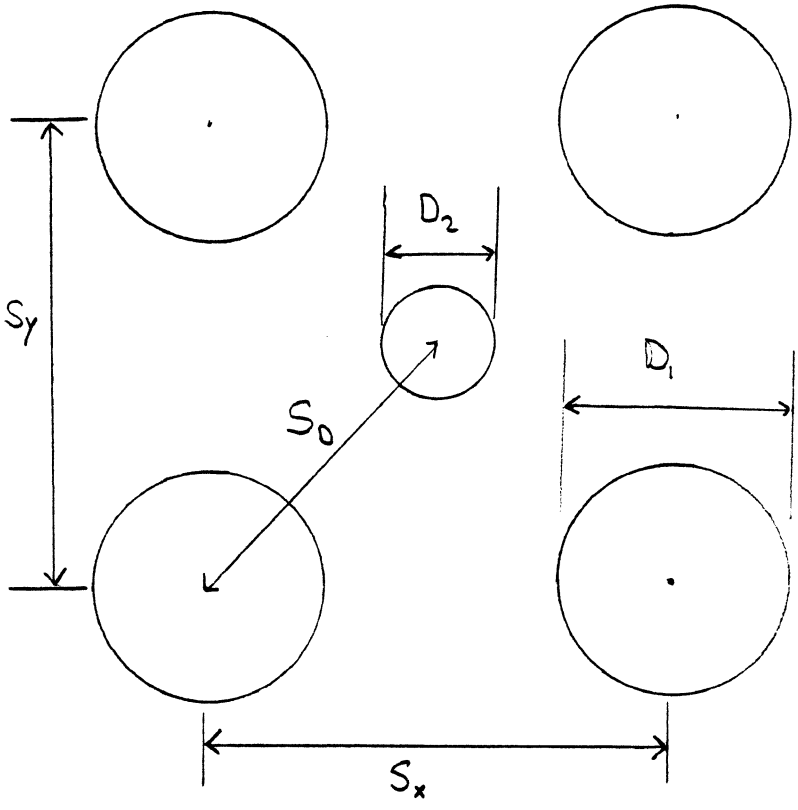

Figure 5.4-1. A portion of the array of Fig. 5.3-5; the elements are circular spirals.

or

$$D_{1max} = 0.472\lambda_1. \tag{5.4-4}$$

The perimeter of the large spiral is then determined by

$$P_1 = \pi D_1 = 1.48\lambda_1. \tag{5.4-5}$$

Because spirals will radiate as long as the perimeter exceeds one wavelength, the large spirals will actually radiate below f_1 to a frequency $\frac{f_1}{1.48} = 0.674 f_1$, thus increasing the operating bandwidth of the array.

5.5 Geometrical Constraints for Wideband Arrays of Square Spirals

Square spirals offer a lower cutoff frequency than circular spirals. This is because the perimeter of a square spiral is $4W_1$ rather than πD_1 for the circular spiral; cutoff occures when the perimeter is one wavelength; thus $W_1 = \frac{\lambda_1}{4} < D_1 = \frac{\lambda_1}{\pi}$. The geometry that yields the minimum spacing for square spirals is shown in Fig. 5.5-1. Other geometries for square spirals would yield smaller spacings, however this would involve rotating some elements differently than others causing phase differences among the elements. As before $S_x = S_y = S$ and the width of the large elements, W_1 , is twice that of the smaller elements, W_2. As before there are two constraints on the spacing of the elements

$$\frac{\sqrt{2}}{2} W_1 + \frac{\sqrt{2}}{2} W_2 < S \tag{5.5-1}$$

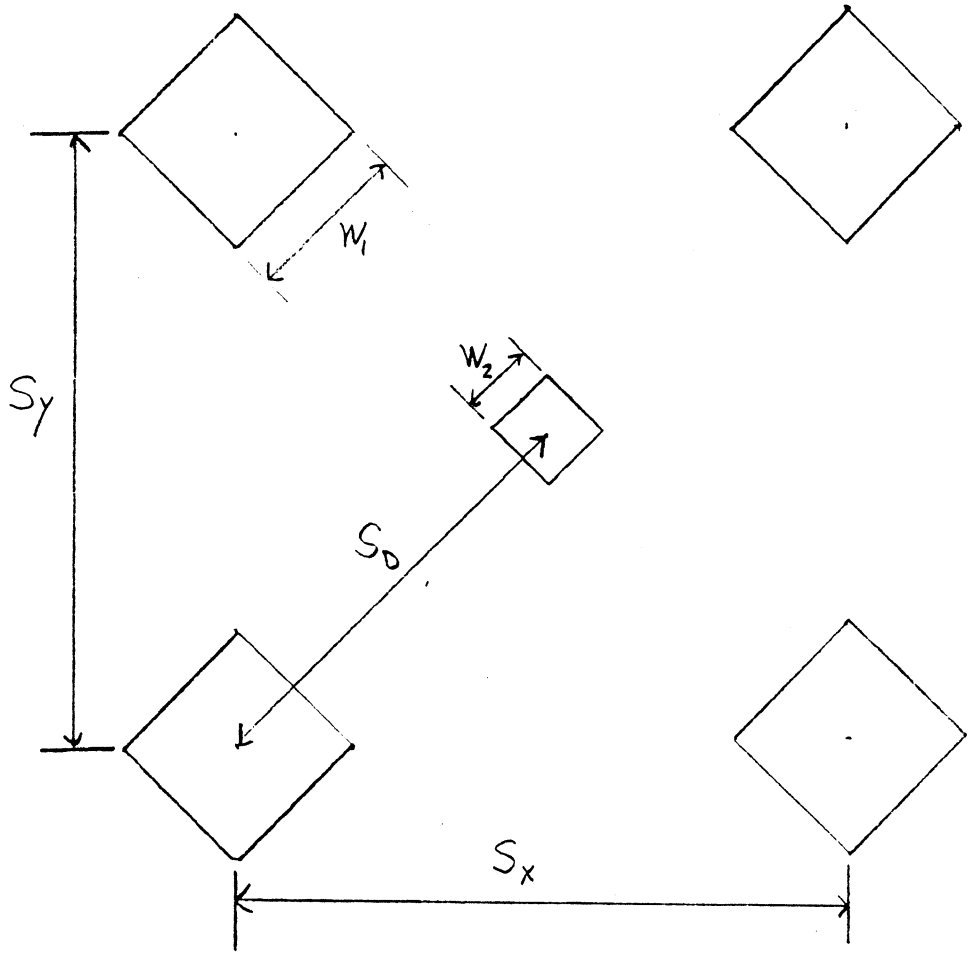

Figure 5.5-1. A portion of the array of Fig. 5.3-5; the elements are square spirals.

$$\sqrt{2}\, W_1 < S. \tag{5.5-2}$$

By replacing W_2 in (5.5-1) with $\frac{1}{2} W_1$ the following inequality results

$$\frac{3}{2\sqrt{2}} W_1 = 1.06 W_1 < S. \tag{5.5-3}$$

For the case of square spirals (5.5-2) is the more restrictive of the two geometrical constraints. If $S = \frac{\lambda_1}{2}$ then the maximum width, $W_{1\,max}$, is given by

$$\frac{\lambda_1}{2} = 1.414 W_{1max}$$

or

$$W_{1max} = 0.354 \lambda_1 \tag{5.5-4}$$

The perimeter of the large spiral is then determined by

$$P_1 = 4W_1 = 1.414 \lambda_1. \tag{5.5-5}$$

As before the spirals will radiate as long as the perimeter is equal to one wavelength. For square spirals the lowest frequency of operation is then $\frac{f_1}{1.41} = 0.707 f_1$. This is close to the value derived for circular spirals but circular spirals will provide a slight increase in bandwidth if the array is allowed to operate below f_1.

5.6 An Improved Wideband Array

Consider the array shown in Fig. 5.6-1 composed of four large elements and four small elements. As before only the large elements radiate in the frequency range f_1 to f_2 and all eight elements radiate in the frequency range f_2 to f_4 This array maintains radiative properties similar to those of the arrays desribed in Sec. 5.3 and is composed of only eight elements. In this case, when the array is projected onto a principal axis the amplitude distribution is 1:2:2:2:1 when all of the elements are active. This array configuration thus exhibits an amplitude taper on the outer array elements which has been noted to produce low sidelobes [1]. When only the large elements are radiating the amplitude distribution is 1:2:1 which again exhibits an amplitude taper. On the diagonal axis the amplitude distribution becomes 3:2:3 when all elements are active. Sidelobe levels in the diagonal plane would naturally be higher than those in the principal planes. Sidelobe levels were calculated as before and remain below -9.7 dB across the frequency band and are the same in both principal planes. This is shown in Fig. 5.6-2. The sidelobes in the diagonal plane are slightly higher and are shown in Fig. 5.6-3. The inclusion of an array element in the center of the array did not significantly change the array performance and actually made sidelobes rise at the higher frequencies. Radiation patterns were calculated as before and are shown in Figs. 5.6-4 through 5.6-6 for frequencies f_1, f_2, and f_4, respectively. As before, note the pattern improvement in Fig. 5.6-5 when the small elements are activated. The directivity of this array is plotted in Fig. 5.6-7 and is slightly lower than that of the array of Sec. 5.3.

When circular spirals are used as elements the packing constraints are exactly the same as those derived for the previous array geometry in Sec. 5.4, i.e. Eq. (5.4-5) holds. If squares are used as elements then the minimum spacing is given by (5.5-3) instead of

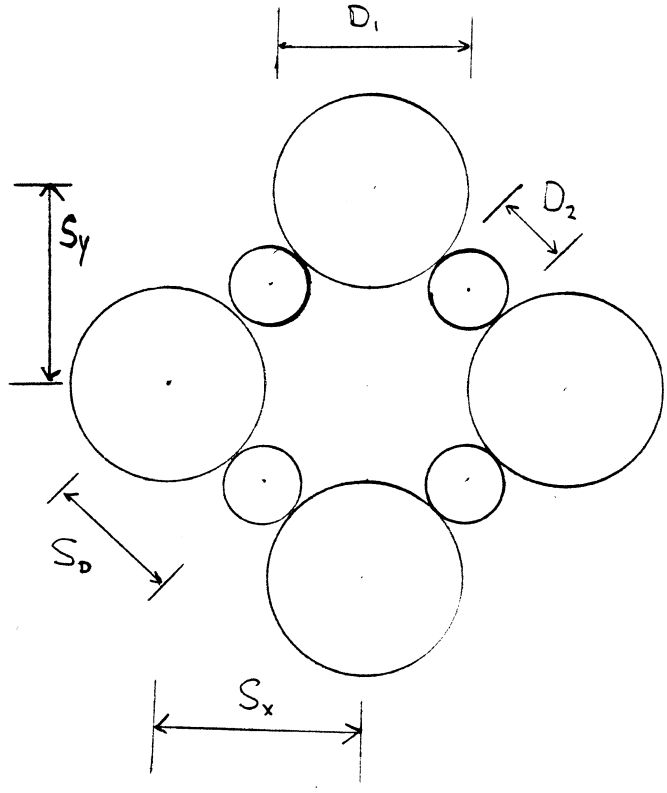

Figure 5.6-1. Wideband planar array designed for two octave bandwidth with element pattern (4.2-2).

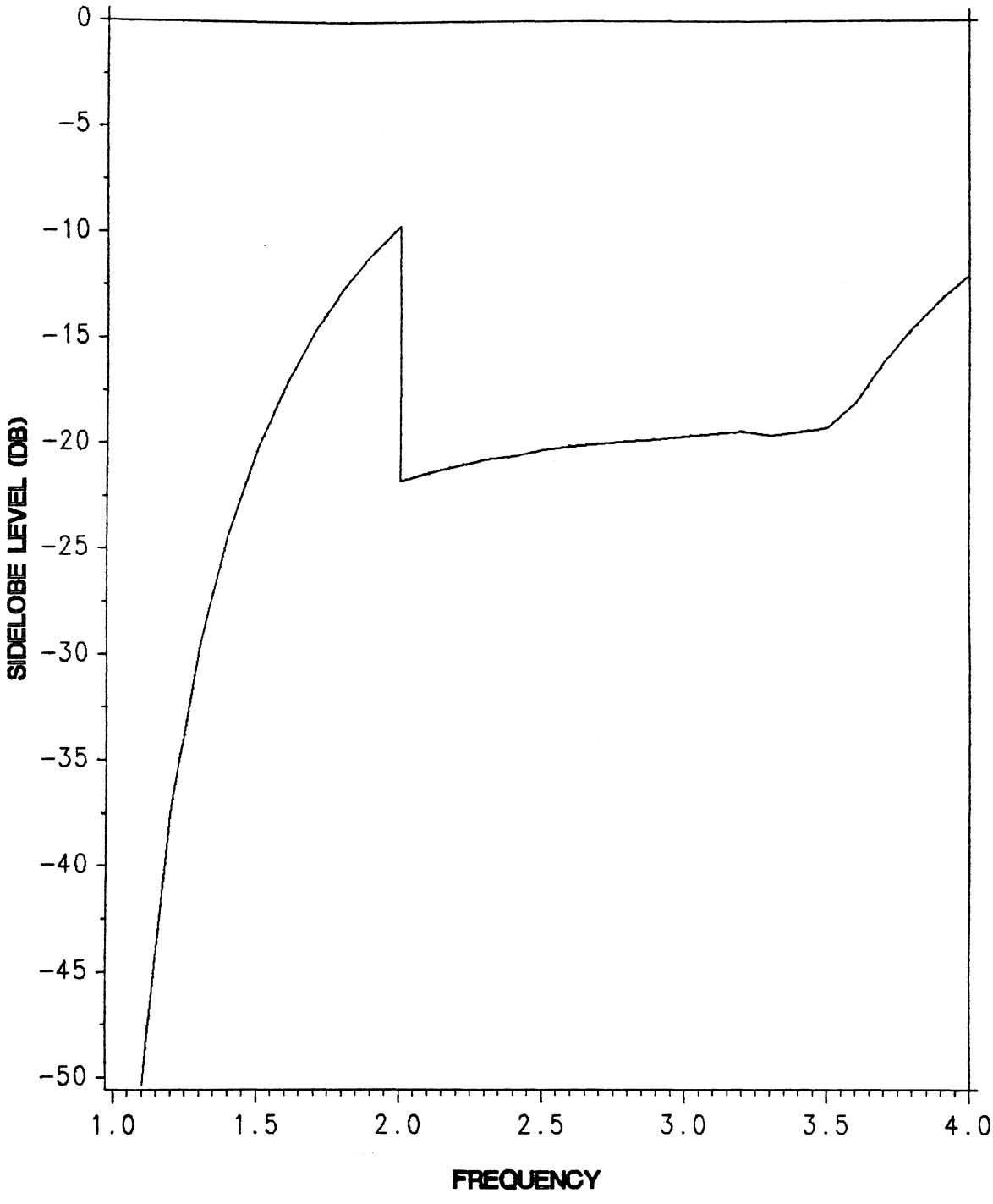

Figure 5.6-2. Calculated principal plane sidelobe level for the array of Fig. 5.6-1 with uniform amplitude and phase excitation. Abscissa is normalized to f_1. The four large elements are active up to $2f_1$. Above $2f_1$ all elements are active.

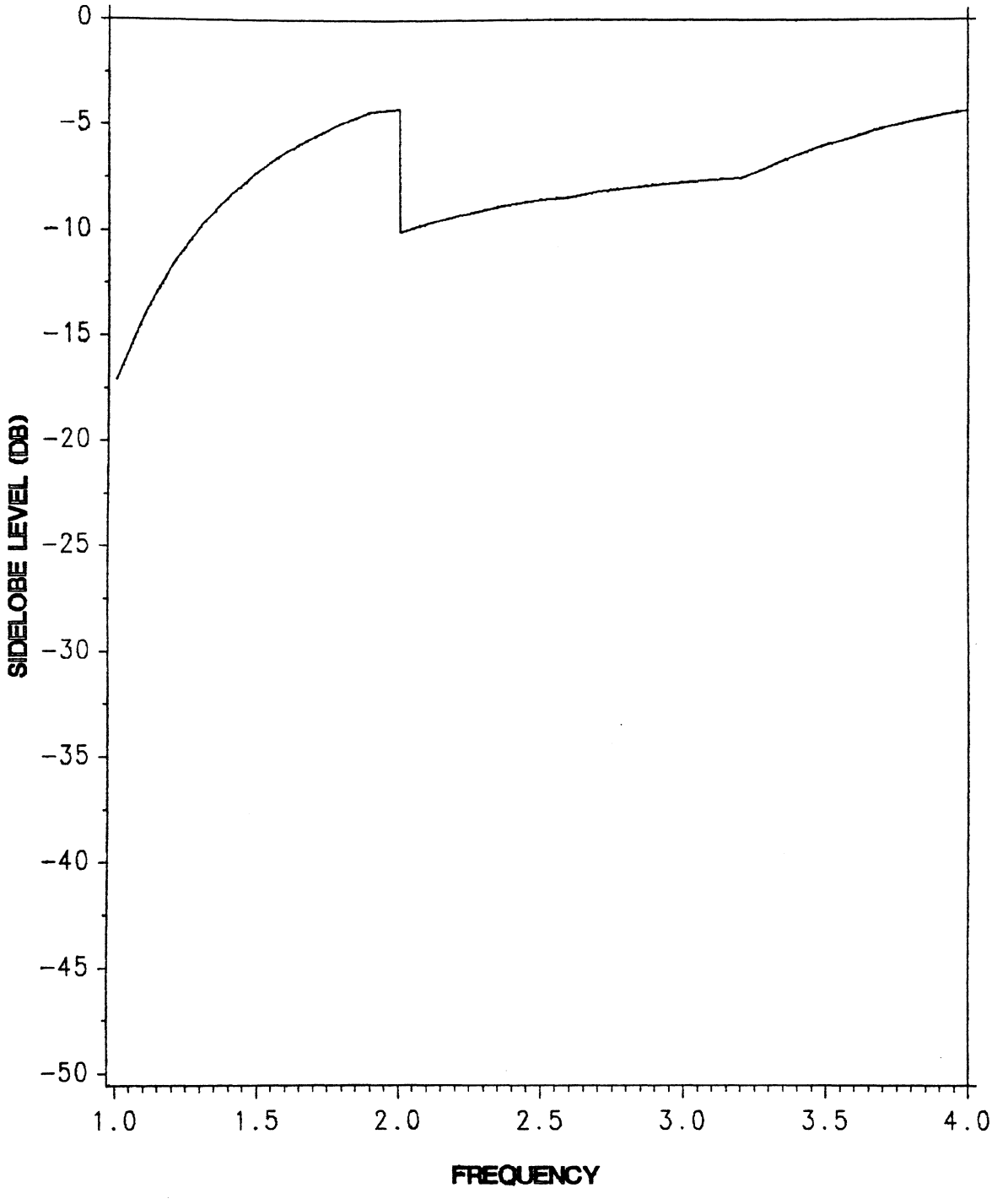

Figure 5.6-3. Calculated diagonal plane sidelobe level for the array of Fig. 5.6-1 with uniform amplitude and phase excitation. Abscissa is normalized to f_1. The four large elements are active up to $2f_1$. Above $2f_2$ all elements are active.

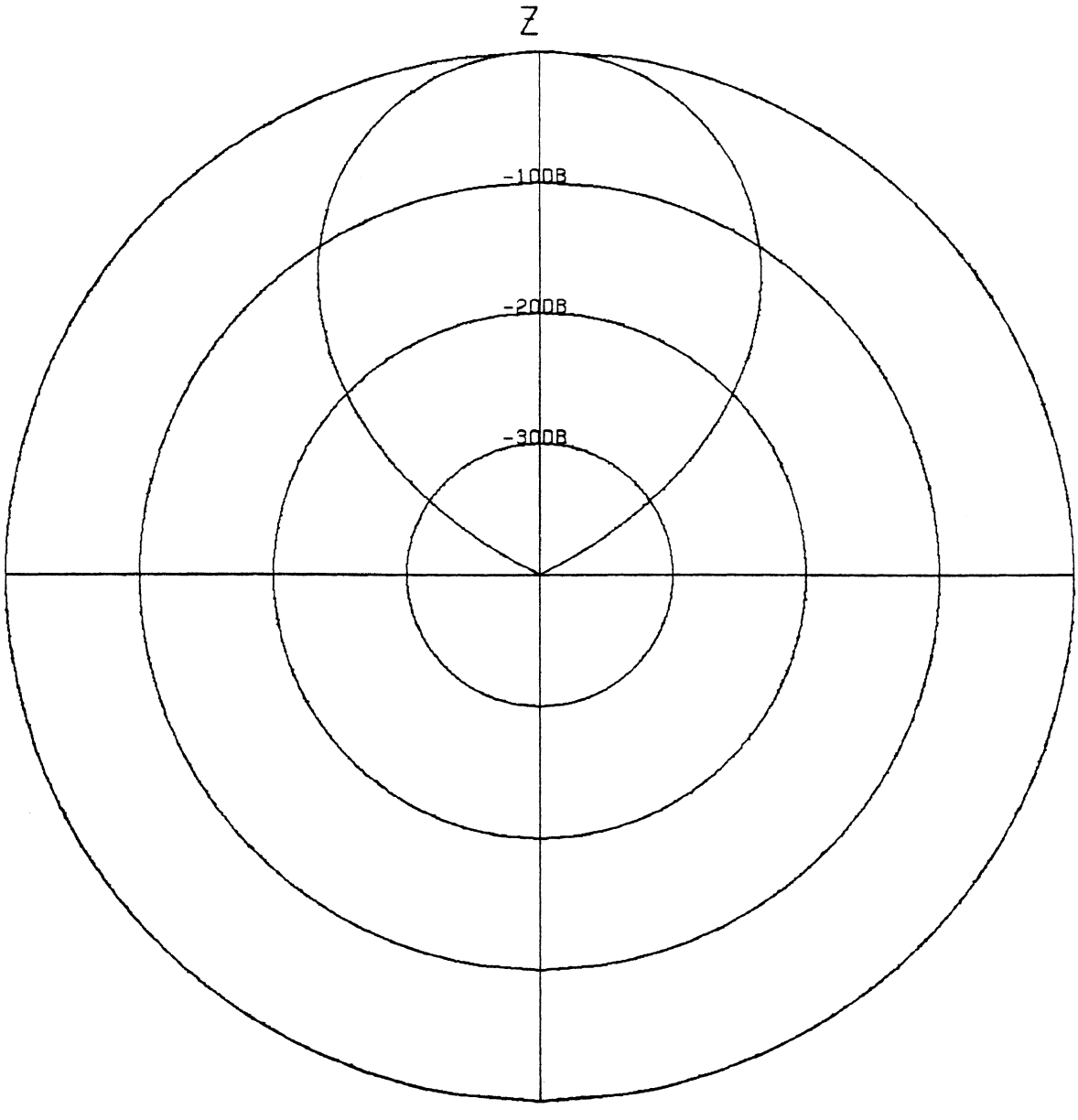

Figure 5.6-4. Calculated principal plane radiation pattern for the array of Fig. 5.6-1 with the four large elements radiating at frequency f_1 and uniform amplitude and phase excitation.

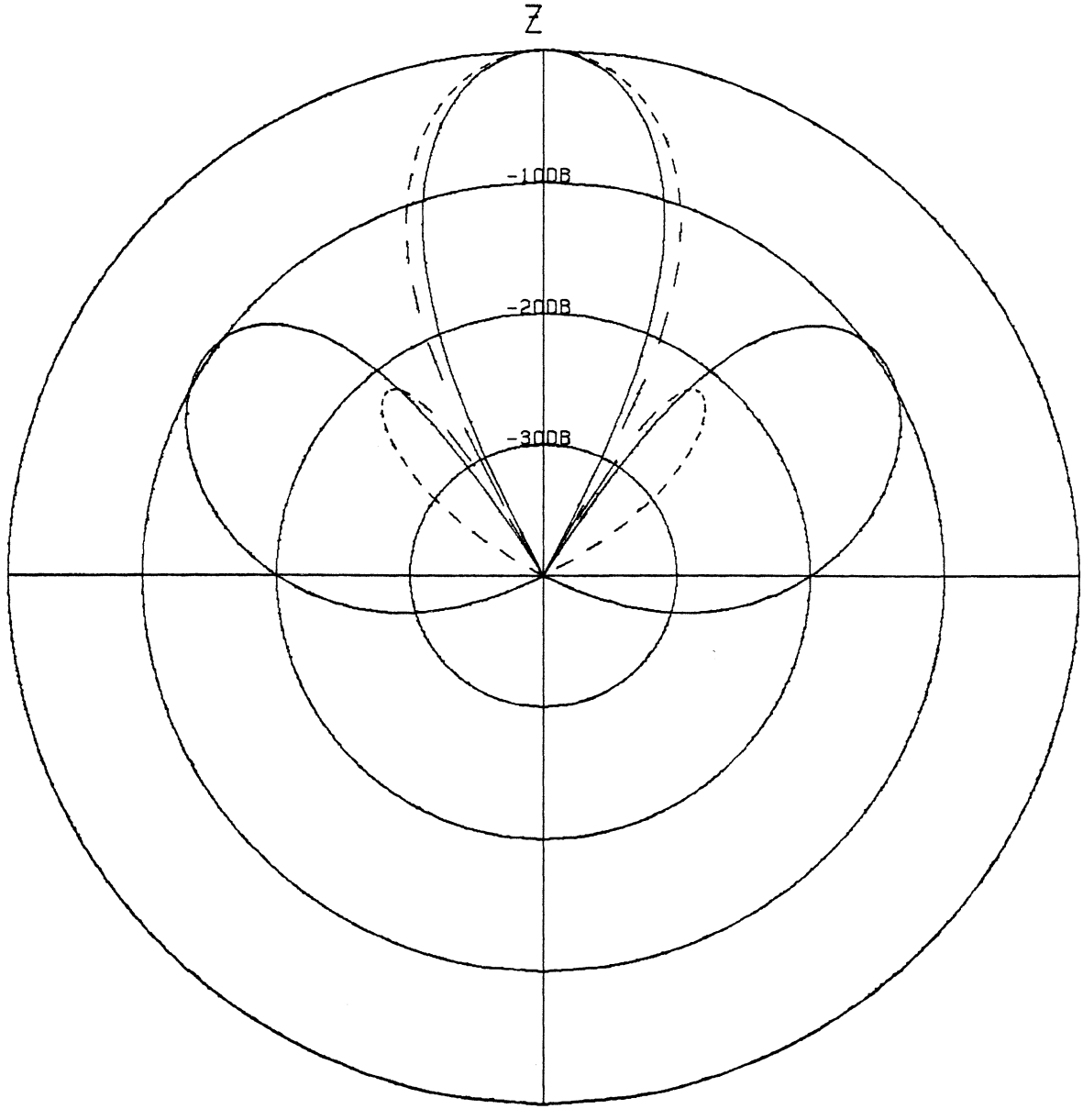

Figure 5.6-5. Calculated principal plane radiation patterns for the array of Fig. 5.6-1 at frequency f_2 with uniform amplitude and phase excitation (4 large elements active-solid, all 8 elements active-dashed).

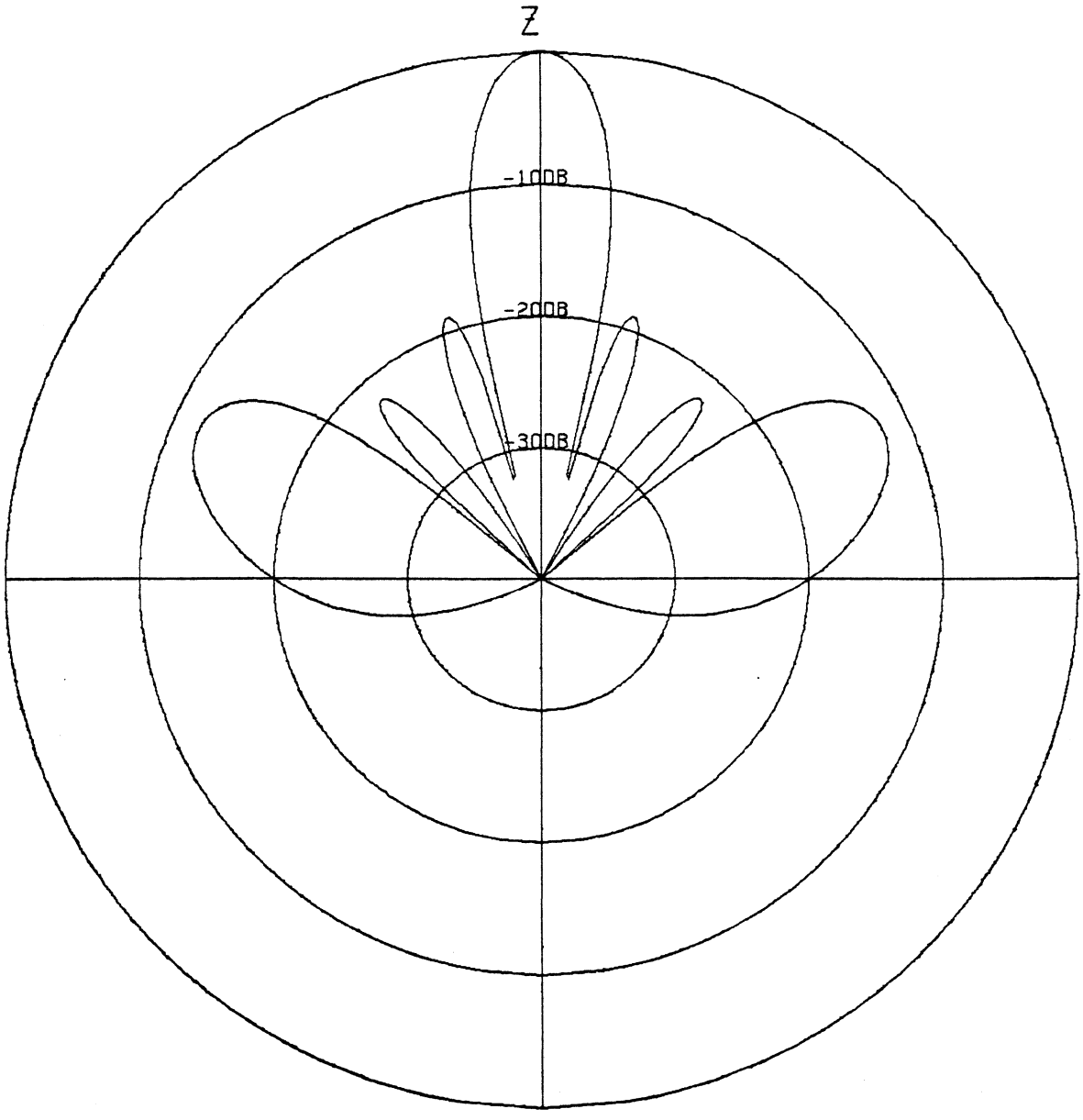

Figure 5.6-6. Calculated principal plane radiation pattern for the array of Fig. 5.6-1 with all 8 elements radiating at frequency f_4 and uniform amplitude and phase excitation.

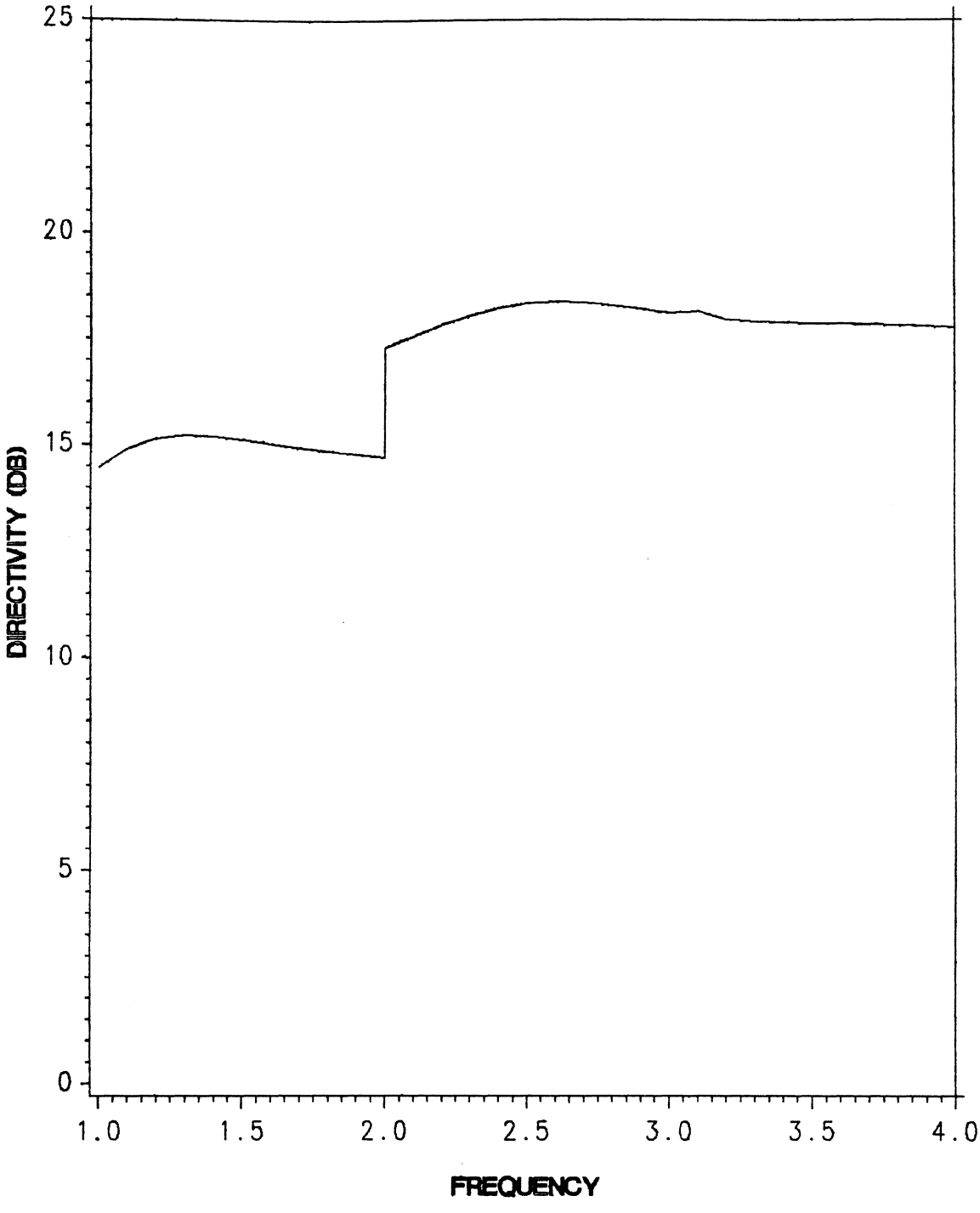

Figure 5.6-7. Calculated directivity for the array of Fig. 5.6-1 with uniform amplitude and phase excitation. Abscissa is normalized to f_1. The four large elements are active up to $2f_1$. Above $2f_1$ all elements are active.

(5.5-2) because of the missing element in the center of the array. The maximum width $W_{1\,max}$ is then given by

$$W_{1max} = .472\lambda_1 \tag{5.6-1}$$

instead of (5.5-4). The perimeter for the large square spiral is then given by

$$P_1 = 4W_1 = 1.89\lambda_1. \tag{5.6-2}$$

Thus, the array will operate below f_1 to a frequency equal to $\frac{f_1}{1.89} = 0.529f_1$

VI. Construction and Testing of a Wideband Array

6.1 Element Construction

An array having the geometry considered in Sec. 5.6 was constructed. The two octave frequency range was chosen to be 2.5 GHz through 10.0 GHz. Circular Archimedean spirals were chosen as the elements for the array instead of square spirals because the performance of circular spirals is well documented. Further discussion concerning moment method modeling of spirals may be found in [12].

With $f_1 = 2.5$ GHz ($\lambda_1 = 12.0$ cm) the diameter of the large spirals is found from Eq. (5.4-4) to be $D_{1\,max} = 5.66$ cm. The diameter of the small spirals is then $\frac{D_1}{2} = 2.83$ cm. Each large spiral was made with 8 turns per spiral arm with an arm width of 0.03 inch. The small spirals each had 4 turns per spiral arm with the same arm width as the large spirals. Both sets of spirals were made to be righthand circularly polarized. The spirals were constructed in the Virginia Tech Hybrid Microelectronics Laboratory using copper etching techniques. Each spiral is mounted on teflon with a relative dielectric constant of 2.1.

Each array element was backed with a cavity made of aluminum foil and filled with microwave absorber to prevent radiation from travelling in the -z direction behind the structure.. This also serves to enhance wideband operation. Each spiral was fed by a coax cable and a wideband balun for balanced excitation. The baluns were constructed from semirigid 50 ohm coaxial cable and were made by gradually stripping away the outside conductor of the coax until the outside conductor was the same diameter as the inside conductor. Each balun is approximately 2.25 inches in length. Such a balun works over a wide range of frequencies and also provides a gradual transition of characteristic impedance. Archimedian spirals have a theoretical impedance of $189+j0$ Ohms. A more detailed discussion concerning element and balun modelling may be found in [12]. The element details are given in Table 6.1-1.

6.2 Element Testing

Element radiation patterns were measured on the Virginia Tech far field antenna range; the results of the element testing are discussed in this section. The elements were operated as the receiving antenna and were rotated 360° while the power level was recorded. The transmit antennas used were linearly polarized standard gain horns. For more information on the antenna range refer to [19].

Figures 6.2-1 to 6.2-3 show the measured patterns for a large spiral at frequencies $f_1 = 2.5$ GHz, $f_2 = 5.0$ GHz and $f_4 = 10.0$ GHz. The latter two figures show the best agreement to the modeled pattern. The pattern measured at 2.5 GHz is wider than expected at $+-90°$. Figures 6.2-4 and 6.2-5 show pattern measurements for a small spiral at frequencies $f_2 = 5.0$ GHz and $f_4 = 10.0$ GHz. These patterns show close agreement to

Table 6.1-1
Spiral Element Antenna Characteristics

	Large Spiral	Small Spiral
Number of Arms	2	2
Number of turns per arm	8	4
Diameter of arm extent	5.66 cm 2.23 in	2.83 cm 1.11 in
Frequency at which perimeter equals one wavelength	1.7 GHz	3.4 GHz
Balun length	2.25 in	2.25 in
Cavity diameter	2.25 in	1.14 in
Cavity depth	0.75 in	0.75 in
Cavity filler	absorber	absorber

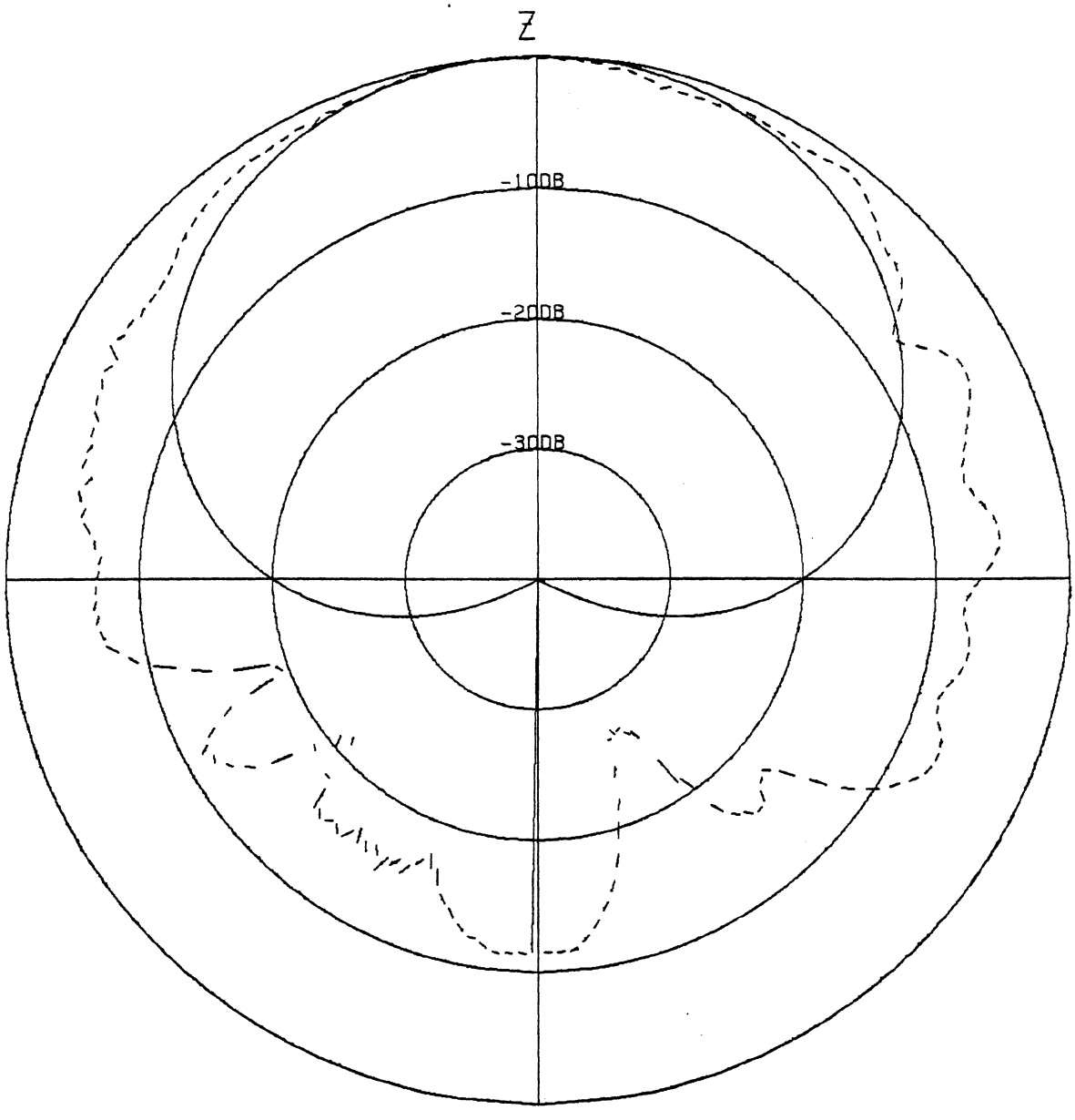

Figure 6.2-1. Radiation pattern of the large spiral at 2.5 GHz (measured-dashed, calculated-solid).

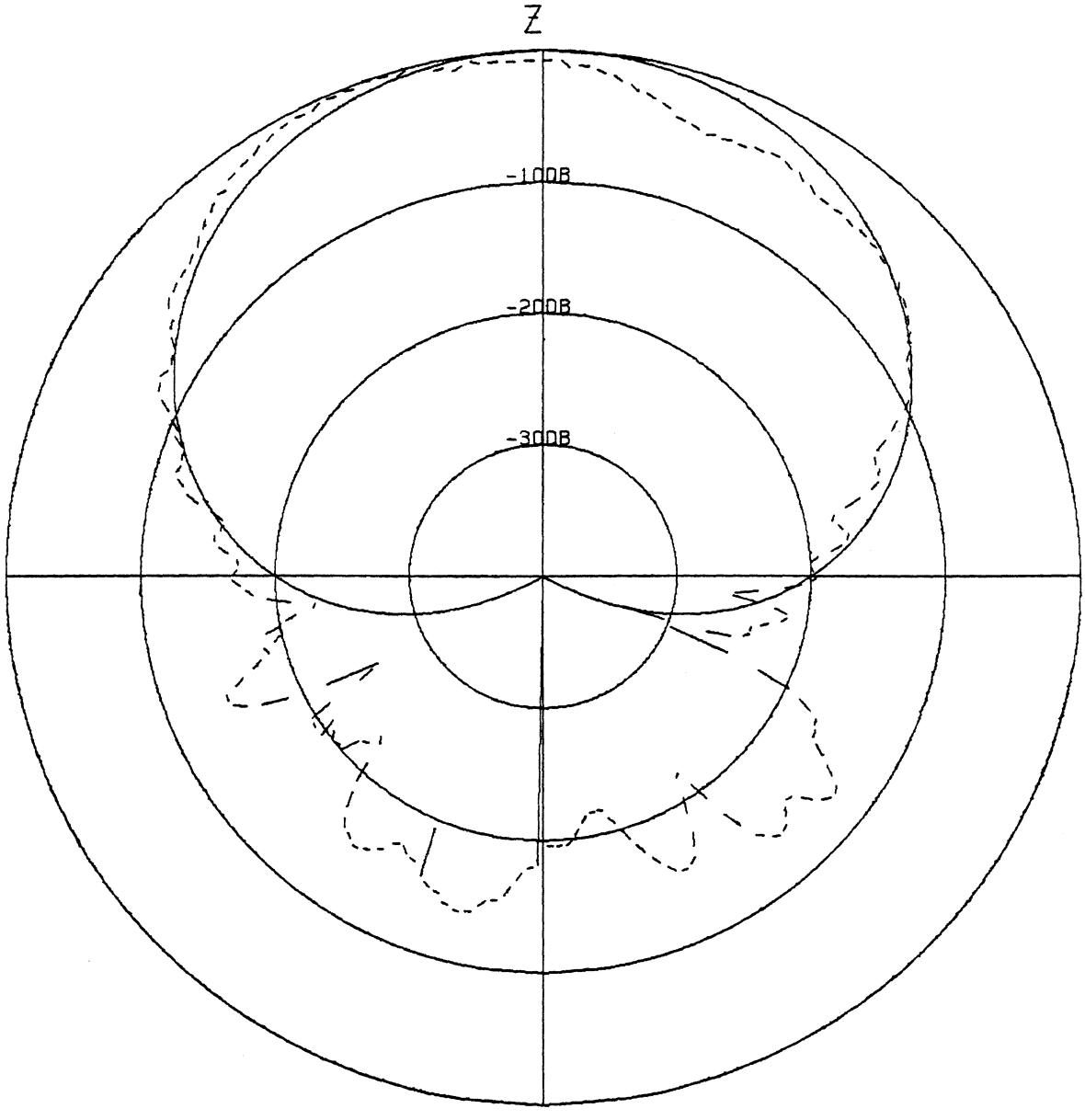

Figure 6.2-2. Radiation pattern of the large spiral at 5.0 GHz (measured-dashed, calculated-solid).

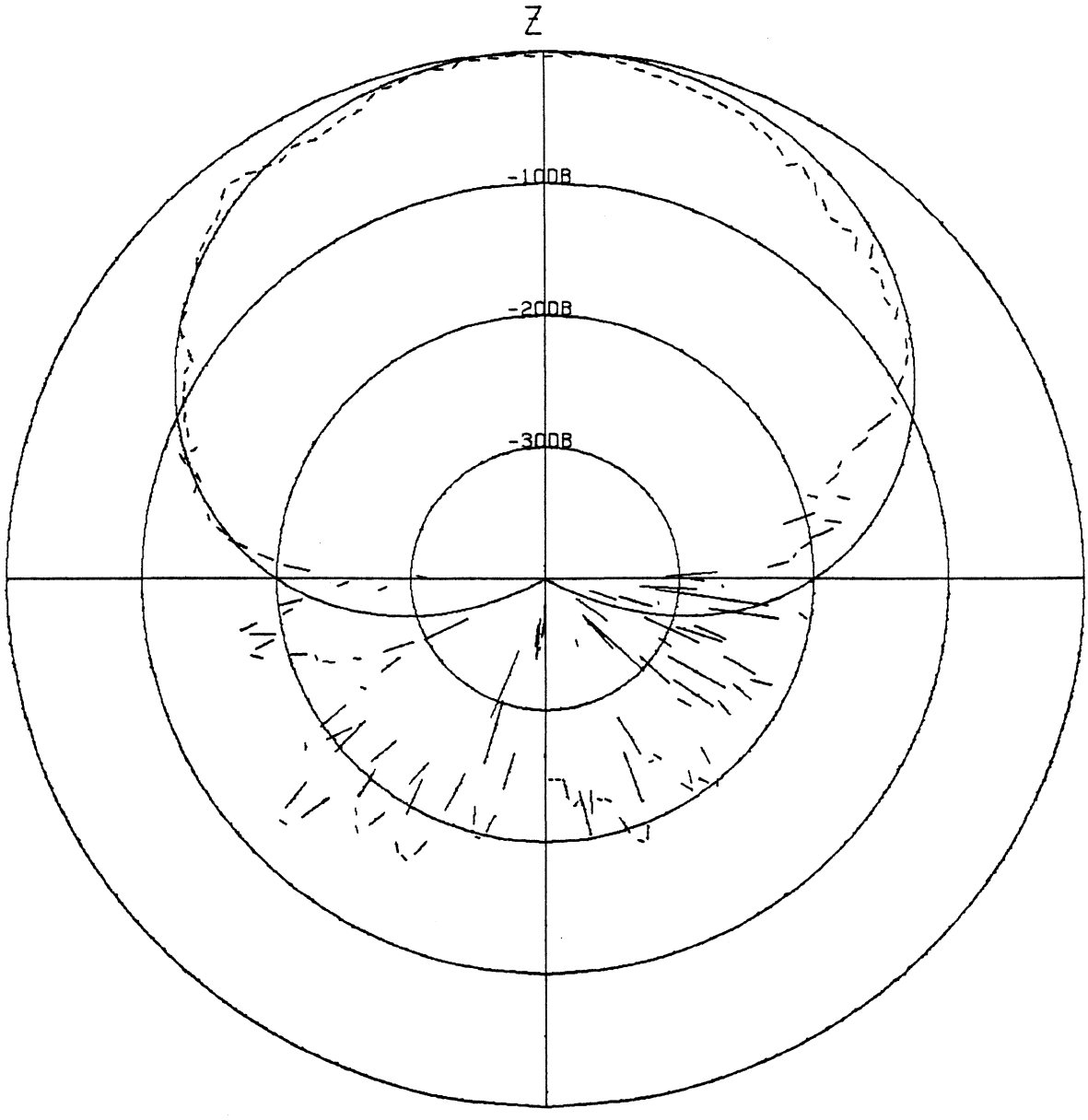

Figure 6.2-3. Radiation pattern of the large spiral at 10.0 GHz (measured-dashed, calculated-solid).

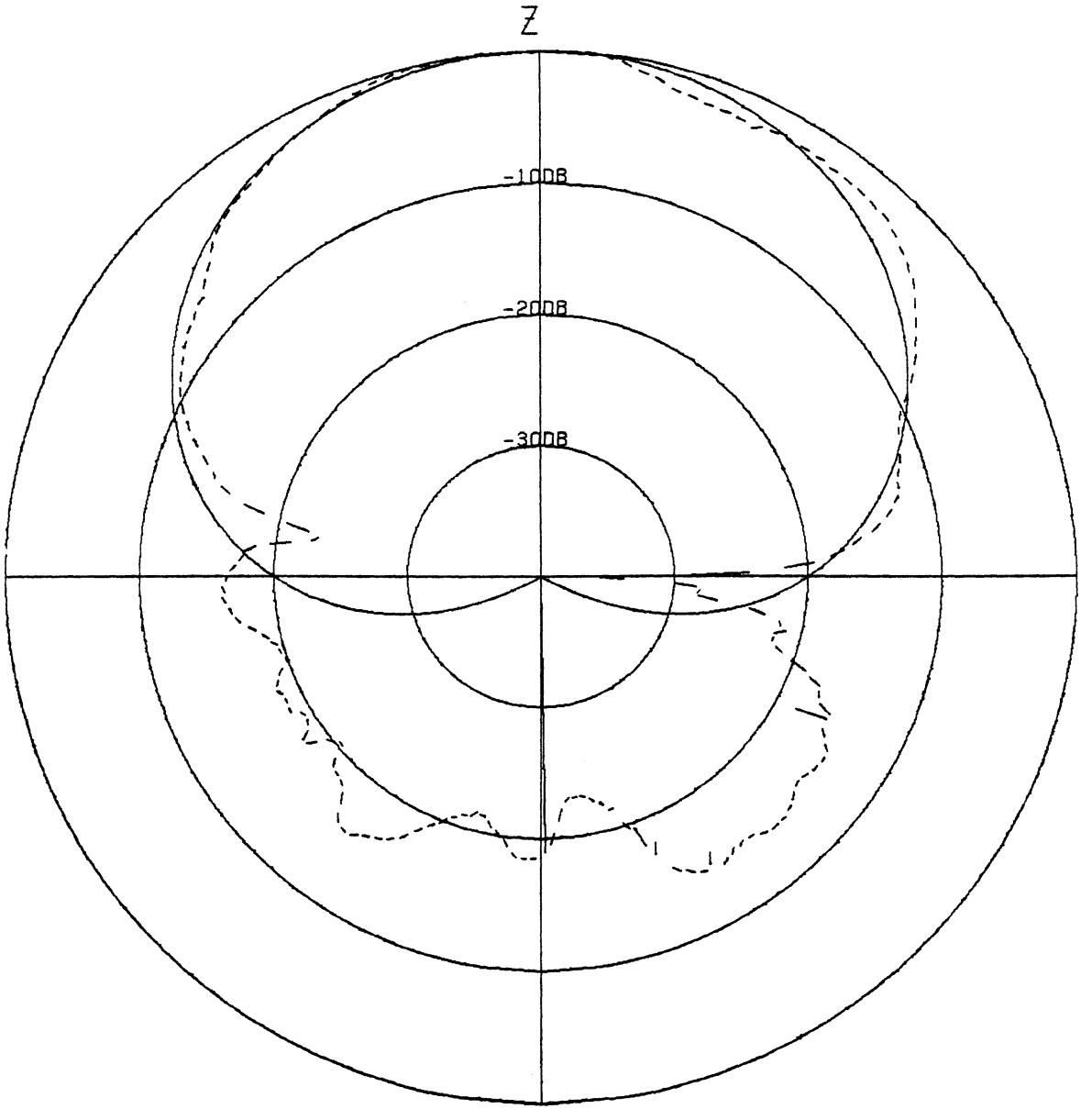

Figure 6.2-4. Radiation pattern of the small spiral at 5.0 GHz (measured-dashed, calculated-solid).

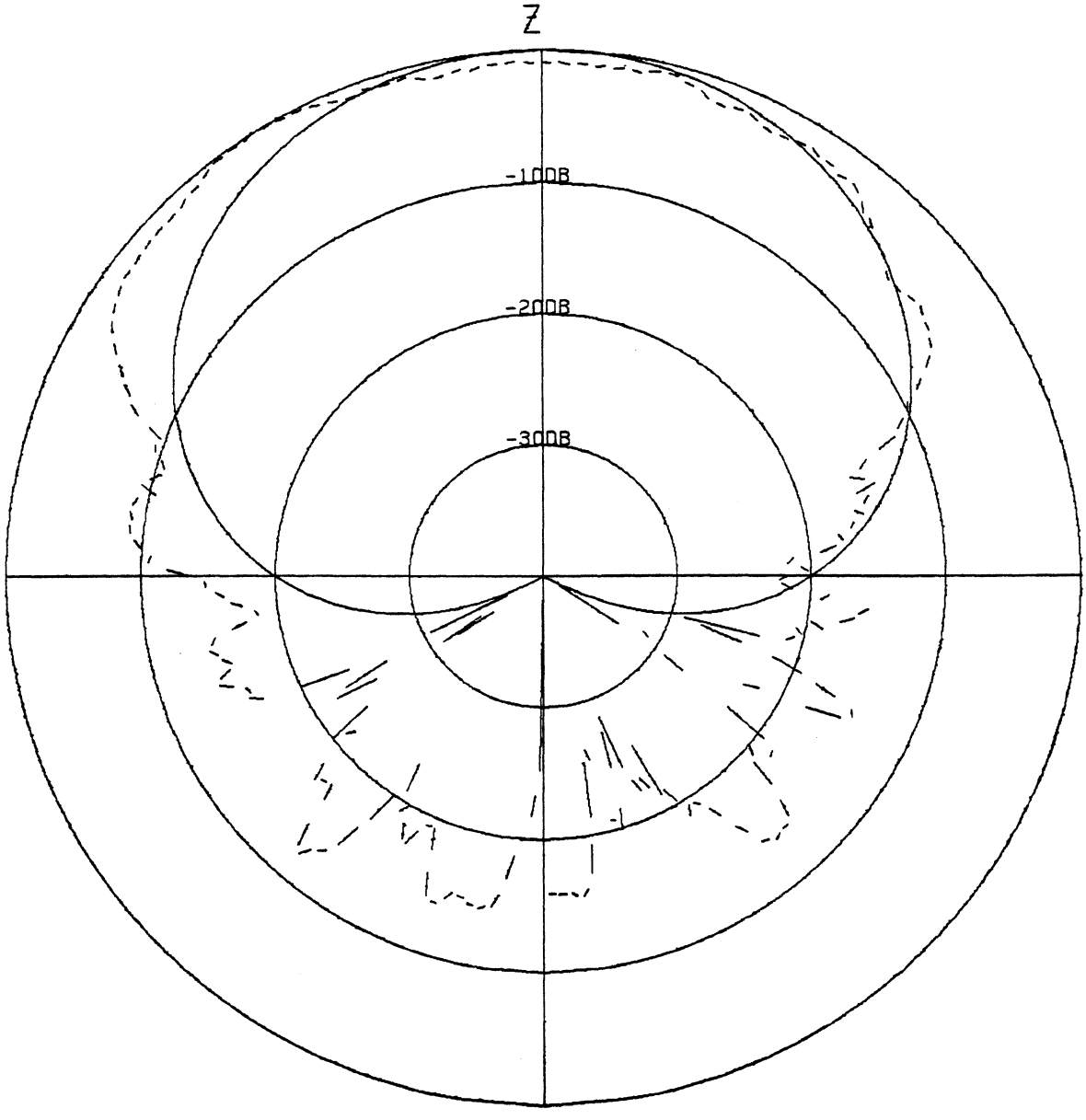

Figure 6.2-5. Radiation pattern of the small spiral at 10.0 GHz (measured-dashed, calculated-solid).

the modelled pattern of (4.2-2) which is overlayed in each of the figures. The large backlobes seen in all of the measured patterns could be caused by imperfections in the cavity that is behind each spiral and also by antenna range reflections. Although the axial ratio for the elements was found to be no worse than 3 dB the radiation pattern of the spirals may have some dependence on the angle ϕ because of the small number of turns and large interconductor spacing in the spirals.

6.3 Wideband Array Construction

The four large and four small spirals were arranged into the planar array configuration shown in Figure 6.3-1. The feed points of the spiral were placed parallel to the x axis with the center conductor of the coax balun connected to the right spiral arm and the outer coax conductor connected to the left spiral arm. The spirals were connected together electrically using two coax "T" connector feed networks as shown in Fig. 6.3-2. The "T"connectors used had one male and two female terminations which allowed direct connection of two or more "T" connectors. The "T" connectors were connected to the spirals with 12 inch sections of RG-405 coaxial cable. For the lower octave the 1:4 transition is used and for the upper octave of operation the 1:8 transition is used. Because these networks do not provide any isolation, reflections caused by impedance mismatches can reappear in another element. Although this is not the best way to connect antennas in an array, it does avoid the high cost of wideband power combiners or stripline feeding networks. Because of the crude feeding arrangement, however, pattern measurements may not show the expected results.

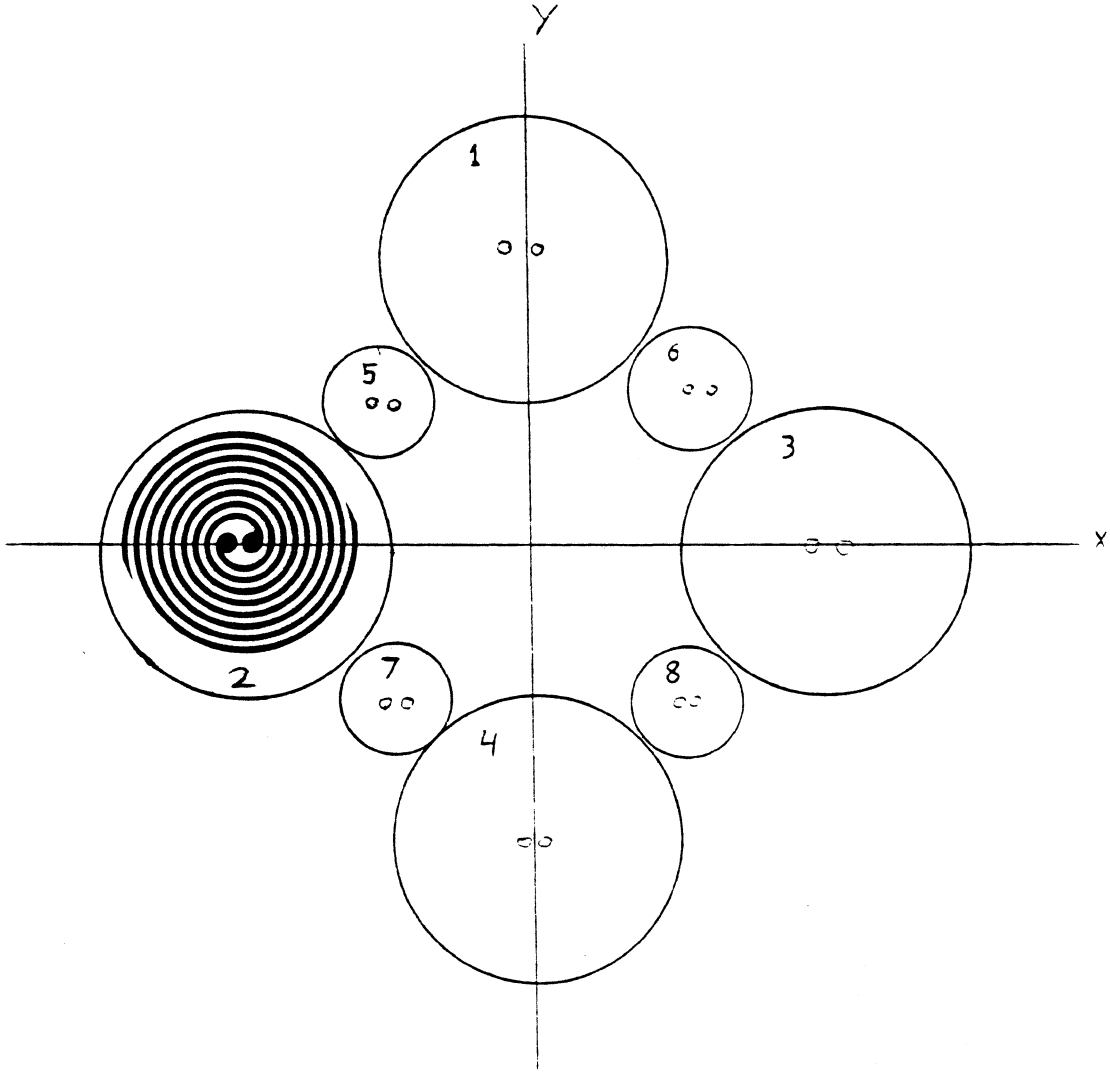

Figure 6.3-1. Front view of the array showing element numbers and element feed points. The center conductor of the balun is the right feed point on each.

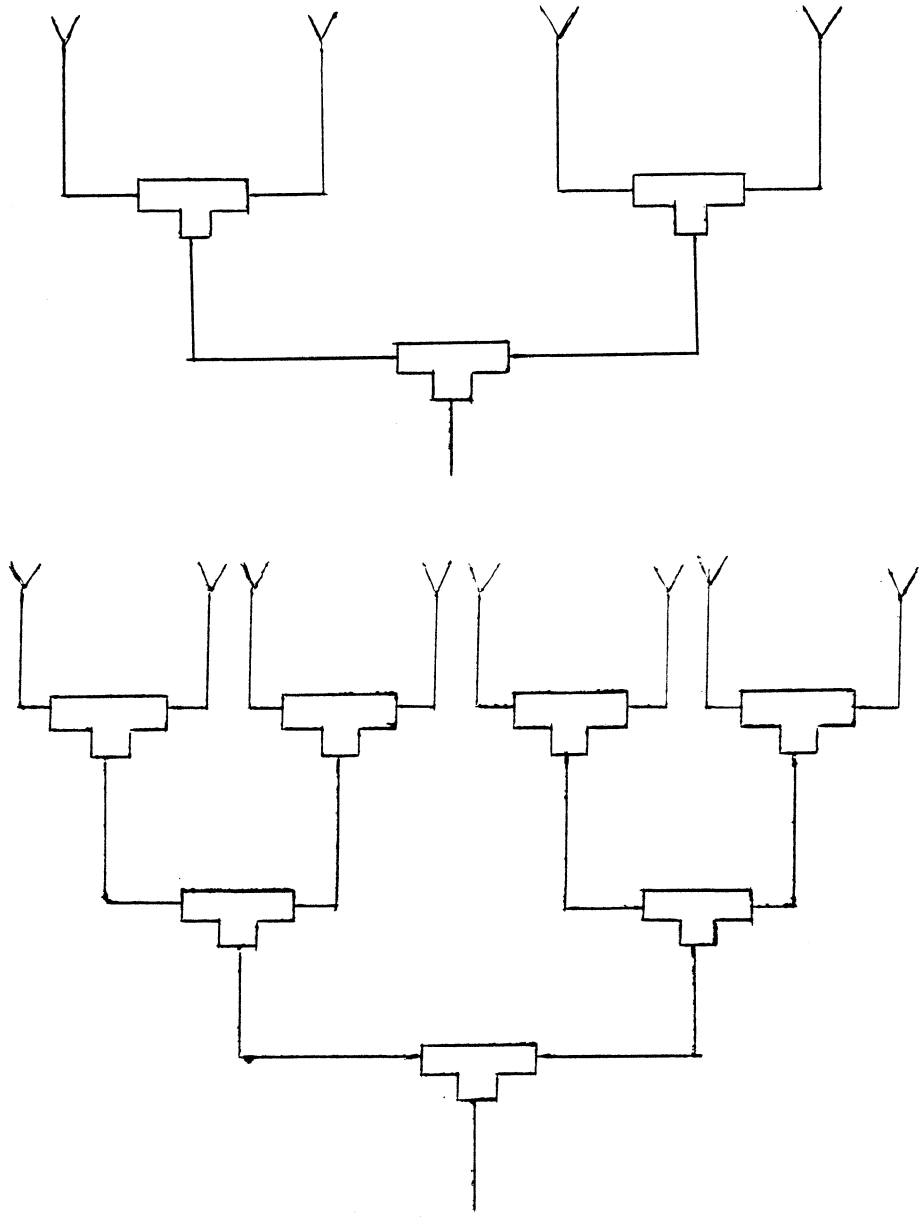

Figure 6.3-2. Feed networks used to feed the array of Fig. 6.3-1. The four element network is used to connect large elements for the first octave and the eight element feed is used to connect all eight elements for the second octave.

6.4 *Array Radiation Pattern Measurements*

Radiation patterns were measured for the array at frequencies 2.5 GHz, 3.75 GHz, 5.0 GHz, 7.5 GHz and 10.0 GHz. For each frequency four patterns were recorded: two patterns for $\phi = 0°$ and two patterns for $\phi = 90°$ (that is, with the array of Fig. 6.3-1 rotated 90° counterclockwise). Two patterns were recorded for each plane because the transmit antennas were not circularly polarized. One pattern was made with the linearly polarized transmit antenna oriented vertically and another with the transmit antenna oriented horizontally. At 5.0 GHz two complete sets of patterns were recorded, the first with only four elements and the second with all eight elements. Array patterns show only the region from +90° to −90° because of the large number of patterns included. As in the element patterns, large backlobes were seen in the array patterns as a result of the cavities that back each element and antenna range reflections.

Figure 6.4-1 shows the four radiation patterns measured at 2.5 GHz for the four element array. All of the patterns show close agreement to the predicted pattern in the shape of the main lobe. The predicted nulls at $+-90°$ are not evident in the measured patterns. This could be caused by differences in individual element radiation patterns or by nonuniform amplitude and phase across the elements introduced by the feed network. The predicted nulls are seen in the $\phi = 90°$ horizontally polarized pattern although the shape of the main lobe is somewhat distorted.

Measured patterns at 3.75 GHz are shown in Figure 6.4-2. Sidelobes are higher than predicted but remain below -10 dB with the exception of the $\phi = 0°$ horizontally polarized pattern. The main beams are all close to that predicted. The $\phi = 90°$ vertically polarized pattern shows the best agreement with the predicted pattern, although one sidelobe is higher than predicted. A small mechanical misalignment of the array

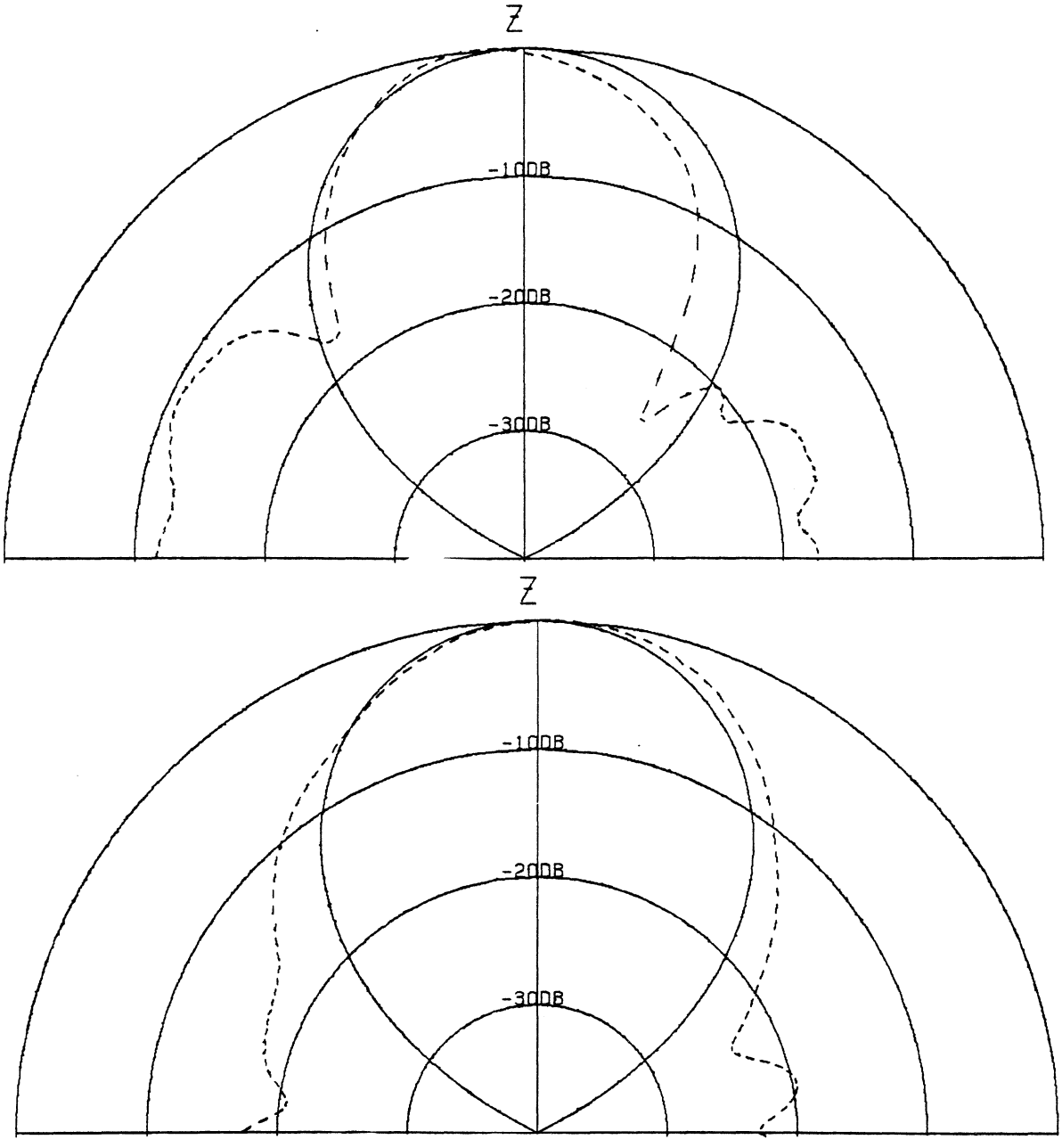

Figure 6.4-1. Radiation patterns of the array of Fig. 6.3-1 at 2.5 GHz with four elements radiating: top- $\phi = 0°$ plane plane pattern horizontal polarization, bottom- $\phi = 90°$ plane pattern vertical polarization. Measured dashed and theoretical solid.

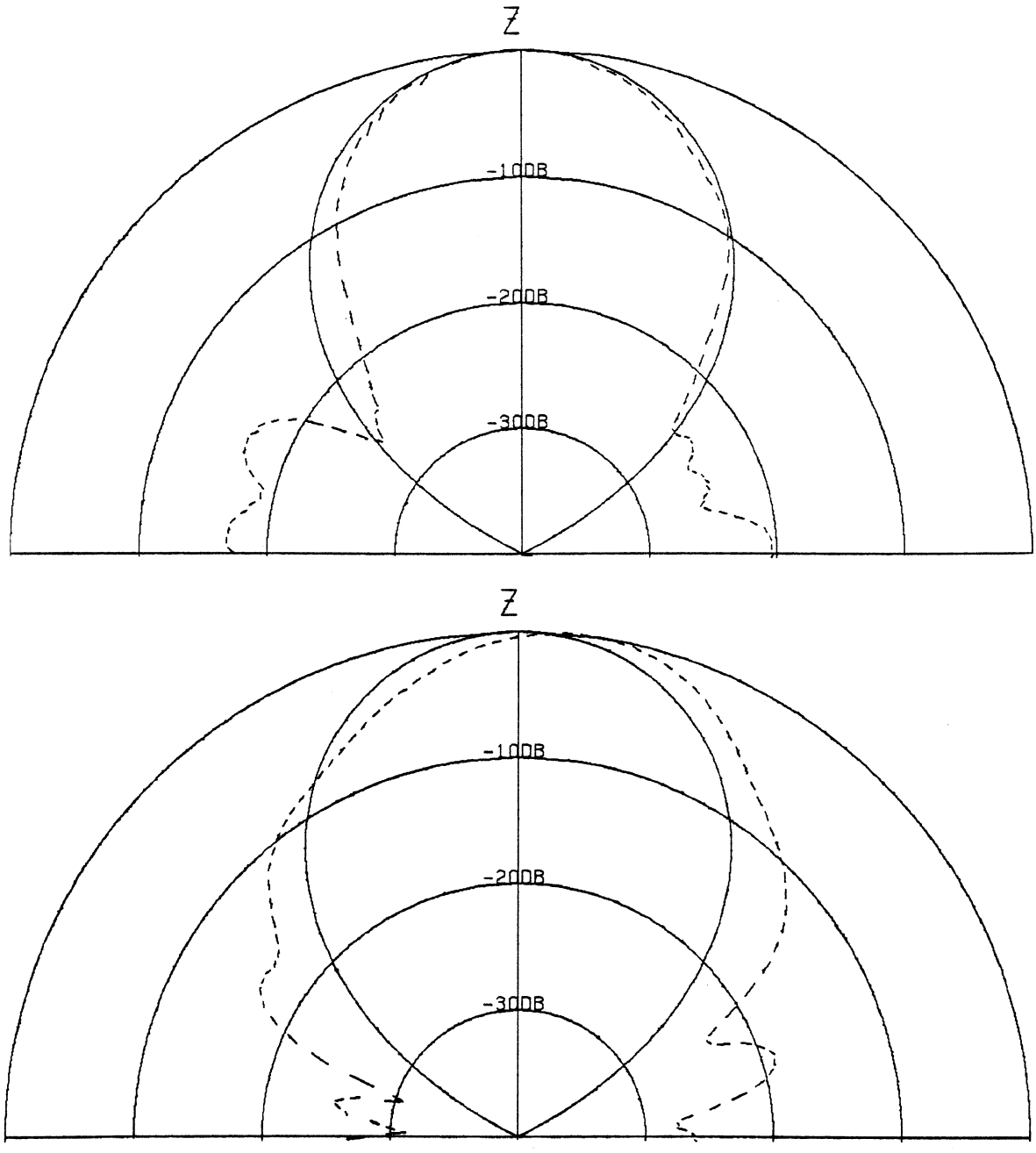

Figure 6.4-1. (continued) top- $\phi = 0°$ plane pattern vertical polarization, bottom- $\phi = 90°$ plane pattern horizontal polarization.

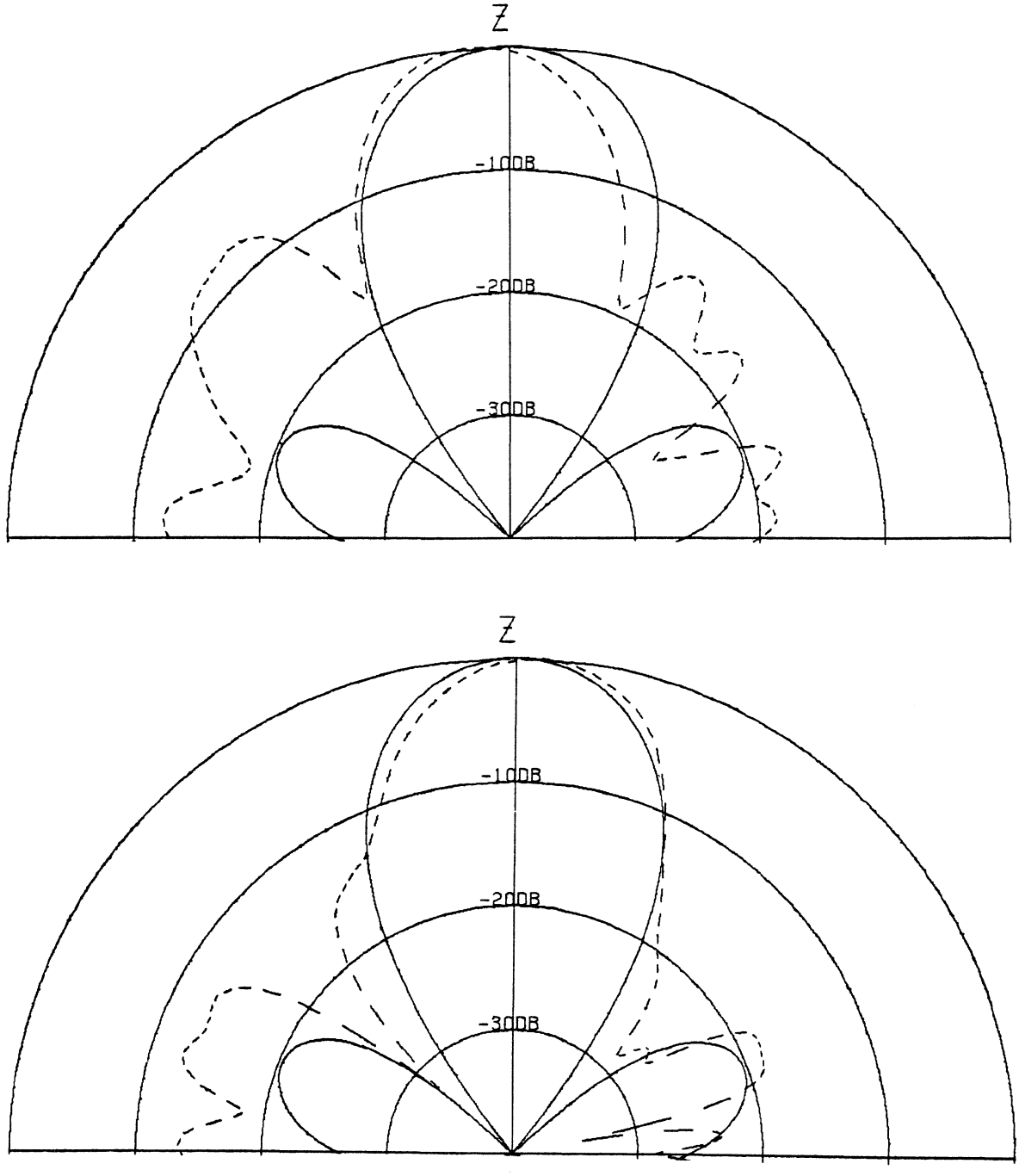

Figure 6.4-2. Radiation patterns of the array of Fig. 6.3-1 at 3.75 GHz with four elements radiating: top- $\phi = 0°$ plane pattern horizontal polarization, bottom- $\phi = 90°$ plane pattern vertical polarization. Measured dashed and theoretical solid.

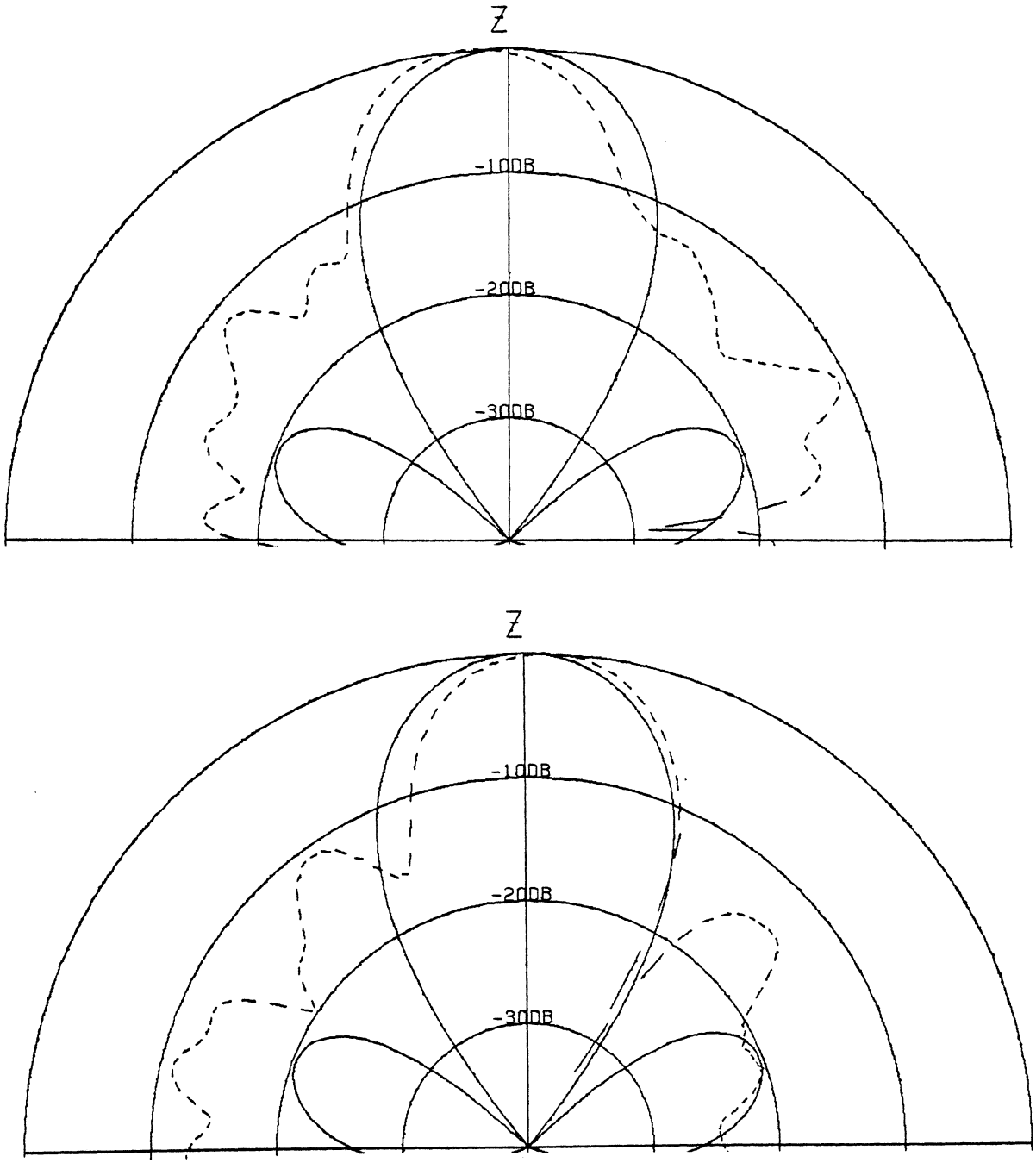

Figure 6.4-2. (continued) top- $\phi = 0°$ plane pattern vertical polarization, bottom- $\phi = 90°$ plane pattern horizontal polarization.

boresight can be seen in all of the patterns. High sidelobes and null filling could be caused by amplitude differences across the array created by the simple feed network.

Figure 6.4-3 shows patterns measured at 5.0 GHz for the four element array. The vertically polarized patterns show the best agreement; in both patterns the predicted main lobe and sidelobes are seen. However, in both cases the sidelobes are higher than expected and the nulls are filled in substantially. The horizontally polarized patterns show less agreement even in the region of the main lobe.

Figure 6.4-4 shows patterns measured at 5.0 GHz with all eight elements radiating. All of the patterns show good agreement for the main lobe. The vertically polarized patterns show the best agreement for deep nulls and low sidelobes. All of the patterns show the correct sidelobe locations although the sidelobes are higher than predicted. The predicted pattern improvement caused by doubling the number of elements can be seen when these patterns are compared to those of Fig. 6.4-3.

Measured patterns at 7.5 GHz are shown in Figure 6.4-5. All of the patterns show close agreement to the predicted pattern with the exception of the $\phi = 90°$ horizontally polarized pattern. The vertically polarized patterns and the $\phi = 0°$ horizontally polarized pattern exhibit close agreement in the main lobe region and show the correct sidelobe locations. As in the 5.0 GHz eight element case, the sidelobes have run together somewhat and are higher than predicted. This effect is so bad in the $\phi = 90°$ horizontally polarized case that the measured pattern is almost unrecognizeable.

Figure 6.4-6 shows measured patterns for the eight element array at 10.0 GHz. The $\phi = 0°$ vertically polarized pattern shows the best agreement to the predicted pattern. The predicted grating lobes are seen although the sidelobes have run together or have become part of the main lobe. The $\phi = 90°$ vertically polarized pattern shows higher sidelobes and grating lobes but retains more definition between the lobes. The horizontally polarized patterns show less agreement to the predicted pattern although the

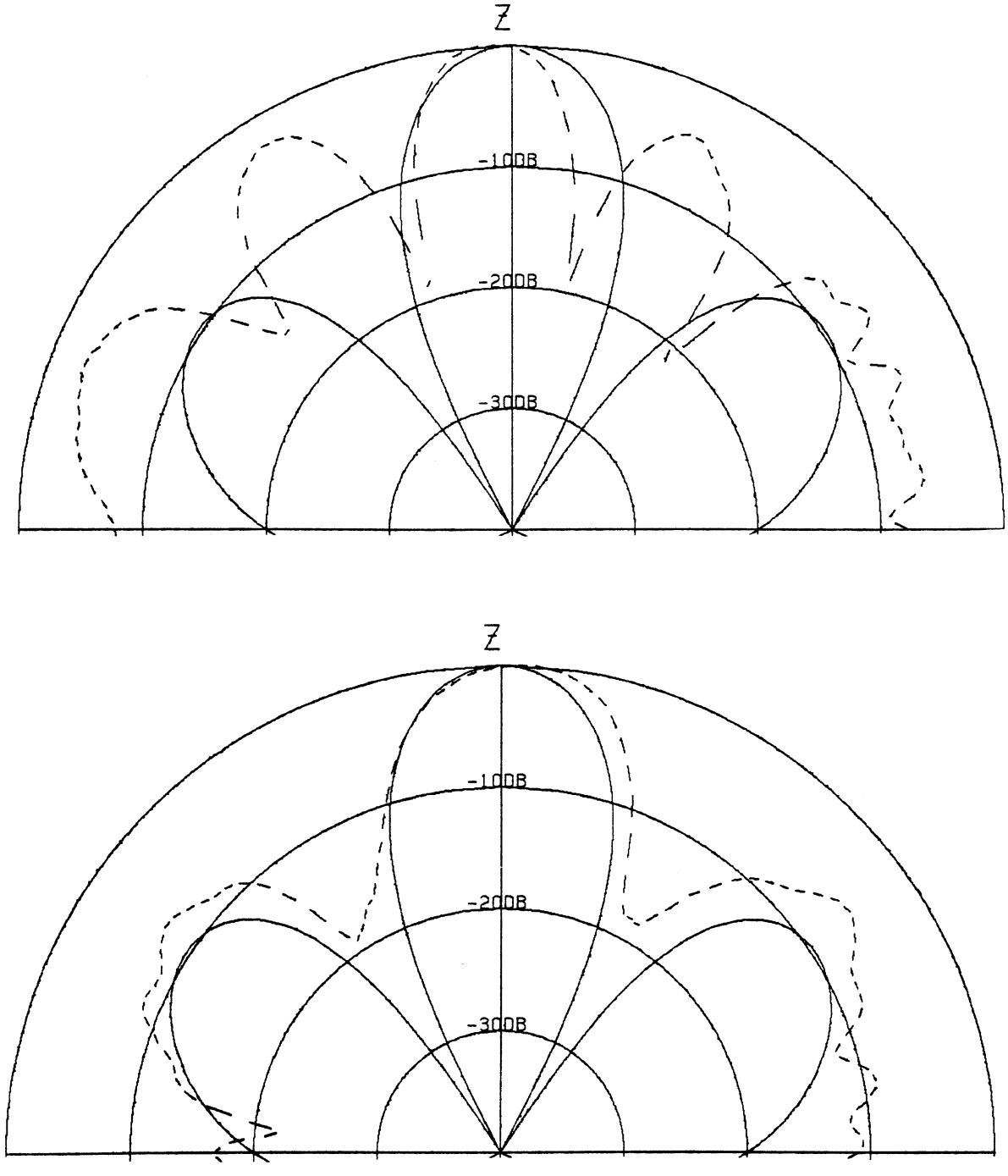

Figure 6.4-3. Radiation patterns of the array of Fig. 6.3-1 at 5.0 GHz with four elements radiating: top- $\phi = 0°$ plane pattern horizontal polarization, bottom- $\phi = 90°$ plane pattern vertical polarization. Measured dashed and theoretical solid.

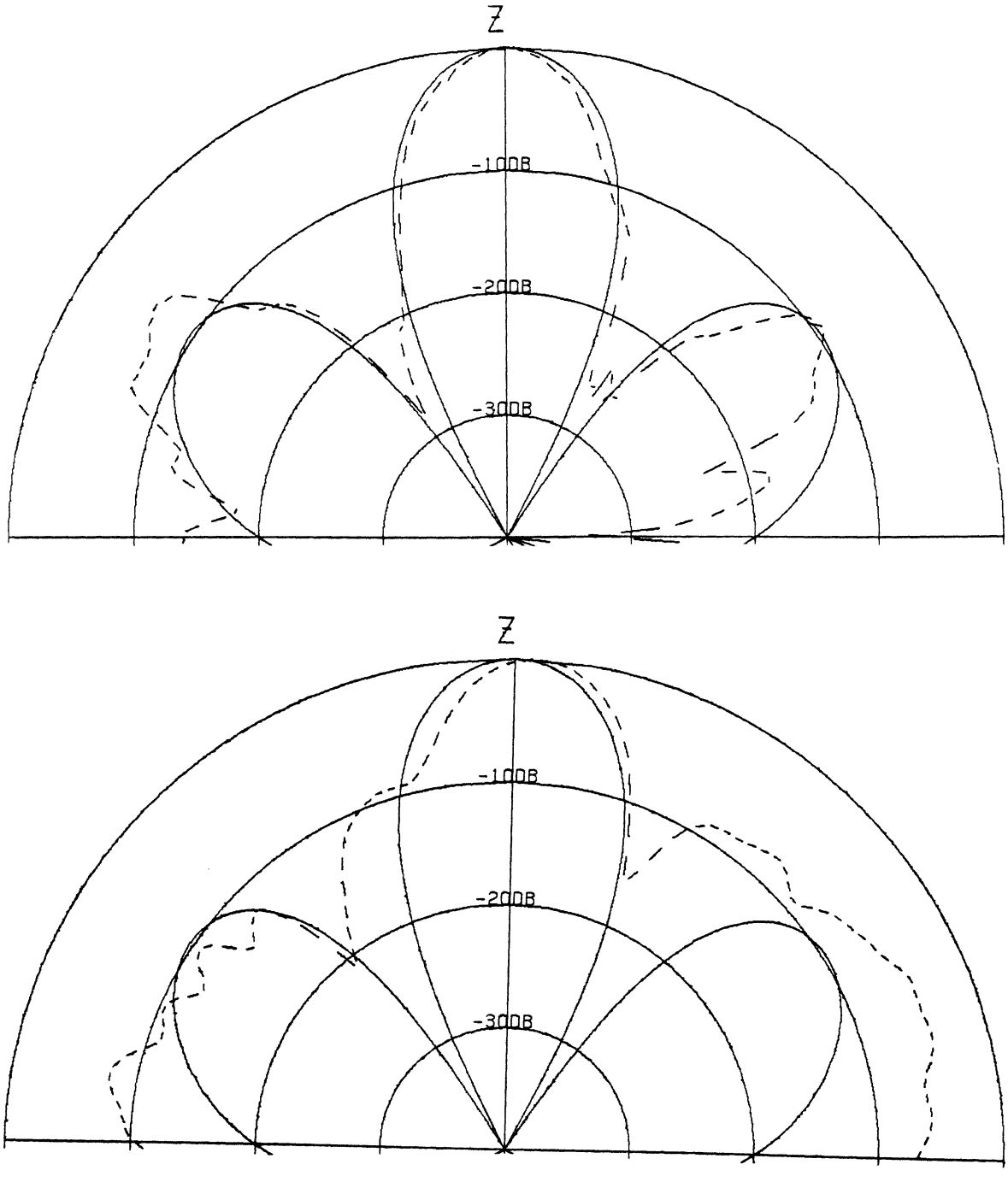

Figure 6.4-3. (continued) top- $\phi = 0°$ plane pattern vertical polarization, bottom- $\phi = 90°$ plane pattern horizontal polarization.

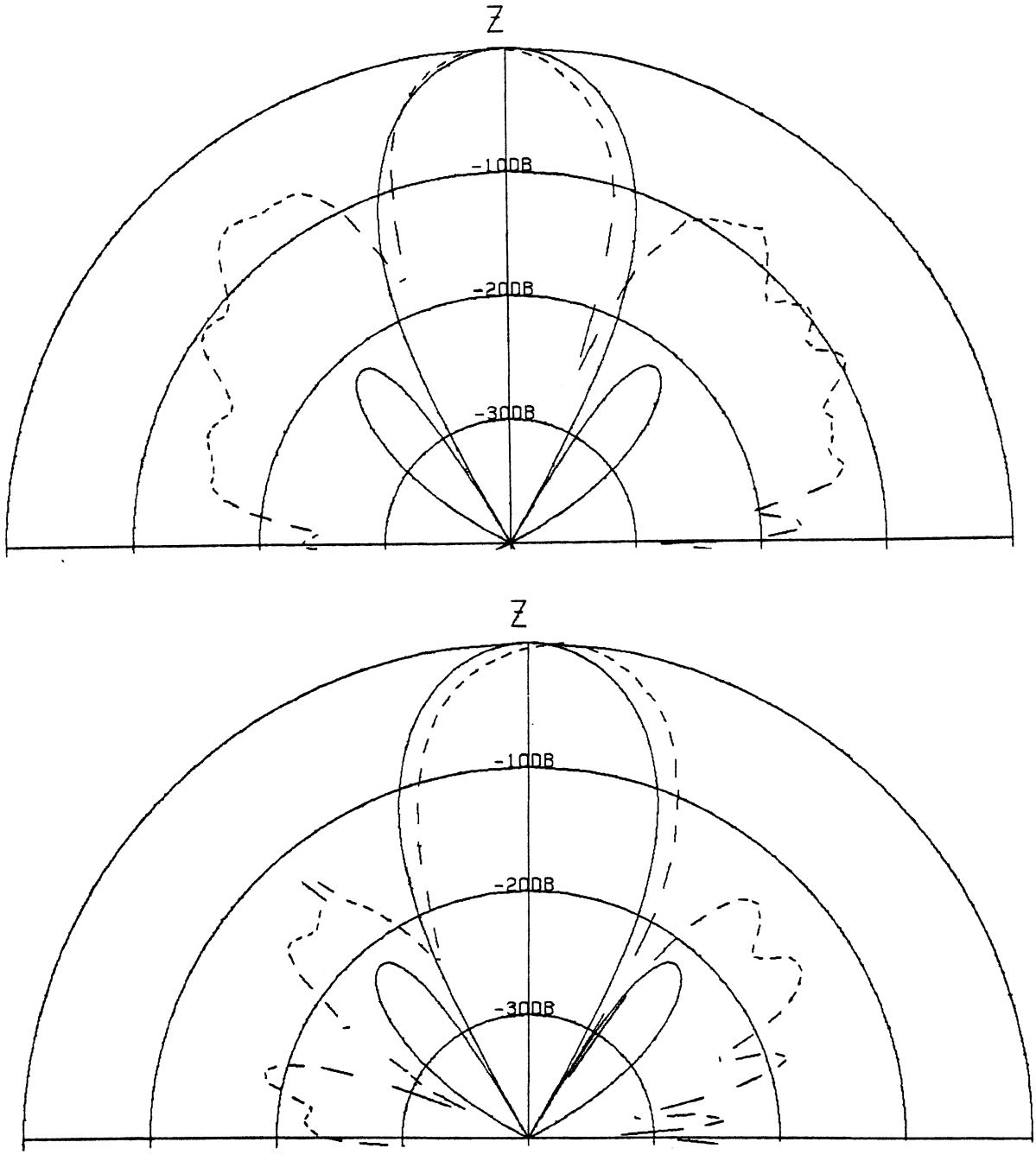

Figure 6.4-4. Radiation patterns of the array of Fig. 6.3-1 at 5.0 GHz with eight elements radiating: top- $\phi = 0°$ plane pattern horizontal polarization, bottom- $\phi = 90°$ plane pattern vertical polarization. Measured dashed and theoretical solid.

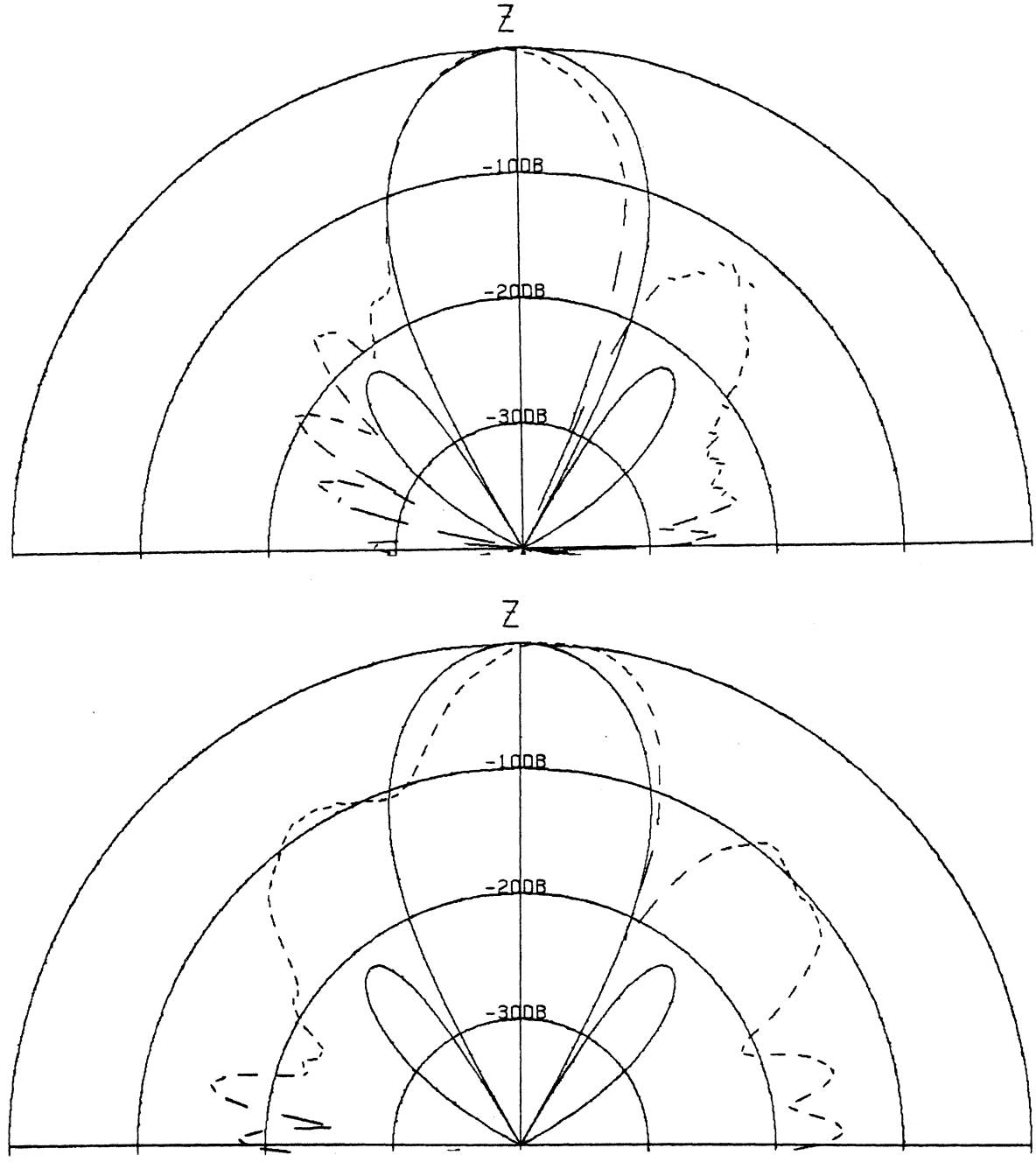

Figure 6.4-4. (continued) top- $\phi = 0°$ plane pattern vertical polarization, bottom- $\phi = 90°$ plane pattern horizontal polarization.

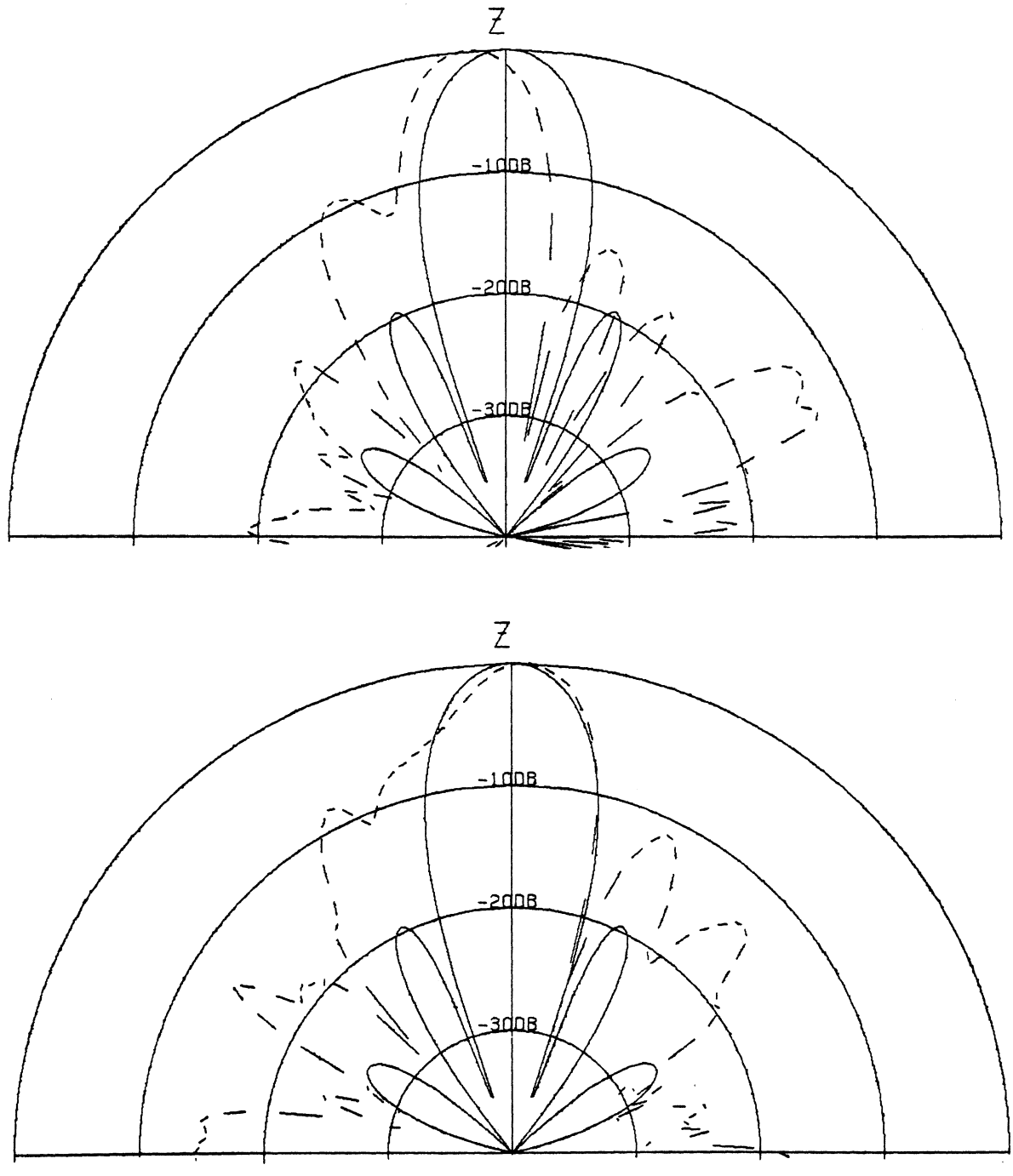

Figure 6.4-5. Radiation patterns of the array of Fig. 6.3-1 at 7.5 GHz with eight elements radiating: top- $\phi = 0°$ plane pattern horizontal polarization, bottom- $\phi = 90°$ plane pattern vertical polarization. Measured dashed and theoretical solid.

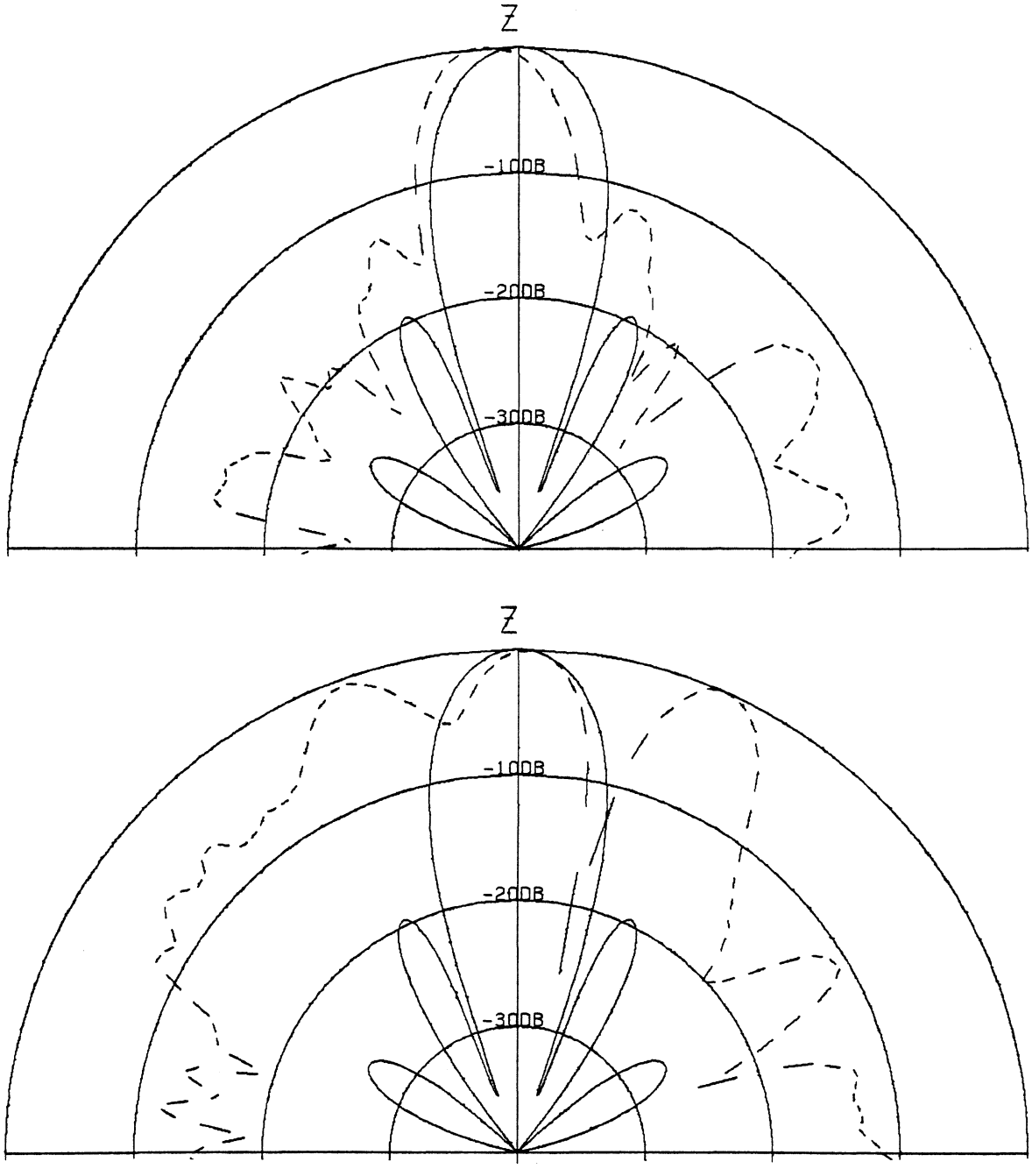

Figure 6.4-5. (continued) top- $\phi = 0°$ plane pattern vertical polarization, bottom- $\phi = 90°$ plane pattern horizontal polarization.

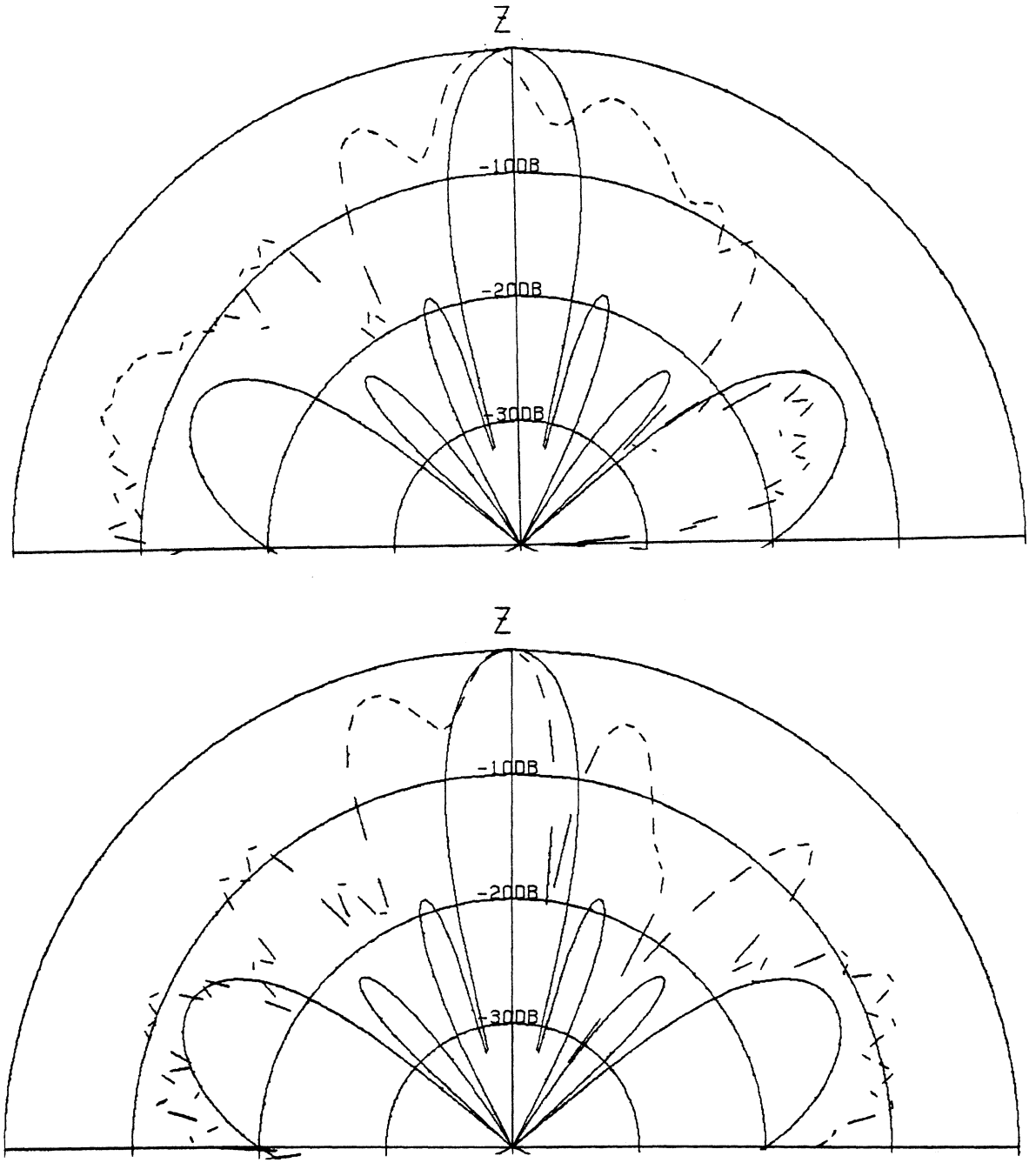

Figure 6.4-6. Radiation patterns of the array of Fig. 6.3-1 at 10.0 GHz with eight elements radiating: top- $\phi = 0°$ plane pattern horizontal polarization, bottom- $\phi = 90°$ plane pattern vertical polarization. Measured dashed and theoretical solid.

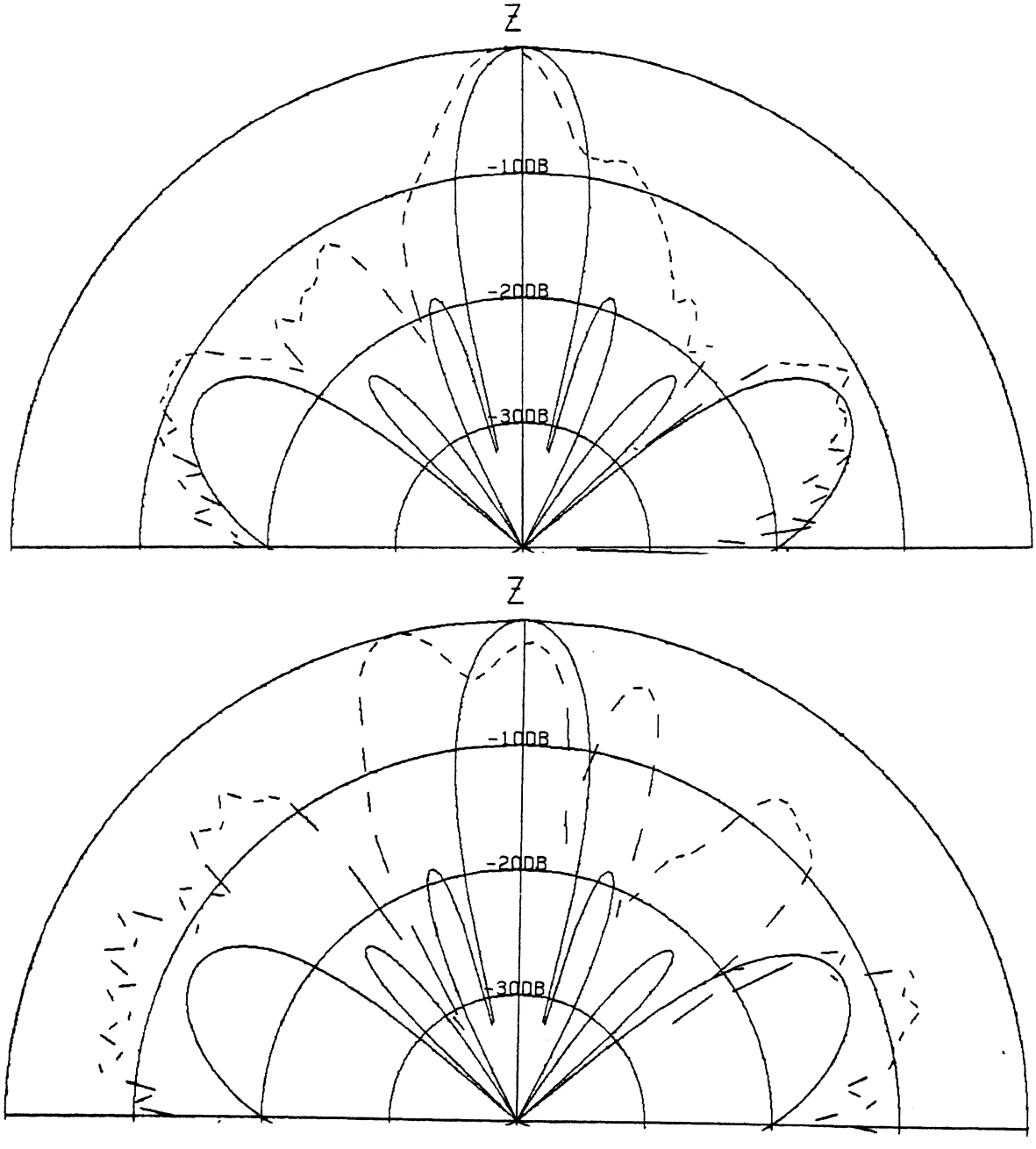

Figure 6.4-6. (continued) top- $\phi = 0°$ plane pattern vertical polarization, bottom- $\phi = 90°$ plane pattern horizontal polarization.

same general shape can be seen in all of the patterns. These effects could be caused by unequal element amplitudes and mismatches associated with the feed network. As expected this effect has grown worse as frequency is increased.

6.4.1 Summary of Measurements

In almost all of the measured patterns the predicted main beam is well formed and agrees with predictions. Some of the measurements exhibit a small mechanical pointing error of two to three degrees which should be ignored. Correct sidelobe heights are seen in some cases as well as correct null locations. Null filling and high sidelobes are evident in most of the horizontally polarized patterns. Patterns at 5.0 GHz and below show the best agreement with the predictions. The closest agreement is seen at 5.0 GHz with four elements radiating and vertical polarization. When eight elements are activated at this frequency, the predicted pattern improvement is obtained as seen in Fig. 6.4-4 for the vertical polarization measurements. Above 5.0 GHz the measured patterns degraded. Although sidelobes are located at the predicted locations, the sidelobe height is much higher than predicted in all cases. In some cases the sidelobes have blended together or have become part of the main beam. At 10.0 GHz the $\phi = 0°$ vertical polarization pattern shows the predicted grating lobes, although the other sidelobes have blended together. The axial ratio for the entire array was found to be between 2 and 3 dB.

6.5 *Array Impedance Measurements*

In an attempt to understand the effects of the feeding network on the radiation pattern measurements, the S_{11} reflection coefficient was measured using a Hewlett-Packard 8410 network analyzer. Measurements were taken from 2.0 to 12.0 GHz for each array element individually, the four large elements connected together, the four small elements connected together and finally all eight elements connected together. Element numbers are shown in Fig. 6.3-1.

As can be seen in Figs. 6.5-1 through 6.5-4, the reflection coefficient for the individual elements is similar although not exactly the same. For the small spirals, elements 5 through 8, the portion of the plot below 5.0 GHz is of no interest although the region of cutoff can be seen at about 2.5 GHz and below. Differences in the reflection coefficient amplitude could be caused by differences in the individual baluns that feeds each spiral, minor differences in the connector to balun solder joint, and minor differences in the balun to spiral connections. These differences in S_{11} amplitude from element to element could cause errors in the radiation pattern if power reflected from one element is re-radiated from another element. This could certainly happen with the feed arrangement used.

Fig. 6.5-5 shows the S_{11} for groups of four large and reflection coefficient for groups of four large and four small spirals. These curves are similar which shows that as a group the four large and four small spirals perform similarly although individual elements may still have current amplitude differences. In the frequency range of 2.5 to 5.0 GHz the S_{11} magnitude of the large elements is that of the operational array with four elements radiating. The upper octave of operation with all eight elements radiating is shown in Figure 6.5-6 where the portion of the graph below 5.0 GHz can be ignored.

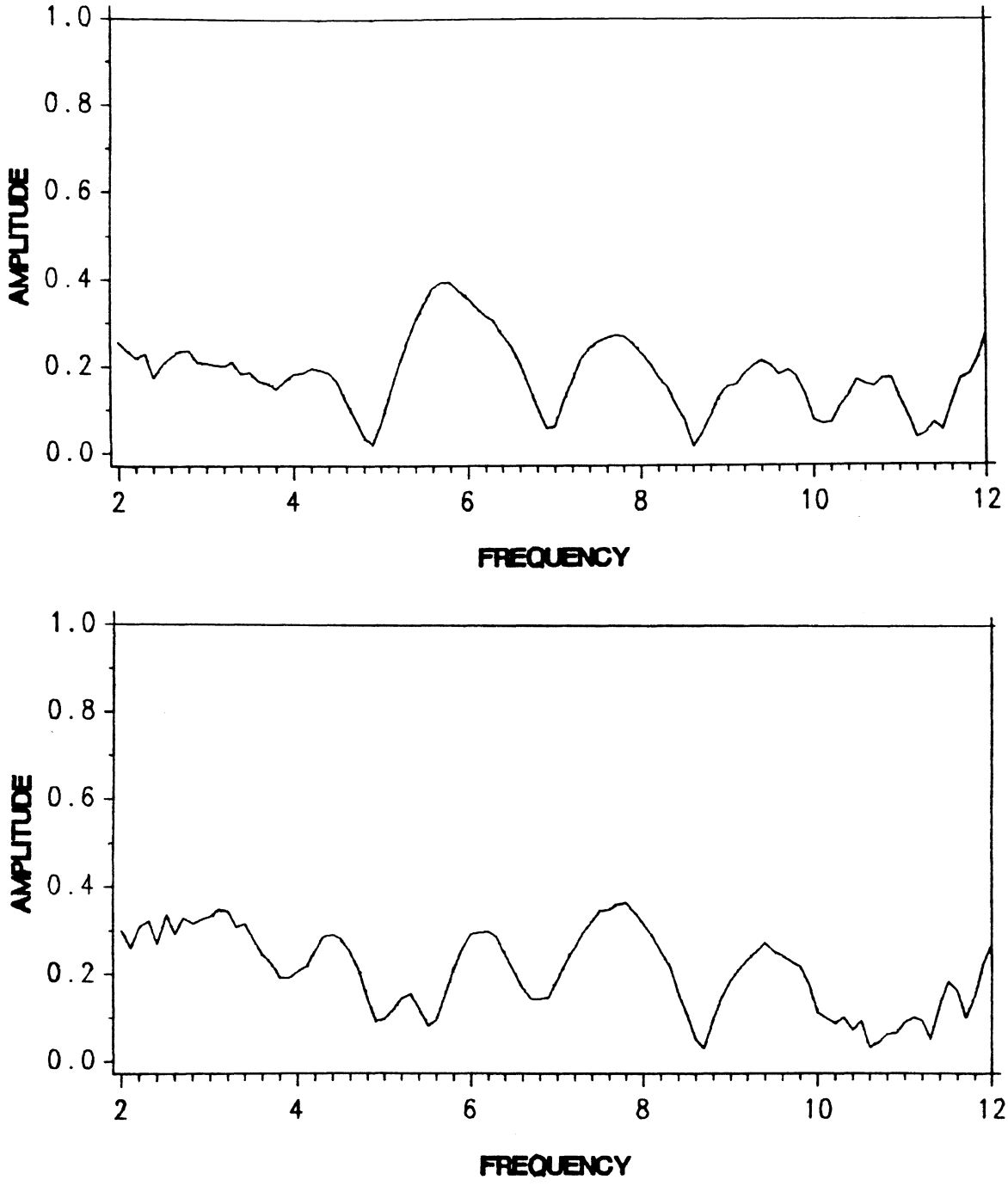

Figure 6.5-1. S_{11} magnitude for array elements 1 and 2 (1-top, 2-bottom). Frequency is shown in GHz.

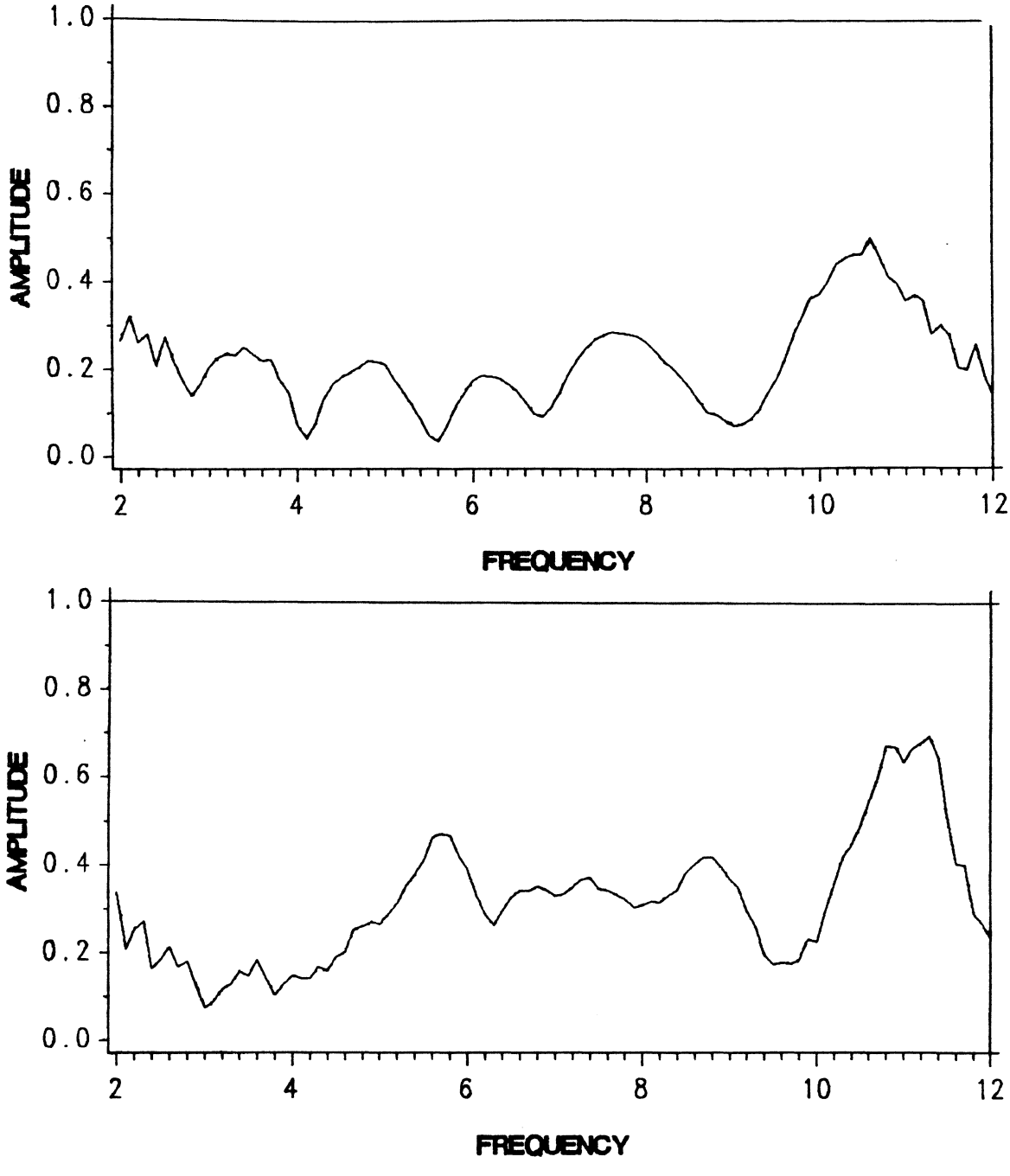

Figure 6.5-2. S_{11} magnitude for array elements 3 and 4 (3-top, 4-bottom). Frequency is shown in GHz.

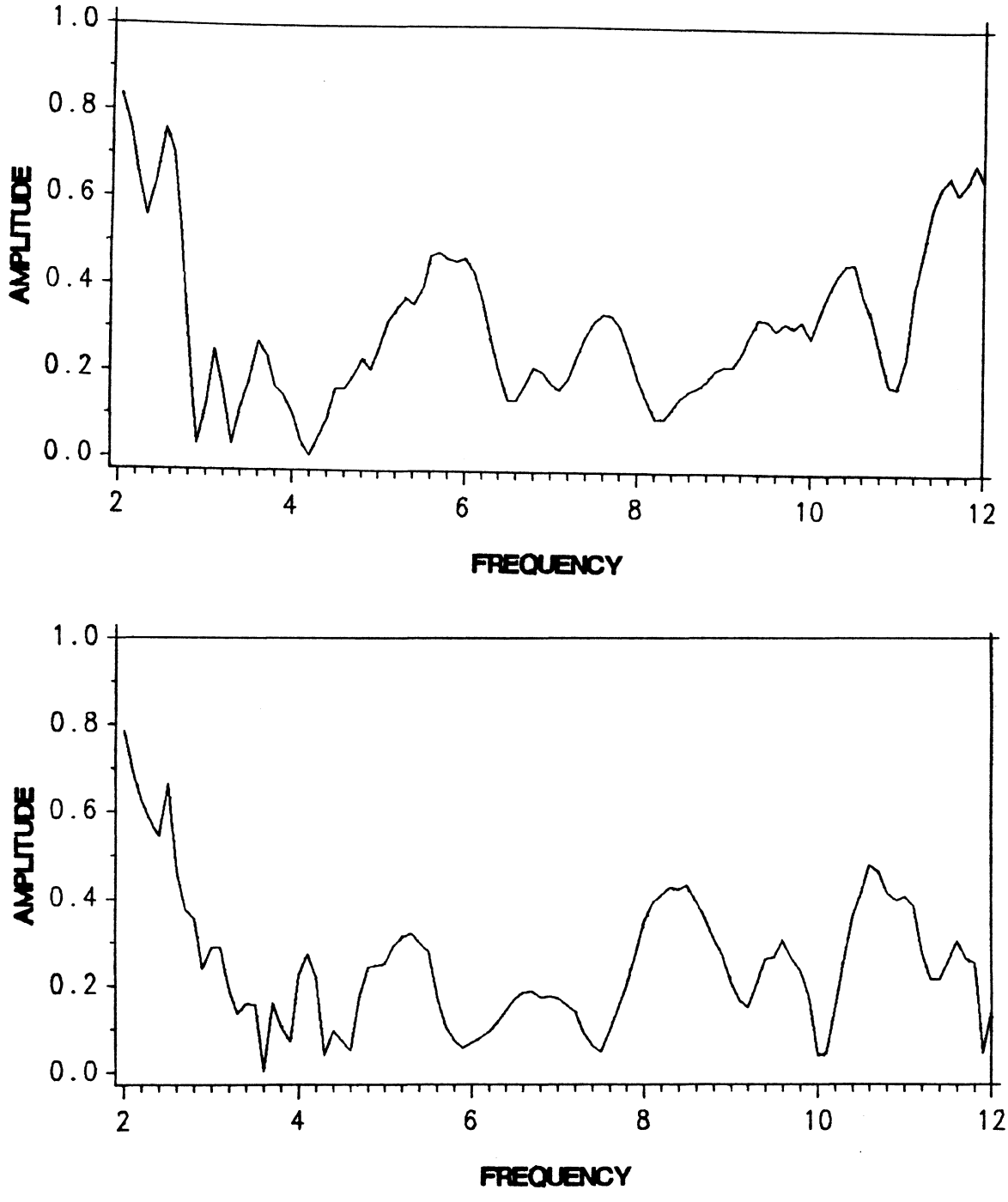

Figure 6.5-3. S_{11} magnitude for array elements 5 and 6 (5-top, 6-bottom). Frequency is shown in GHz. The data below 5.0 GHz can be ignored.

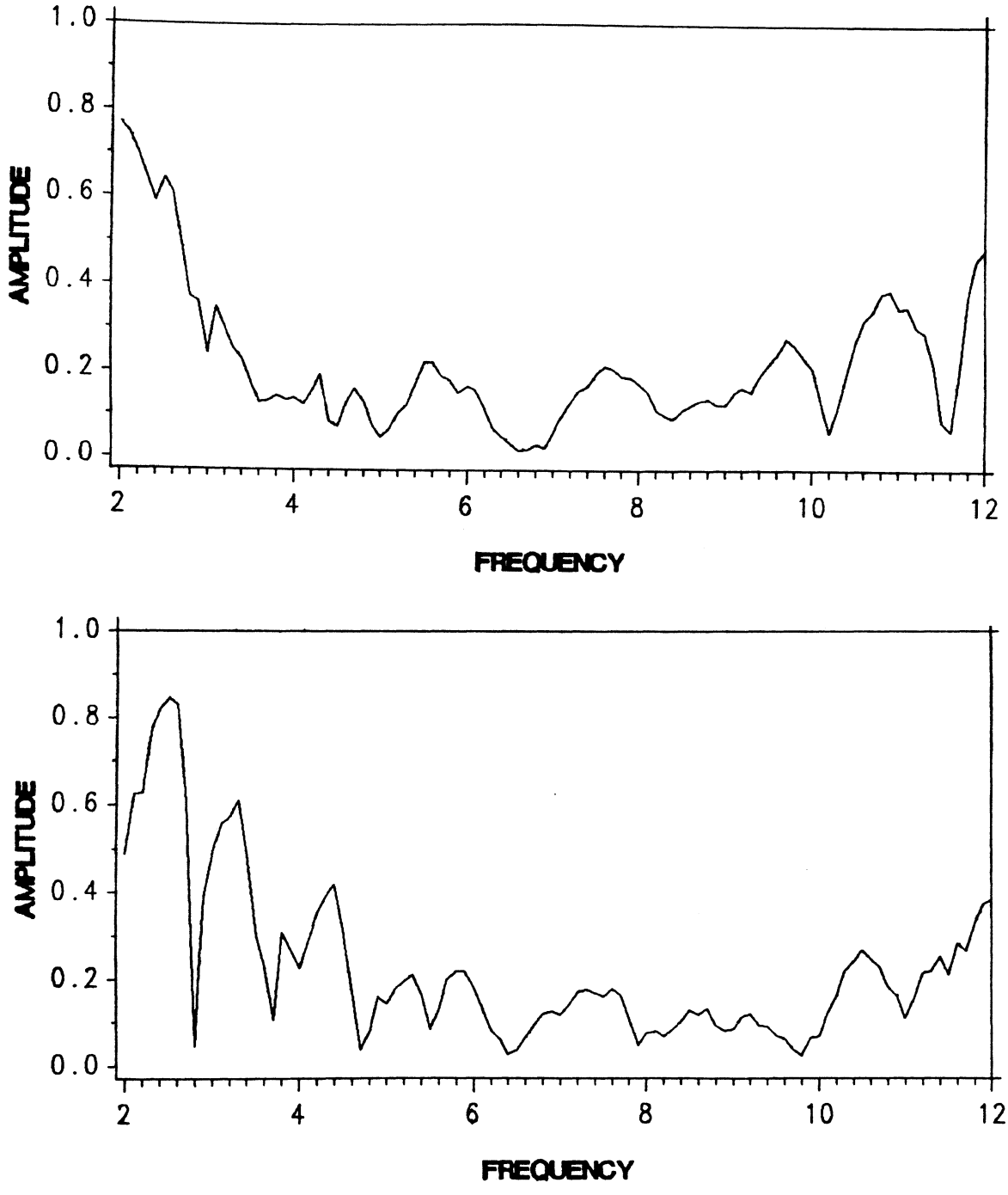

Figure 6.5-4. S_{11} magnitude for array elements 7 and 8 (7-top, 8-bottom). Frequency is shown in GHz. The data below 5.0 GHz can be ignored.

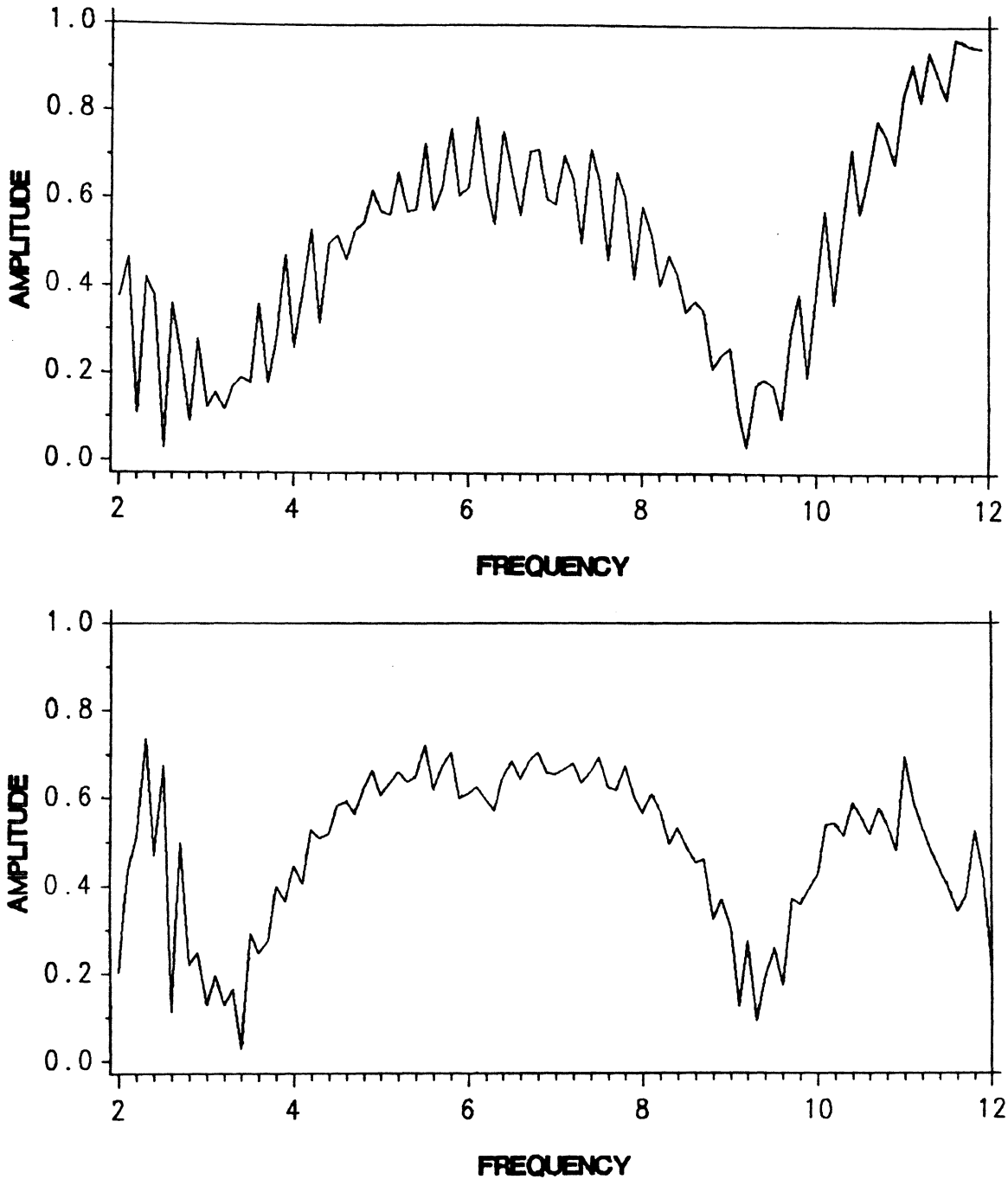

Figure 6.5-5. S_{11} magnitude for groups of four elements (large elements-top, small elements-bottom). Frequency is shown in GHz. The data in the lower plot below 5.0 GHz can be ignored.

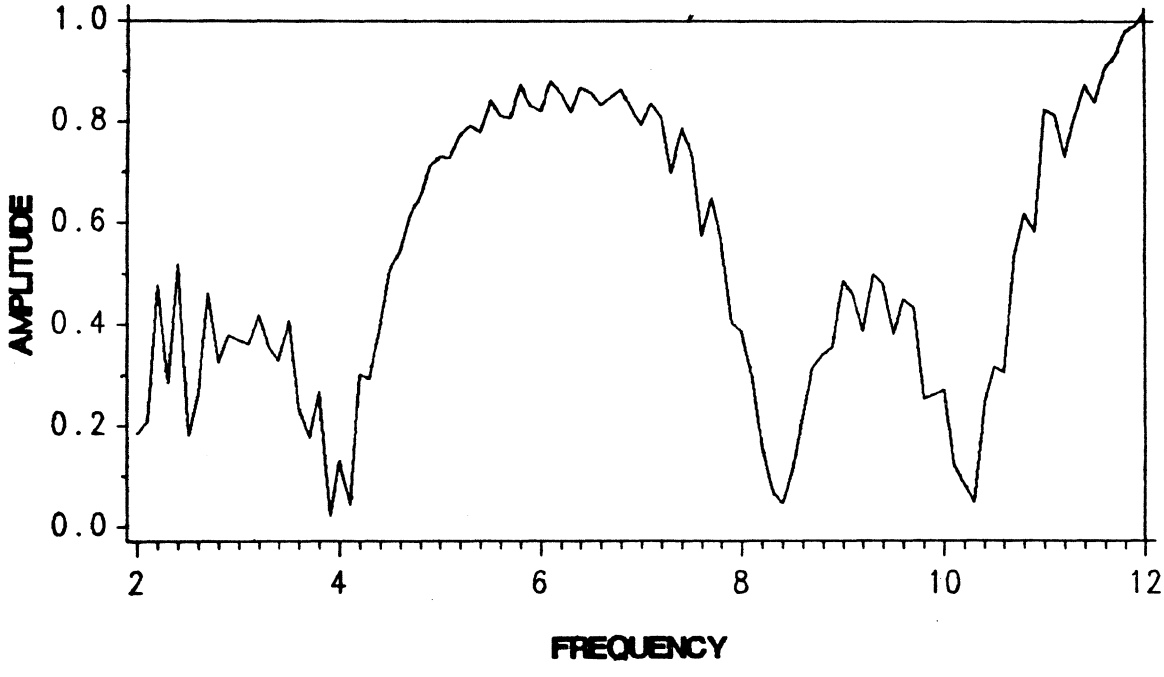

Figure 6.5-6. S_{11} magnitude for the entire eight element array. Frequency is shown in GHz. Note the array is not operated with all eight elements below 5.0 GHz so the data below 5.0 GHz can be ignored.

VII. Conclusions

In this research project array architectures for wideband operation were examined. The design goal was two octaves of frequency over which the directivity did not degrade nor did the sidelobes become excessively high (very much worse than -10 dB). Such design relies on elements with some forward directivity. Archimedean spiral antennas were chosen for the array element because of their nearly constant radiation pattern over a wide frequency range and small size. The element pattern model in Fig. 4.2-1 was used in all investigations.

Two octaves of operation was found to be possible with several array configurations if two sizes of elements are used with the smaller elements activated only in the upper octave of frequency. The smaller elements are half the diameter of the larger elements and all elements are equally spaced with the larger being 1/2 wavelength apart at the lowest frequency of operation. Element spacings remain between 1/2 and 1 wavelength across the complete operating band by increasing the number of active elements in the array. A linear array example is shown in Fig. 5.2-1 where as frequency increases the small elements begin to radiate whan the spacing between the large elements becomes one wavelength (at the end of the first octave). The element spacing becomes 1/2

wavelength when the small elements are activated at the end of the first ocatve. As frequency is increased to two full octaves the element spacing again becomes one wavelength. In this manner a two octave frequency range can be covered. Principal plane sidelobes for this array remain below -10 dB across the entire bandwidth as shown in Fig. 5.2-2. Directivity, shown in Fig. 5.2-3, remains nearly constant for the bandwidth considered. It was found that removing the small array element on the end of the array did not significantly alter the array performance. This can be seen in Figs. 5.2-7 and 5.2-8.

The linear array idea was then extended to two dimensions to form the planar array shown in Fig. 5.3-1. Principal plane sidelobes for this array also remain below -10 dB, although a larger change in directivity can be seen in Fig. 5.3-3. The small elements outside of the large elements were removed and, as in the linear array case, the array performance did not change drastically.

An improved planar array geometry, shown in Fig. 5.6-1, was then considered. Using only eight elements, this array maintains principal plane sidelobes below -9.7 dB over the two octave frequency range as shown in Fig. 5.6-2. The directivity for this array, shown in Fig. 5.6-7, shows less fluctuation than that of the two previous planar arrays (Figs. 5.2-3 and 5.3-3).

Two sizes of spirals were constructed in the Virginia Tech Microelectronics Laboratory on a dielectric substrate using copper etching techniques. The individual spiral characteristics are given in Table 6.1-1. The spiral antenna radiation patterns in Figs. 6.2-1 through 6.2-5 show that the element pattern model of (4.2-2) is valid for both sizes of spirals over the frequency ranges of interest. Individual element pattern differences could cause the array patterns to deviate from the predicted patterns. Although ideally the element pattern should be the same in any plane, the spirals constructed had a low number of turns and may not exhibit this property completely. A large amount of

backward radiation was seen in the element patterns and the array patterns. This could be caused by imperfections in the feed cavities and backscatter from the antenna range at Virginia Tech.

The planar array of Fig. 6.3-1 was constructed and it performed as expected, although measured sidelobes were higher than those predicted in most cases. In almost all of the measured patterns the correct main beam was measured. The measured patterns in Figure 6.4-3 with vertical polarization illumination show the best agreement with the predicted pattern. Above the midband frequency (5.0 GHz) when all eight elements are allowed to radiate the pattern improvement over only four large elements is obsevred in Fig. 6.4-4, again for the vertically polarized patterns. Above 5.0 GHz the patterns are further degraded with the best agreement shown in Figure 6.4-6 for the $\phi = 0°$ vertically polarized case at 10.0 GHz.

Possible reasons for differences between the measured and predicted patterns include element pattern differences, element magnitude differences and problems associated with the feed network having no port-to-port isolation. The reflection coefficient measurements for individual elements shown in Figs. 6.5-1 through 6.5-4 indicate that reflections are present. These reflections can couple to other elements by the feed network since there is no isolation between the elements. Differences between vertically and horizontally polarized patterns could be caused by the element patterns exhibiting some dependence on the angle ϕ although the measured axial ratio of the elements and the total array are acceptable.

Improvements on the array are certainly possible. Better cavities and baluns would improve the radiation patterns of the elements and the entire array. Spiral elements constructed with more turns and spiral arms spaced closer together would also improve the element performance. An improved feeding network utilizing broadband power dividers would equalize the amplitude of each array element which should improve the

array performance. Although switching mechanisms used to turn the small array elements on and off were not considered here, measurements could be made across the entire bandwidth with all array elements connected. Likewise, switches that do not alter the input impedance of the array could be designed and tested.

VIII. References

1. Stutzman, W.L. and G. Thiele, *Antenna Theory and Design* , John Wiley and Sons: New York, 1981.

2. King, D. D., R.F. Packard, and R.K. Thomas, "Unequally Spaced, Broad-Band Antenna Arrays", *IRE Trans. on Ant. and Prop.* , vol. AP-8, pp.380-384, July 1960.

3. Chen, Y. S. and A. Ishimaru, "Thinning and Broadbanding Antenna Arrays by Unequal Spacings", *IEEE Trans. on Ant. and Prop.* , vol. AP-13, pp.34-42, January 1965.

4. Bratkovic, Frank., "Synthesis of Broad Band Arrays with Arbitrary Frequency Independent Elements", *IEEE Trans. on Ant. and Prop.* , vol. AP-21, pp. 211-213, March 1973.

5. DuFort, E.C., "Optical Technique for Broadbanding Phased Arrays", *IEEE Trans. on Ant. and Prop.* , vol. AP-23, pp. 516-523, July 1975.

6. Byron, E.V., G.J. Laughlin and T.C. Cheston, "Very Wide-Band Phased-Array Antenna", *IEEE Trans. on Ant. and Prop.* , vol. AP-20, pp. 699-704, November 1972.

7. Boyns, J.E. and J.H. Provencher, "Experimental Results of a Multifrequency Array Antenna", *IEEE Trans. on Ant. and Prop.* , vol. AP-20, pp. 106-107, January 1972.

8. Stutzman, W. L., "Near Field Feasibility Study, Part 1: Probe Antenna Element Investigation", New Mexico State University Physical Science Laboratory Report Number PN01049, November 1983.

9. Stutzman, W. L., "Wide Bandwidth Antenna Array Design", *Proceedings of the IEEE Southeastern Meeting* (Raleigh, NC), pp. 97-95, April 1985.

10. Newman, E.H. and M.R. Schrote, "A Wide-Band Electrically Small Superdirective Array", *IEEE Trans. on Ant. and Prop.* , vol. AP-30, pp. 1172-1176, November 1972.

11. Mosko, J. A., "An Introduction to Wideband, Two-Channel Direction Finding Systems", *Microwave Journal* , vol. 27, pp. 91-106, February 1984.

12. Werntz, P. C., *Design, Analysis and Fabrication of Archimedean Spiral Antennas* , Thesis, May 1988.

13. Donnellan, John R., "A Spiral Doublet Scanning Array", *IEEE Trans. on Ant. and Prop.* , vol. AP-9, pp. 276-279, May 1961.

14. Close, R.T., and John R. Donnellan, "A Spiral Grating Array", *IRE Trans. on Ant. and Prop.* , vol. AP-9, pp. 291-296, May 1961.

15. AEL Model ASM-1601A Cavity Backed Spiral Antenna Data Package, June 1982, American Equipment Laboratories, Inc., Montgomery PA.

16. Lee, S., and Y. Rahmat-Samii, "Directivity of Planar Array Feeds for Satellite Reflector Applications", *IEEE Trans. on Ant. and Prop.* , vol AP-31, pp. 463-470, May 1983.

17. Forman, Barry, "Directivity Characteristics of Scannable Planar Arrays", *IEEE Trans. on Ant. and Prop.* , vol. AP-20, pp. 245-252, May 1972.

18. Elliot, R. S., *Antenna Theory and Design* , Prentice Hall, Inc.: Englewood Cliffs, NJ, 1981.

19. Shively, D. G. and W. L. Stutzman, *The Virginia Tech Antenna Laboratory: Documentation and Performance* , The Bradley Department of Electrical Engineering, Virginia Tech, Blacksburg, VA.

Appendices

Appendix A. Directivity Program

The following program computes the directivity for a planar array antenna defined by (4.1-1) with the beam solid angle defined by (4.3-1). An IMSL subroutine is called to perform the numerical integration. Element coordinates, amplitude and phase are input in a data file. The output is a directivity value for each frequency in the two octave bandwidth.

```
      INTEGER IER,I,N,L
      REAL DBLIN,F,AX,AY,BX,BY,AERR,ERROR,C,PI,PI2
      REAL A(20),B(20),FF,D,S(20),T(20)
      EXTERNAL F,AY,BY
      COMMON N,A,B,PI,PI2
      PI = 3.14159
      PI2 = PI/2.0
      AERR = 0.0001
      AX = 0.0
      BX = PI2
      READ(12,1)N
    1 FORMAT(I5)
      DO 10 I = 1,N
      READ(12,5)S(I),T(I)
    5 FORMAT(F6.3,F8.3)
```

```
 10  CONTINUE
     WRITE(13,2)N
  2  FORMAT('NUMBER OF ELEMENTS = ',I2)
     DO 20 I = 1,N
     WRITE(13,15)S(I),T(I)
 15  FORMAT(F7.4,5X,F7.4)
 20  CONTINUE
     DO 100 L = 10,40
     AERR = 0.0001
     FF = L/10.0
     DO 25 I = 1,N
     A(I) = S(I)*FF
     B(I) = T(I)*FF
 25  CONTINUE
     C = DBLIN(F,AX,BX,AY,BY,AERR,ERROR,IER)
     D = 10.0*LOG10(PI/C)
     WRITE(13,30)FF,D
 30  FORMAT(F5.2,'  ',F6.3)
100  CONTINUE
     STOP
     END
     REAL FUNCTION F(X,Y)
     REAL X,Y,A(20),B(20),PI,PI2,M
     COMPLEX G
     INTEGER I,N
     COMMON N,A,B,PI,PI2
     M = N
     G = (0.0,0.0)
     DO 50 I = 1,N
     G = G + CEXP(2.0*PI*(0.0,1.0)*((A(I)*SIN(Y)*COS(X)) + (B(I)*SIN(Y)
    C*SIN(X))))
 50  CONTINUE
     F = ((CABS(G)/M)**2)*SIN(Y)*((COS(0.53*Y))**11.6)
     RETURN
     END
     REAL FUNCTION AY(X)
     REAL X
     AY = 0.0
     RETURN
     END
     REAL FUNCTION BY(X)
     REAL X,A(20),B(20),PI,PI2
     INTEGER N
     COMMON N,A,B,PI,PI2
     BY = PI2
     RETURN
     END
```

Appendix B. Sidelobe Level Program

The following program calculates sidelobe levels for planar array antennas as a function of frequency. The radiation pattern expression (2.3-1) is evaluated by first evaluating the array factor expression (2.3-3) and then the element pattern expression (4.2-2). Element coordinates, amplitude and phase are input from a data file. Frequency and sidelobe level are output.

```
const
  pi = 3.14159;
var
  ardat                              : text;
  k,i,n,kk,j                         : integer;
  sll,sllmax,aftemp,m,phir                 : real;
  afreal,afimag,afmax,af,f,theta,temp,phi  : real;
  x1,y1,x2,y2,a,alpha                      : array[0..20] of real;
  down                               : boolean;
begin
    assign(ardat,'array.dat');
    reset(ardat);
    clrscr;
    writeln('SLL program');
    writeln('Input # of elements');
    readln(n);
    m:=n;
    afmax:=20.0*(ln(m)/ln(10.0));
    writeln('Input phi');
    readln(phi);
    phir:=phi*(pi/180.0);
    for i:= 1 to n do begin
     readln(ardat,x1[i],y1[i],a[i],alpha[i]);
     end;
    for i:=1 to n do begin
     writeln(x1[i]:6:2,y1[i]:6:2,a[i]:6:2,alpha[i]:6:2);
     end;
    repeat until keypressed;
    clrscr;
    writeln('# of elements = ',n,'  Phi = ',phi:4:1);
    writeln;
    for j:= 10 to 40 do begin
    down:=true;
    aftemp:=100.0;
    sll:=-100.0;
    sllmax:=-100.0;
    f:=j/10.0;
```

```
    for k:= 0 to 135 do begin
    theta:=k*(pi/180.0);
    afreal:=0.0;
    afimag:=0.0;
     for i:= 1 to n do begin
     x2[i]:=x1[i]*f;
     y2[i]:=y1[i]*f;
     temp:=(x2[i]*sin(theta)*cos(phir))+(y2[i]*sin(theta)*sin(phir));
     afreal:=afreal + (a[i]*cos((2.0*pi*temp)+alpha[i]));
     afimag:=afimag + (a[i]*sin((2.0*pi*temp)+alpha[i]));
     end;
    af:=sqrt(sqr(afreal)+sqr(afimag));
    af:=20.0*(ln(af)/ln(10.0));
    af:=af+(20.0*5.8*(ln(cos(0.53*theta))/ln(10.0)))-afmax;
    if (down=false) and (af <= aftemp) then sll:= af;
    if sll > sllmax then sllmax:=sll;
    if af <= aftemp then down:=true else down:=false;
    aftemp:=af;
    end;
    writeln('FF = ',f:4:1,' SLL = ',sllmax:5:2,' dB');
    end;
end.
```

Appendix C. Radiation Pattern Program

The following program evaluates the radiation pattern for a planar array antenna at a single frequency. Eq. (2.3-1) is evaluated with (4.2-2) and (2.3-3) to form the complete pattern. Element locations, amplitude, phase, frequency are input as well as the phi value for the plane of interest. The output is given in degree values of theta and relative power level in logarithmic form.

```
const
  pi = 3.14159;
var
  ardat,data,max                          : text;
  k,i,n,kk                               : integer;
  afreal,afimag,afmax,af,f,theta,temp,phi    : real;
  x,y,a,alpha                             : array[0..20] of real;
begin
    assign(ardat,'array.dat');
    assign(data,'pat.dat');
    assign(max,'max.dat');
    rewrite(data);
    rewrite(max);
    reset(ardat);
    afmax:= -100.0;
    clrscr;
    writeln('Input # of elements');
    readln(n);
    writeln('Input frequency factor');
    readln(f);
    writeln('Input phi');
    readln(phi);
    phi:= phi*(pi/180.0);
    for i:= 1 to n do begin
     readln(ardat,x[i],y[i],a[i],alpha[i]);
     x[i]:= x[i]*f;
     y[i]:= y[i]*f;
     alpha[i]:= alpha[i]*(pi/180.0);
     end;
    for i:= 1 to n do begin
    writeln(x[i]:6:2,y[i]:6:2,a[i]:6:2,alpha[i]:6:2);
    end;
    for k:= -135 to 135 do begin
     theta:= abs(k*(pi/180.0));
       afreal:= 0.0;
```

```
      afimag:=0.0;
      for i:= 1 to n do begin
      temp:=(x[i]*sin(theta)*cos(phi)) + (y[i]*sin(theta)*sin(phi));
      afreal:=afreal + (a[i]*cos((2.0*pi*temp)+alpha[i]));
      afimag:=afimag + (a[i]*sin((2.0*pi*temp)+alpha[i]));
      end;
     af:=sqrt(sqr(afreal)+sqr(afimag));
     af:=20.0*(ln(af)/ln(10.0));
     af:=af+(20.0*5.8*(ln(cos(0.53*theta))/ln(10.0)));
     if af<-40.0 then af:=-40;
     if af>afmax then afmax:=af;
     writeln(data,k:4,af:7:2);
     end;
    writeln(max,afmax:7:2);
    close(ardat);
    close(data);
    close(max);
end.
```

The vita has been removed from the scanned document